POLITECNICO DI MILANO
POLO TERRITORIALE DI COMO

Scuola di Ingegneria dell'Informazione

Master of Science in
Computer Engineering

Design of an active noise control solution for a DVB-T device

Thesis Supervisor
Prof. Luigi Piroddi

Assistant Supervisor
Prof. Fabio Salice

Candidate

Marco Ludovico Perego
Student Id 800547

Academic Year 2015/2016

POLITECNICO DI MILANO
POLO TERRITORIALE DI COMO

Scuola di Ingegneria dell'Informazione

Laurea Magistrale in
Ingegneria Informatica

Progettazione di una soluzione di controllo attivo del rumore per un dispositivo DVB-T

Relatore
Prof. Luigi Piroddi

Co-relatore
Prof. Fabio Salice

Candidato

Marco Ludovico Perego
Matricola 800547

Anno Accademico 2015/2016

Active Noise Control
Master thesis in Computer Science,
Politecnico di Milano - Polo territoriale di Como.
© 2016 Marco Ludovico Perego. All rights reserved.

Politecnico di Milano: www.polimi.it

Scuola di Ingegneria Industriale e dell'Informazione: www.ingindinf.polimi.it

Author's email: marcoludovico.perego@mail.polimi.it

Ringraziamenti

Un ringraziamento particolare al Prof. Piroddi e al Prof. Salice, che mi hanno permesso di lavorare con loro per portare a termine questo lavoro di tesi, dedicandomi tempo e pazienza. Vorrei ringraziare i miei genitori. Per ogni giorno che mi hanno dedicato, per ogni preoccupazione e per tutta la pazienza di cui si sono muniti. Sono orgoglioso di avervi al mio fianco e un giorno spero di poter ricambiare anche in minima parte tutti i vostri sforzi. Grazie a Massi e Teo, vi voglio bene e sarò sempre grato di avervi come fratelli. Un Singing Ja Ja enorme per Stefanino e il suo sorriso, la luce più bella in questo anno passato. Grazie a mia nonna Carla, per tutte le lavate di capo e l'amore che ha dato a tutti i suoi nipoti. Grazie a mia zia Mara, Stefano, Paolo e le vostre famiglie, meritate tutti gli abbracci e il bene del mondo. Il grazie più grande va a Bianca, non sarei qui senza di te. Hai riportato vita e colore dove tutto stava sbiadendo. Questa laurea è anche tua. Grazie a Laura ed Ennio, praticamente la mia seconda famiglia. Vorrei ringraziare di cuore tutti gli amici del PDD, del Lago, di Brugherio, di Anzani, del Gruppo Classe e del Libra, la famiglia di Casa Neri e tutte le persone che ho conosciuto suonando. Siete veramente troppi per elencarvi tutti e siete la base della mia felicità. Grazie a Luca e Cafa, suonare nei Bantha mi ha arricchito profondamente. Grazie a Staglia e Luke per aver condiviso con i me i loro Wet Floor. Grazie a Ema e Valli, Rava e Tanzino, per una vita passata assieme.

Dedico questo lavoro ai miei nonni: Carla, Lidia, Gianni e Angelo. Nessun libro o università potrà mai rimpiazzare le vostre parole.

Brugherio, Dicembre 2016 Marco Ludovico Perego

"What can be done must be done"
Ai miei nonni.

Contents

Introduction **1**

1 State of the art **5**
1.1 The acoustic noise problem 5
1.1.1 Active Noise Canceler vs Passive Noise Canceler . . 6
1.1.2 The superposition principle 7
1.1.3 Classification of ANC systems 7
1.2 Operative principles of an ANC system 9
1.3 Broadband feedforward ANC systems 13
1.3.1 The LMS algorithm 13
1.3.2 Secondary path effects 14
1.3.3 The FxLMS algorithm 16
Feedback compensation 17
Estimation of the acoustic paths 18
1.4 Narrowband feedforward ANC systems 20
1.4.1 Adaptive notch filter 21
1.4.2 Multiple frequency ANF 23
1.4.3 Narrowband input applied to a broadband ANC . . 25

2 Theoretical background **29**
2.1 Convergence analysis 29
2.2 Estimation errors 33
2.3 Phase delay compensation 34
2.4 Eigenvalue equalization 34
2.5 Leaky FxLMS 42

3 Signal analysis **45**
3.1 Signal analysis 45
3.2 Spectral analysis and beat frequency 46
3.3 Flow noise 50

4 The proposed ANC method **51**
4.1 Hybrid ANC method . . . 52
4.2 Filtered-error parallel narrowband ANC . . . 55
4.3 The proposed method . . . 56

5 Hardware implementation **63**
5.1 The digital signal processor . . . 63
5.2 The audio signal chain . . . 64
The analog-to-digital converter . . . 65
The digital-to-analog converter . . . 65
The microphones . . . 66
The canceling loudspeaker . . . 67
5.3 Signal acquisition . . . 68
5.4 Some considerations on the physical ANC system . . . 69
Causality . . . 69
Sampling frequency and filter length . . . 70
Sensor and actuator placement . . . 71
The duct case . . . 71

6 Software implementation **73**
6.1 Lookup tables and delay compensation . . . 73
6.2 Reduced-order path estimation . . . 75

7 Test beds **81**
7.1 Initial test setup procedure . . . 81
7.2 Case 1 - ANC system inside the duct . . . 82
7.2.1 The EE-FxLMS validation . . . 83
7.2.2 Attenuation performances . . . 86
7.2.3 Pros and cons . . . 89
7.3 Case 2 - ANC system outside the duct . . . 89
7.3.1 Configurations . . . 89
7.3.2 Attenuation performances . . . 91
7.3.3 Pros and cons . . . 96
7.4 Case 3 - ANC system without the duct . . . 99
7.4.1 Attenuation performances . . . 102
7.4.2 Pros and cons . . . 103

8 Results with the DBV-T **107**
8.1 Test with the duct . . . 107
8.2 Test without the duct . . . 113

Conclusions 115

List of Figures

1 DBV-T Device under study 2

1.1 Superposition principle: Two identical sine waves with some phase difference between them are shown on the left column. The right column shows the result of adding the two waves. When the waves are exactly out of phase (bottom plots) the addition of the two waves results in no wave motion. . . . 8

1.2 Two plane acoustical monopoles in an infinite duct: the monopole at distance x_P represents the noise source, while the monopole at x_S is the secondary source which should reduce the noise produced by the previous source for $x > x_S$. 10

1.3 The elements of an ANC system: the noise source and $P(z)$ belong to the acoustic domain, the remaining blocks instead belong to the electrical domain. 11

1.4 Single-channel Feedforward ANC systems: the main difference in these two systems is the acquisition block for the reference signal. In the broadband case **(a)** the reference signal is picked up by a microphone. In the narrowband case **(b)**, instead, a non-acoustic sensor is used. 12

1.5 LMS algorithm scheme: the reference signal $x(n)$ and the error signal $e(n) = y(n) - d(n)$ are used in the LMS algorithm to update the adaptive filter $W(z)$. 15

1.6 Block diagram of an LMS-based ANC system. 16

1.7 Block diagram of the FxLMS algorithm: the ANC system stability is ensured by adding the estimate $\widehat{S}(z)$, it takes into account the distortions introduced by the secondary path $S(z)$. 17

1.8 Block diagram of ANC system with feedback: $F(z)$ represents the transfer function from the loudspeaker to the reference microphone. 18

1.9 ANC system with feedback neutralization: the estimation $\widehat{F}(z)$ is introduced to eliminate the feedback between loudspeaker and reference microphone. 19
1.10 Off-line modeling of the secondary and feedback paths. . . 20
1.11 Block diagram of the single frequency Adaptive Notch Filter: the sinusoidal input signal $x(n)$ is acquired by a non-acoustic sensor or by a pre-designed lookup table. The filter coefficients $a(n)$ and $b(n)$ have the task of correcting the phase and the amplitude of $x(n)$ through a FxLMS algorithm. . . 22
1.12 Degradation of the noise attenuation performance of an ANF system as a function of the frequency mismatch (nominal frequency= 500Hz). 23
1.13 Block diagram of the parallel-form Adaptive Notch Filter (m-th channel). 24
1.14 Efficient parallel narrowband ANC system (m-th channel): a summing node is added to convey the signals of all channels to a single update signal. After the filtering with the estimate $\widehat{S}(z)$, the band-pass filters $BP_m(z)$ decomposes again the signal in its main components. 26

2.1 Examples of the filter and reference signal used in this Chapter. **(a)**: an example of a 180-Tap secondary path **(b)**: FFT of the DVB-T cooling fans noise in the frequency range of interest ($0 \div 4000$ Hz). 30
2.2 Example for delay compensation in a Narrowband ANF scheme. 35
2.3 Magnitude comparison: original $\widehat{S}(z)$ (blue) and after the Eigenvalues Equalization (orange). 36
2.4 Phase comparison: original secondary path (blue) and after the Eigenvalues Equalization (orange). 37
2.5 Filter coefficient comparison between the original $\widehat{S}(z)$ taps and the Eigenvalues Equalization version. 38
2.6 Magnitude comparison: original $\widehat{S}(j\omega)$ (blue) and after the Eigenvalues Equalization (orange). The EE-version is based only on the inverse magnitude of the reference signal. Thus, the minimum value of $|\widehat{S}_{EE}(j\omega)|$ is at the fundamental frequency $f_0 = 1136$Hz. 39
2.7 Filter coefficient comparison between the original $\widehat{S}(z)$ taps and the Eigenvalues Equalization version based on the reference signal. 40

2.8 Comparison between convergence times using the original $\widehat{S}(z)$ (blue) and the Eigenvalues Equalization version (orange). Results refer to a noise with 33 tones, each separated from the others by 25 Hz in the frequency range of [200÷1000] Hz. 41

2.9 Block diagram of an ANC system with the FxFeLMS algorithm. 42

3.1 Details of the refrigerant fans in the DBV-T device without the protective grid. 46

3.2 Graphic representation of the beat phenomenon: the upper subplot shows two sinusoids of equal amplitude but with slightly different frequency, (the blue sinusoid has frequency $f_b = 200$Hz, the orange sinusoid has a frequency $f_o = 210$Hz). The bottom subplot shows the sum of these two sinusoids. 47

3.3 Temporal behavior of the reference signal around the fundamental frequency $F_0 = 1136$Hz. 48

3.4 Spectrogram of the fan signal near the fundamental frequency, i.e. in the frequency range of $[1125, 1150]$ Hz. . . . 49

3.5 Magnitude of the DBV-T noise signal. 49

3.6 Individual spectrum analysis of the fans. 50

4.1 Hybrid feedforward ANC scheme: the system consists of three subsystems, a SNC (red) that 'cleans' the reference signal from selected sinusoidal components, a broadband FxLMS-based active noise canceler (blue) and a second SNC (green) that takes into account the secondary path and eliminates the sinusoidal components neglected by the broadband subsystem. 53

4.2 Parallel filtered-error narrowband FxLMS ANC scheme: the highlighted block $H_m(z)$ represents the m-th band-pass filter, used to make the update equation error-selective in each m-th system in parallel. 55

4.3 Block diagram of the proposed hybrid method: the broadband ANC subsystem (blue) filters the input signal with a high-pass filter $H_{HP}(z)$ in order to eliminate the flow noise components. The narrowband ANC subsystem (green) handles the cancellation of the narrowband component at 227 Hz. This component is not present in the input signal x(n) entering the broadband subsystem, due to the highpass filtering applied to obtain that signal. Hence, the broadband subsystem is not capable of attenuating this narrowband component, which motivates the introduction of the narrowband subsystem to correct the antinoise signal. The band-pass filter $H_{BP}(z)$ is included to make the update equation of the narrowband subsystem error-selective. . . 58
4.4 Spectrogram of the antinoise output $y(n)$ in the case of system instability due to flow noise. 60

5.1 STM32F4 DISCOVERY evaluation board. 64
5.2 Audio signal chain. 65
5.3 FourPointSurround^{TM} Speaker System. 67
5.4 PicoScope2000 digital oscilloscope. 68

6.1 Filter coefficients comparison between the 180-taps estimation $\widehat{H}(z)$ and its reduced version $\widehat{H}_k(z)$. 76
6.2 Magnitude comparison between the 180-taps estimation $\widehat{H}(z)$ (blue) and its reduced version $\widehat{H}_k(z)$ (orange). 76
6.3 Phase comparison between the 180-taps estimation $\widehat{H}(z)$ (blue) and its reduced version $\widehat{H}_k(z)$ (orange). 77
6.4 Filter coefficients comparison between the 180-taps estimation $\widehat{H}(z)$ (blue) and its reduced version $\widehat{H}_{d,k}(z)$ (orange). 78
6.5 Magnitude comparison between the 180-taps estimation $\widehat{H}(z)$ (blue) and its reduced version $\widehat{H}_{d,k}(z)$ (orange). . . . 79
6.6 Phase comparison between the 180-taps estimation $\widehat{H}(z)$ (blue) and its reduced version $\widehat{H}_{d,k}(z)$ (orange). 79

7.1 Case 1: wooden duct with all the sensors and actuators of the ANC system located internally. 83
7.2 Case 1: impulse response magnitudes of the FIR filters $\widehat{S}(z)$ (top) and $\widehat{F}(z)$ (bottom). 84
7.3 Case 1: convergence times comparison between the standard-FxLMS algorithm and the EE-FxLMS algorithm. 85

7.4 Case 1: attenuation performances achieved using the EE-FxLMS algorithm. 86
7.5 Case 1: comparison between the residual noise acquired at the error microphone and the one acquired at the workstation with the laptop's built-in microphone. 87
7.6 Case 1: attenuation performance at the error microphone using the proposed method applied to the DVB-T fans noise signal. 88
7.7 Case 2: impulse response magnitudes of the FIR filters $\widehat{S}(z)$ (top) and $\widehat{F}(z)$ (bottom). 90
7.8 Case 2: wooden duct with all the sensors and actuators of the ANC system located internally. 92
7.9 Case 2: magnitude comparison between the frequency response of $\widehat{S}(z)$ and $\widehat{F}(z)$ identified using three different loudspeaker configurations. 93
7.10 Case 2: phase comparison between the frequency response of $\widehat{S}(z)$ and $\widehat{F}(z)$ identified using three different loudspeaker configurations. 94
7.11 Case 2: attenuation perfomances at the error microphone. 95
7.12 Case 2: comparison between the residual noise acquired at the workstation with the laptop's built-in microphone using six different loudspeaker configurations. 97
7.13 Case 2: attenuation performance at the error microphone using the proposed method applied to the DVB-T fans noise signal. 98
7.14 Case 3: ANC system in the free field using one or two cancelling sources. 100
7.15 Case 3: magnitude comparison between the frequency response of $\widehat{S}(z)$ and $\widehat{F}(z)$ identified using one or two loudspeakers. 100
7.16 Case 3: phase comparison between the frequency response of $\widehat{S}(z)$ and $\widehat{F}(z)$ identified using one or two loudspeakers. 101
7.17 Case 3: comparison between the attenuation performances at the error microphone using one or two loudspeakers. . . 102
7.18 Case 3: comparison between the attenuation performances at the workstation using one or two loudspeakers. 103
7.19 Case 3: attenuation performance at the error microphone using one loudspeaker. The proposed method is applied to the DVB-T fans noise signal. 104

7.20 Case 3: attenuation performance at the error microphone using two loudspeakers. The proposed method is applied to the DVB-T fans noise signal. 105

8.1 Detail of the duct applied to the DVB-T device. 108
8.2 Impulse response magnitudes of the FIR filters $\widehat{S}(z)$ (top) and $\widehat{F}(z)$ (bottom) estimated with the duct. 109
8.3 FFT of the noise signal produced by the DVB-T fans acquired inside the duct. 110
8.4 Duct applied close to the DVB-T protective grid 110
8.5 Attenuation performance at error microphone using the duct. 111
8.6 FFT of the noise signal produced by the rear side of the DVB-T. 112
8.7 DVB-T device under analysis. 112
8.8 Positioning of the ANC sensors and actuators for the control of the DVB-T noise in the free field. 113
8.9 Attenuation performance at error microphone in the free field. 114

Sommario

Il lavoro di tesi qui presentato è inserito all'interno del progetto PIANO ("PIAttaforme a basso costo per il coNtrOllo attivo del rumore"), commissionato al Politecnico di Milano nel Febbraio 2011. Scopo del progetto è l'attenuazione del rumore prodotto da due ventole ad alta velocità, per il raffreddamento di un dispositivo di Digital Video Broadcasting – Terrestrial (DVB-T). La soluzione a questo problema adotta una metodologia di controllo attivo del rumore (ANC) sviluppata attraverso hardware. In particolare, essa utilizza un microcontrollore per processare i segnali acquisiti attraverso dei sensori ed effettua la cancellazione generando con degli attuatori elettroacustici il segnale atto ad attenuare il disturbo in una particolare zona dello spazio, detta zona di quiete. Le specifiche di progetto, tuttavia, vietano qualsiasi modifica strutturale del dispositivo ad eccezione dell'installazione di piccoli microfoni ed altoparlanti, purché questi non compromettano le prestazioni. Ad una prima parte focalizzata sull'analisi dello stato dell'arte, segue l'analisi del segnale di rumore emesso dalle ventole. L'implementazione della soluzione specifica per il caso DVB-T è stata raggiunta gradualmente, dapprima analizzando il comportamento del sistema ANC implementato su strutture fisiche standard, già ampiamente trattate nello stato dell'arte, e in seguito aggiungendo o rimuovendo elementi del sistema al fine di trovare la soluzione migliore per il problema legato al dispositivo DVB-T. Conclusa questa fase iniziale di test, è stato implementato il sistema ANC sul dispositivo DVB-T, ottenendo risultati non soddisfacenti a causa del forte rumore di rumore di fondo e alla presenza di componenti di rumore legate al flusso d'aria a cui sono soggetti i sensori. Per questo motivo è stato pensato e consecutivamente proposto un metodo ANC ibrido ad-hoc, il quale sfrutta al contempo le metodologie broadband e narrowband basate sull'algoritmo FxLMS. In questo modo è stato possibile ottenere risultati migliori e garantire la stabilità del sistema.

Abstract

The master thesis here presented is part of the PIANO project (the Italian acronym for "low cost platforms for the active noise control") which was commissioned to Politecnico di Milano in February 2011. The project goal is the attenuation of the noise produced by two high speed cooling fans of a Digital Video Broadcasting – Terrestrial (DVB-T) device. The solution to this problem employs a hardware implemented Active Noise Control (ANC) methodology. In particular, a dedicated digital signal processing microprocessor and electro-acoustic sensors and actuators are employed to generate an anti-noise signal, whose aim is the cancellation of the disturbance at a particular point in space (quiet zone). Nevertheless, the project specifications prohibit any structural modification of the device, with the exception of the installation of small microphones and loudspeakers, provided that the cooling performance is not affected. A study concerning the fan noise signal is presented after a state of the art analysis. The implementation of the specific solution for the DVB-T case was reached gradually, first by analysing the behaviour of the ANC system implemented on standard physical structures, already widely discussed in the state of the art, and subsequently, by adding or removing elements of the system in order to find the best solution to the DVB-T noise problem. After this initial test phase, the ANC system has been implemented on the DVB-T device, obtaining unsatisfactory results because of the loud background noise and the presence of noise components related to the air flow to which the sensors are subject. For this reason, a hybrid ANC ad-hoc method was designed and consecutively proposed, which relies on both the broadband and narrowband methodologies based on the FxLMS algorithm. In this way, it was possible to get better results and ensure the stability of the system.

Introduction

The project carried out in this thesis faces topics related to active noise control both through simulations and practical implementations. Starting from an ANC problem, the goal is the development of a hardware prototype for its solution, implementing a specific algorithm. In particular, the noise problem here considered is related to heating, ventilating and air conditioning systems (HVAC). The fans present in common desktop or laptop computers are needed to avoid overheating and consequent fusion of internal electronic components. These types of fans have standard dimensions of few centimeters and produce a tolerable level of noise. On the contrary, large devices dedicated to signal processing such as the terrestrial infrastructures for digital video broadcasting need a continuous and high computing power. Consequently, the fans installed in these devices produce a loud noise, proportional to their rotational speed. Considering a room dedicated to the development of the digital video broadcasting system, the computing power required necessitates the installation of multiple servers, organized in racks. It is easy to understand how much annoying the generated global noise can be for an operator who has to work nearby.

The goal of this thesis is related to the PIANO project, a research project started in February 2011 in partnership with the Politecnico di Milano. The goal of this project is the reduction of the noise emitted by two high performance cooling fans of a DVB-T (Digital Video Broadcasting - Terrestrial) processing system showed in Figure 1: this type of fan reaches a high rotational speed, in order to dissipate the high amount of heat released by the image processors. The project specifications require to pursue the goal without modifying the device, while the addition of small sensors and actuators is allowed, provided that it does not affect the cooling performance. These restrictions forced the adoption of a hardware (DSP) implemented ANC system. This problem was therefore analyzed from the ANC perspective, implementing an ANC algorithm for the reduction of the acoustic noise produced by the fans. The starting point to reach this goal is the elaboration of several practical implementations of ANC systems

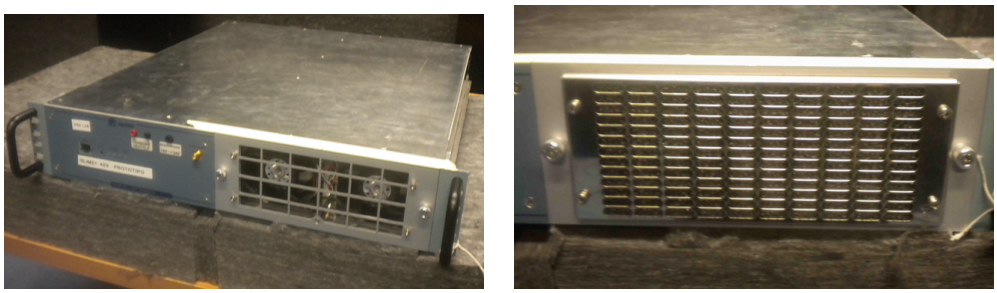

(a) Frontal image of DBV-T device **(b)** Fan grid detail

Figure 1: DBV-T Device under study

for sound control in ducts. Different test beds were built to simulate the behavior of HVAC systems, starting from the most simple case and gradually approaching the DVB-T fans case.

After evaluating the limitations posed by the hardware devices available, a study was carried out on the noise signal generated by the fans and as a result an ANC method that would work the best for this scenario was chosen. Despite this, in the implementation phase various problems and difficulties were detected that could not be accounted for during the simulations. The most significant are the errors in the acoustic paths estimations, the presence of acoustic feedback, the flow noise, resonances related to the duct modes, placement of the sensors and of the secondary sources. Given the limitations of the available instrumentation, a single-channel ANC system has been designed, although a multi-channel ANC system would be more suited to the final aim of this thesis.

The thesis is organized as follows:

In Chapter 1, the state of the art is reviewed. After a brief recap on the acoustic noise problem, the active noise control methodologies are analyzed, namely broadband and narrowband single-channel feedforward ANC methods.

Chapter 2 is devoted to the theoretical background. The problem of stability is presented in relation to the estimate of the secondary path. The stability conditions are discussed together with algorithms to improve system performance.

Chapter 3 addresses the temporal and spectral analysis of the signal produced by the DVB-T fans. The information contained in this chapter will be used to subsequently design an ad-hoc ANC system.

Chapter 4 provides an insight on the ANC method developed in this thesis. Before explaining the new ANC method concerning the PIANO

project, an introduction of two recent feedforward ANC methods is provided. These two new systems will contribute, together with the concepts discussed in previous chapters, to the implementation of the ad-hoc ANC method.

Hardware and software implementations are discussed in Chapters 5 and 6 respectively. In these chapters the attention will be mainly focused on practical problems encountered during the design of the ANC system, as the positioning of the sensors and actuators, the choice of parameters related to the adaptive filters, system optimization to increase performance, etc.

Chapters 7 and 8 report the results of simulations and experiments conducted at first on laboratory test beds, simulating the behavior in the case of noise in ducts, then applying the acquired knowledge to the DBV-T device.

Finally, the conclusions and outlines possible future research directions are described.

Chapter 1

State of the art

A short review on the Feedforward ANC methodologies is provided in this chapter. We start by introducing the acoustic noise problem, and the difference between active and passive solutions for the noise control. The physical mechanism behind active noise control is then discussed. Basic configurations for the realization of ANC systems are then introduced, starting from the Least Mean Square (LMS) algorithm. One of the main constraints in the choice of an adaptive algorithm is its computational complexity. For the application of ANC, it is convenient to choose an algorithm which is computationally very fast. Taking this into consideration, the LMS algorithm became an obvious choice. The operating principle of LMS is the basis for the algorithm used throughout the whole project, the Filtered-x Least Mean Square (FxLMS) algorithm, which is widely used in different types of ANC systems. The FxLMS was developed by Morgan [1]. Burgess [2] has suggested using this algorithm to compensate for the effects of the secondary path in ANC applications. Nowadays, the FxLMS algorithm is one of the most popular adaptive algorithms for Feedforward control and is considered the most effective ANC approach among all other solutions. As a result, several modified FxLMS-type algorithms have been developed.

Broadband and Narrowband ANC schemes based on FxLMS are finally presented and discussed.

1.1 The acoustic noise problem

Acoustic noise problems have become serious with the increased use of industrial equipment, such as engines, fans, blowers, transformers, and compressors. The design of an active noise canceler using a microphone

and an electronically driven loudspeaker to generate a canceling sound was first proposed and patented by Paul Lueg in 1936 [3]. In the 1950s, the first active noise control (ANC) systems were constructed. After that, the development of ANC was halted for twenty years. The lack of required technology didn't permit to implement canceling systems because the characteristics of an acoustic noise source and of the environment are not constant, the frequency content, amplitude, phase, and velocity of the undesired noise are non-stationary (time varying). An ANC system must be adaptive in order to cope with these changing characteristics. With the existing manual analogue techniques, it was extremely difficult to produce secondary sound that had the amplitude and phase required to attenuate the primary noise.

The advent of the microprocessor in 1970s made it possible to apply digital signal processing techniques and devices for ANC and construct practical ANC systems. A duct-noise cancellation system based on adaptive filter theory was developed by Burgess in 1981[2].

Later in the 1980s, research on ANC was dramatically affected by the development of powerful, low-cost digital signal processors (DSPs) that allowed the implementation of advanced adaptive algorithms with faster convergence, increased robustness to interference, and improved system performance for practical applications.

1.1.1 Active Noise Canceler vs Passive Noise Canceler

There are two approaches for controlling acoustic noise: passive and active. Traditional acoustic noise reduction techniques are based on passive noise control, such as earplugs, ear-protectors, sound insulation walls, mufflers, and sound-absorbing materials. These passive techniques are effective for reducing noise over a wide frequency range, by absorbing it. Passive silencers use either the concept of impedance change caused by a combination of baffles and tubes to silence the undesired sound (reactive silencers) or the concept of energy loss caused by sound propagation in a duct lined with sound-absorbing material to provide the silencing (resistive silencers). Reactive silencers are commonly used as mufflers on internal combustion engines, while resistive silencers are used mostly for duct-borne fan noise. Furthermore, these silencers often create an undesired back pressure if there is airflow in the duct.

Passive noise control is very effective in suppressing high-frequency noise, but it becomes cumbersome, costly and inefficient at low frequencies.

On the other hand, ANC is effective for reducing low-frequency noise, which motivates the considerable interest that has been placed in ANC. On the other hand, one of the major limitations of ANC is that the reduction of noise is limited to a localized specific region and has the unwanted side effect of amplifying it elsewhere. In addition, it must be possible to measure the noise signal before it reaches the area of interest.

1.1.2 The superposition principle

ANC is an electro-acoustical technique based on the principle of superposition.

Consider the addition of two identical waves (same frequency and amplitude) shown in Figure 1.1. The net amplitude of the resulting wave depends on the relative phase of the two waves. When the positive antinodes of one wave align with the negative antinodes of the other (exactly out of phase) the combined wave displacement will be zero. The same principle holds for more complicated waveforms and sound fields.

In ANC systems the anti-noise with the same amplitude but opposite phase is generated by secondary source(s), typically a loudspeaker, to cancel unwanted (primary) noise. An error sensor is used to pick up the residual noise, which serves as the error signal for updating the adaptive filter. The adaptive filter that tracks the variations of the primary noise and estimates unknown plants, is typically updated with an adaptive LMS (Least Mean Square) or FxLMS (Filtered-x Least Mean Square) algorithm.

1.1.3 Classification of ANC systems

ANC methods are generally classified into two classes depending on the control structure: feedforward control and feedback control. In this thesis we focus on the feedforward control case, where a primary noise signal is assumed to be available for the adaptive filter. Feedforward ANC systems can be categorized as either broadband or narrowband, depending on the spectral characteristics of the noise.

In the broadband feedforward control case the noise energy is distributed over a large frequency band. Examples of broadband noise are low-frequency noise from jet planes and road noise inside a moving vehicle.

Narrowband noise is related to rotating or repetitive machines and is periodic or nearly periodic. Its energy is concentrated at specific frequencies. In addition to these two major feedforward ANC systems, several hybrid ANC systems have also been developed.

In our applications the feedforward ANC system is based on 4 elements:

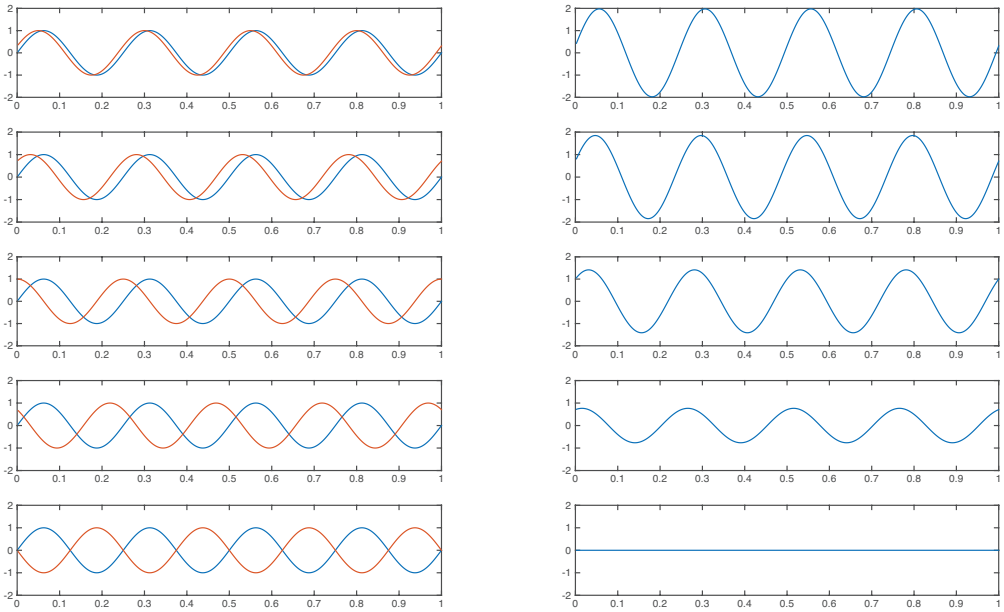

Figure 1.1: Superposition principle: Two identical sine waves with some phase difference between them are shown on the left column. The right column shows the result of adding the two waves. When the waves are exactly out of phase (bottom plots) the addition of the two waves results in no wave motion.

1. a microphone as reference sensor, for detecting the primary noise (also called reference signal);
2. a microphone as error sensor, for detecting the error signal;
3. a loudspeaker as secondary source;
4. a DSP micro-controller, for processing the signals and driving the canceling actuator.

Successful application of ANC requires that there is both a good spatial and a good temporal matching between the fields of the primary and secondary sources. The requirement for spatial matching bounds the upper frequency of ANC, due to the physical requirement that the acoustic wavelength be small compared to the control zone. The requirement for temporal matching requires a signal processing system that can adapt to changes in the primary noise.

Active noise cancelers rely heavily on adaptive signal processing, but they have to take in account the acoustical elements. If the acoustical design of the system is not optimized, the digital controller may not be able to adequately attenuate the undesired noise. Therefore, it is necessary to understand the acoustics of the installation and to design the system adequately.

1.2 Operative principles of an ANC system

ANC uses the principle of destructive interference of sound waves. To cancel an undesired noise, a sound wave with inverse sound pressure is generated. To achieve a significant cancellation, the anti-noise source must generate an inverted version of the original noise signal with great accuracy. In this thesis a model of ANC systems for infinite ducts will be developed, useful for modeling ANC systems for ventilation ducts.

If the sound wave propagates through an infinite duct, and if its wavelength is much longer than the duct diameter, one can assume that it is a plane acoustical wave. When the wavelength is less than the double diameter of the duct, high-order modes are generated in the soundwave propagation. Although most work on active noise control systems in ducts has focused on plane-wave propagation, higher order modes can become a problem for large duct dimensions even for low frequencies.

Plane wave propagation of the sound in the $+x$ axis direction of the Cartesian coordinate system is described by the differential equation

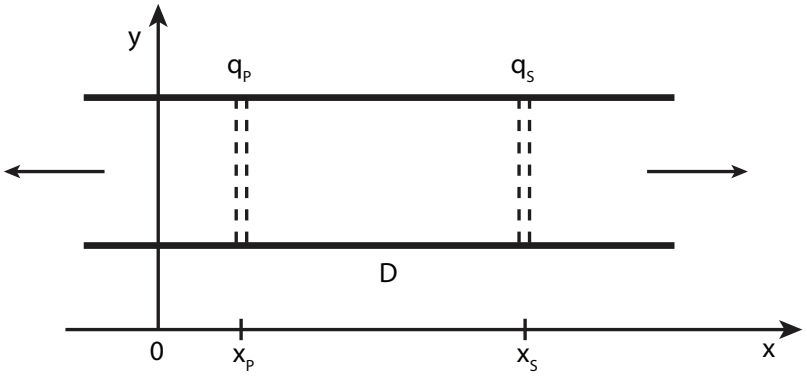

Figure 1.2: Two plane acoustical monopoles in an infinite duct: the monopole at distance x_P represents the noise source, while the monopole at x_S is the secondary source which should reduce the noise produced by the previous source for $x > x_S$.

$$\frac{\delta^2 p}{\delta x^2} - \frac{1}{c_0^2}\frac{\delta^2 p}{\delta t^2} = 0, \tag{1.1}$$

where p denotes sound pressure, t is the time and c_0 is the velocity of the sound propagation. The simplest anti-noise source for the infinite duct case is one loudspeaker fixed on the wall of the duct. At low frequencies, neglecting the area close to the loudspeaker, one can assume that the anti-noise sound wave is a plane wave, and can model the loudspeaker as a plane acoustical monopole in the infinite duct.

A plane acoustical monopole can be imagined as a pair of two massless pistons at infinitesimal distance, moving in opposite directions, their motion being controlled by the time-varying volume velocity of the monopole $q(t)$. If the sound wavelength is large compared to the physical dimensions of the loudspeaker, the volume velocities of the monopole and the loudspeaker will be the same.

If the noise source is located in the x_P point on the x-axis, and the secondary source in the x_S point (Figure 1.2), and if their volume velocities are q_P an q_S, respectively, the sound pressure will be canceled for $x > x_S$ if the following equation is satisfied:

$$q_S = q_P(t - \frac{D}{c_0}) \tag{1.2}$$

where D denotes the distance between the two sources.

To satisfy (1.2), the time delay between q_S and q_P must be equal to the time the sound waves take to propagate between the two sources. In

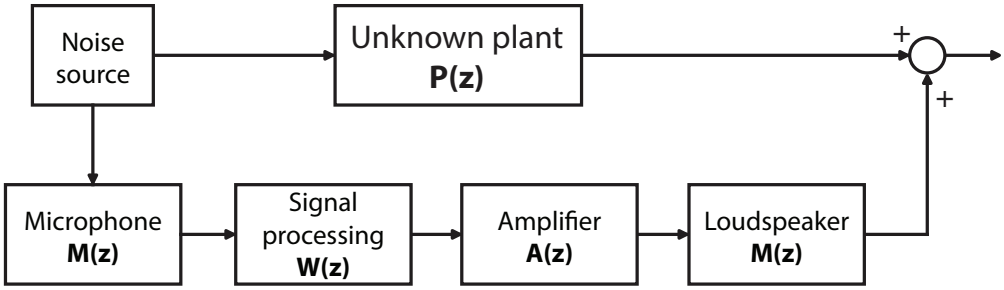

Figure 1.3: The elements of an ANC system: the noise source and $P(z)$ belong to the acoustic domain, the remaining blocks instead belong to the electrical domain.

practice one has to detect the original noise signal using an appropriate sensor, and transduce the acoustic signal to its electrical equivalent. The electrical signal has to be processed to ensure the time delay condition, and after suitable amplification, brought to the actuator (loudspeaker). This chain is described by Figure 1.3.

All the elements of an ANC system have their own transfer functions: $P(z)$ is the transfer function of the primary channel, representing the acoustic path from the reference microphone to the error microphone. The secondary path $S(z)$ includes the transfer functions of all the electronic devices needed by the ANC system. It takes also into account the transfer function of the acoustic path from the loudspeaker to the error microphone. $S(z)$ introduce amplitude and phase changes in the system. The purpose of the signal processor is to compensate these changes, and to ensure an overall time delay that matches condition (1.2), by properly designing its transfer function $W(z)$. In order to compensate the phase change the residual signal (output of the node), is detected by the error microphone and used to update $W(z)$.

The complete schemes for single-channel Feedforward Broadband and Narrowband ANC systems are presented in Figure 1.4. Most of the concepts and methodologies that will be presented later are based on Kuo and Morgan works [4, 5, 6]. Academic books and materials were also consulted during the entire project [7, 8, 9].

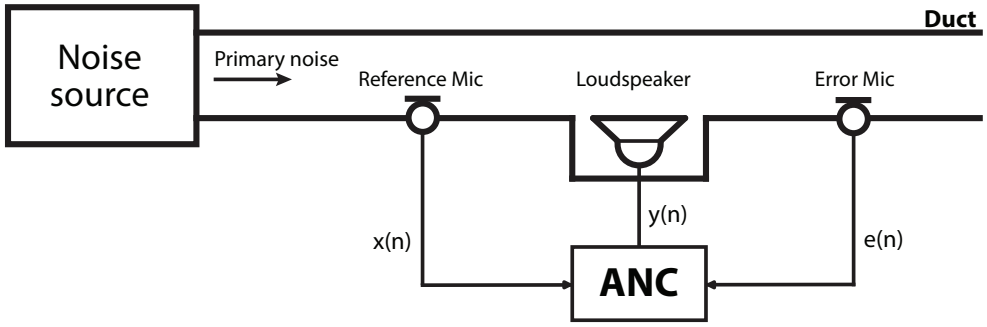

(a) Broadband ANC system

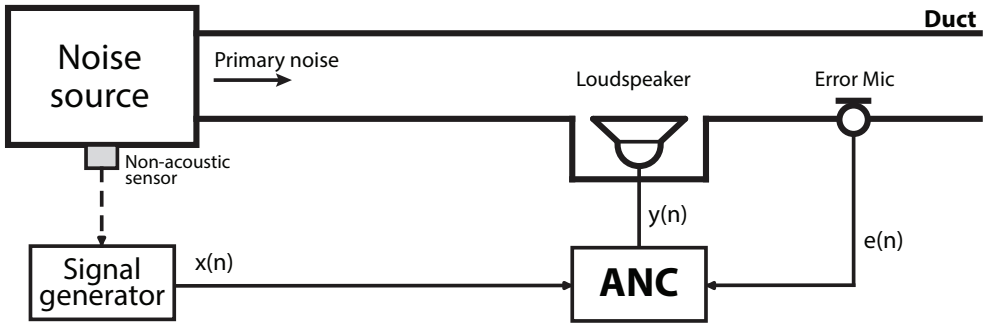

(b) Narrowband ANC system

Figure 1.4: Single-channel Feedforward ANC systems: the main difference in these two systems is the acquisition block for the reference signal. In the broadband case **(a)** the reference signal is picked up by a microphone. In the narrowband case **(b)**, instead, a non-acoustic sensor is used.

1.3 Broadband feedforward ANC systems

1.3.1 The LMS algorithm

The LMS algorithm for adaptive noise cancellation is illustrated in Figure 1.5. The objective is to cancel the disturbance signal $d(n)$ with the output of the adaptive filter $y(n)$. The error signal $e(n)$, which is the sum of the disturbance and the adaptive filter output, is used for adapting the adaptive filter $W(z)$ so that the error is minimized. The adaptive filter consists of two elements, the filter itself and an adaptive algorithm that tunes it. The filter is in most cases a finite impulse response (FIR) filter.

The LMS algorithm is based on the steepest descent method from numerical optimization where the cost function is the mean-squared error signal $\xi(n) = \mathbf{E}[e^2(n)]$. In the adaptation, also the reference signal $x(n)$ is needed. The reference signal contains information about the disturbance and thus correlates with it.

The update equation for the FIR filter coefficients will now be derived. The error $e(n)$ is a function of the filter coefficient vector $\mathbf{w}(n) = [w_0(n), w_1(n), \cdots, w_{L-1}(n)]^T$ and can be visualized as a surface in an L-dimensional space whose coordinates correspond to the filter coefficients. The error signal is expressed as

$$e(n) = d(n) - y(n) = d(n) - \mathbf{w}^T(n)\,\mathbf{x}(n) \tag{1.3}$$

where $\mathbf{w}(n)$ is the filter coefficient vector and $\mathbf{x}(n)$ is the reference signal vector.

The mean-square error can be written as

$$\xi(n) = \mathbf{E}[e^2(n)] = \mathbf{E}[d^2(n)] + 2\,\mathbf{p}^T\,\mathbf{w}(n) + \mathbf{w}^T(n)\,\mathbf{R}\,\mathbf{w}(n) \tag{1.4}$$

where $\mathbf{p} = \mathbf{E}[d(n)\,\mathbf{x}(n)]$ is the cross-correlation vector between the disturbance and the reference signal and $\mathbf{R} = \mathbf{E}[\mathbf{x}(n)\,\mathbf{x}(n)^T]$ is the autocorrelation matrix of the reference signal.

Equation (1.4) requires the computation of the cross-correlation vector and autocorrelation matrix. The computational burden is significant because the optimal filter coefficients have to be calculated constantly. To overcome this problem, the method of steepest descent is employed. The filter coefficients are updated towards the negative gradient at each time step following the rule:

$$\mathbf{w}(n+1) = \mathbf{w}(n) - \frac{\mu}{2}\,\nabla\xi(n) \tag{1.5}$$

where μ is the step-size used for controlling the stability and the rate of convergence.

An instantaneous version of the squared error, $\widehat{\xi}(n) = e^2(n)$, is used to estimate the mean-square error $\xi(n)$. The gradient vector estimate of this squared error surface is given by

$$\begin{aligned}\nabla\widehat{\xi}(n) = \nabla e^2(n) &= \frac{\partial e^2(n)}{\partial \mathbf{w}(n)} = 2\,e(n)\,\frac{\partial e(n)}{\partial \mathbf{w}(n)} \\ &= 2\,e(n)\,\cdot\,[\frac{\partial e(n)}{\partial w_0(n)}, \frac{\partial e(n)}{\partial w_1(n)}, \cdots, \frac{\partial e(n)}{\partial w_{L-1}(n)}]^T \\ &= -2\,e(n)\,\mathbf{x}(n)\end{aligned} \tag{1.6}$$

where the final equality follows from the fact that the (un)desired noise signal $d(n)$ is not a function of the filter coefficient vector $\mathbf{w}(n)$, so $\partial d(n)/\partial \mathbf{w}(n) = \mathbf{0}$.

The direction of the steepest descent of the squared error surface is given by the negative gradient, that is, $-\nabla e^2(n) = 2e(n)\mathbf{x}(n)$. Hence, in order to reduce the squared error, we can substitute the Equation (1.6) into Equation (1.5) and the filter coefficient vector is updated as follows

$$\mathbf{w}(n+1) = \mathbf{w}(n) + \mu\,e(n)\,\mathbf{x}(n) \tag{1.7}$$

which is called the LMS algorithm.

The block diagram of the adaptive filter in Figure 1.5 shows that there is a feedback loop from the error signal back to the adaptive algorithm block. The amount of feedback depends upon the value of the step-size μ. To ensure the convergence of the algorithm, the step size of the LMS algorithm has to be chosen so that

$$0 < \mu < \frac{2}{L_w\,\sigma_x^2} \qquad , \tag{1.8}$$

where σ_x^2 is the variance of the reference signal and L_w is the length of the filter coefficient vector.

1.3.2 Secondary path effects

The use of the adaptive filter for ANC application is complicated by the fact that the summing junction in Figure 1.3 represents the acoustic superposition in space from the canceling loudspeaker to the error microphone, the transfer function between these two elements being called

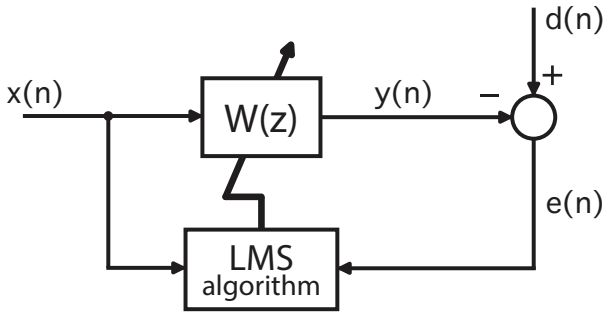

Figure 1.5: LMS algorithm scheme: the reference signal $x(n)$ and the error signal $e(n) = y(n) - d(n)$ are used in the LMS algorithm to update the adaptive filter $W(z)$.

secondary path $S(z)$. This transfer function is from $y(n)$ to $e(n)$ and includes the digital-to-analog (D/A) converter, the reconstruction filter, the power amplifier, the loudspeaker, the acoustic path from loudspeaker to error microphone, the error microphone, the preamplifier, the anti-aliasing filter, and the analog-to-digital (A/D) converter. We can represent the actual LMS system by the block diagram of Figure 1.6.

The Z-transform of the error signal is

$$E(z) = [P(z) - S(z)\,W(z)]X(z) \tag{1.9}$$

where $P(z)$ is the transfer function of the unknown path.

Ideally, after the convergence of the adaptive filter the residual error is zero, and the optimal filter coefficients of $W(z)$ become

$$W^o(z) = \frac{P(z)}{S(z)} \tag{1.10}$$

In other words, the adaptive filter $W(z)$ has to simultaneously model $P(z)$ and inversely model $S(z)$, for this reason the optimal filter can become unstable if in the secondary path the gain of the transfer function goes to zero for some frequency.

For these obvious reasons, the secondary path has to be compensated in some way to achieve successful control. Without compensation the convergence of the adaptation process cannot be ensured. In addition, a sufficiently high-order adaptive FIR filter is required to approximate a rational function $1/S(z)$. Another important issue is that if the delay in the secondary path is greater than that of the primary path, the adaptive filter is non-causal.

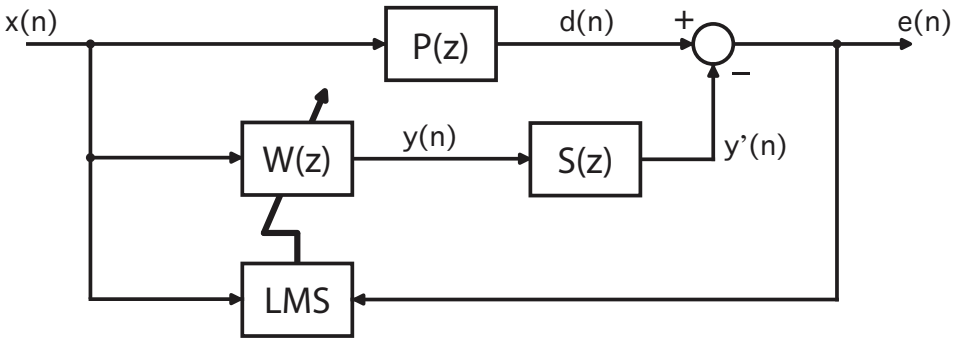

Figure 1.6: Block diagram of an LMS-based ANC system.

1.3.3 The FxLMS algorithm

The FxLMS algorithm accounts for the effect of the secondary path transfer function on the ANC system. The output signal is thus modified by the secondary path transfer function before it reaches the cancellation point at the error sensor. In active noise control, the error signal becomes

$$e(n) = d(n) - y'(n) = d(n) - \mathbf{s}(n) * y(n) = d(n) - \mathbf{s}(n)[\mathbf{w}^T(n)\,\mathbf{x}(n)] \quad (1.11)$$

where $\mathbf{s}(n)$ is the impulse response of the secondary path.

The compensation of $S(z)$ is achieved by placing a filter identical to $S(z)$ in the path of the reference noise signal $x(n)$ to the LMS weight update block. In this way, the filtered reference signal $x'(n)$, differs from the original signal in the same way that $y'(n)$ differs from the output $y(n)$ of the adaptive filter.

The gradient term in the LMS algorithm is then expressed as

$$\nabla\widehat{\xi}(n) = 2\,[\nabla e(n)]\,e(n) \cong -2\,[\mathbf{s}(n) * \mathbf{x}(n)]\,e(n) = -2\,\mathbf{x}'(n)\,e(n) \quad (1.12)$$

Substituting the gradient term into the equation of the steepest descent algorithm yields

$$\mathbf{w}(n+1) = \mathbf{w}(n) + \mu\,\mathbf{x}'(n)\,e(n) \quad (1.13)$$

which is the filtered-reference (or filtered-x) LMS (FxLMS) algorithm. The block diagram of the FxLMS algorithm is given in Figure 1.7. An estimate transfer function $\widehat{S}(z)$ is used rather than $S(z)$ itself, because in practice the secondary path transfer function is rarely known exactly and needs to be estimated.

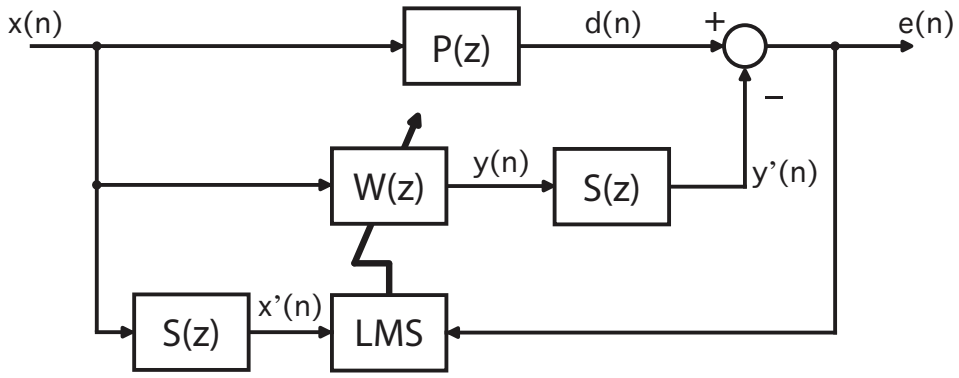

Figure 1.7: Block diagram of the FxLMS algorithm: the ANC system stability is ensured by adding the estimate $\widehat{S}(z)$, it takes into account the distortions introduced by the secondary path $S(z)$.

It has been shown that the maximum step size for the FxLMS algorithm is approximately

$$\mu_{max} = \frac{1}{\sigma_{x'}^2 \left(L_w + \Delta_S\right)} \tag{1.14}$$

where $\sigma_{x'}^2$ is the variance of the filtered reference signal, L_w is the length of the adaptive filter and Δ_S is the number of samples corresponding to the overall delay in the secondary path. The delay in the secondary path is the most significant factor influencing the dynamic response of the feedforward active noise control system. Therefore, the delay should be kept small by decreasing the distance between the secondary source and the error sensor and reducing the delay of the control system components. Since Δ_S is a positive number, the upper bound on the step size in FxLMS is lower than that for the LMS, hence the convergence may be slower.

Feedback compensation

The above FxLMS structure performs well if the reference microphone measures only the reference noise signal $x(n)$. However, depending on the practical setup, the anti-sound loudspeaker also radiates upstream to the reference microphone, resulting in a corrupted reference signal and creating a feedback loop in the system.

The structure in Figure 1.7 can be modified as shown in Figure 1.8 include the feedback from the secondary source to the reference sensor, where $x(n)$ is the reference signal, $x_r(n)$ is the primary noise signal picked up by the reference sensor, and $F(z)$ is the feedback path transfer function

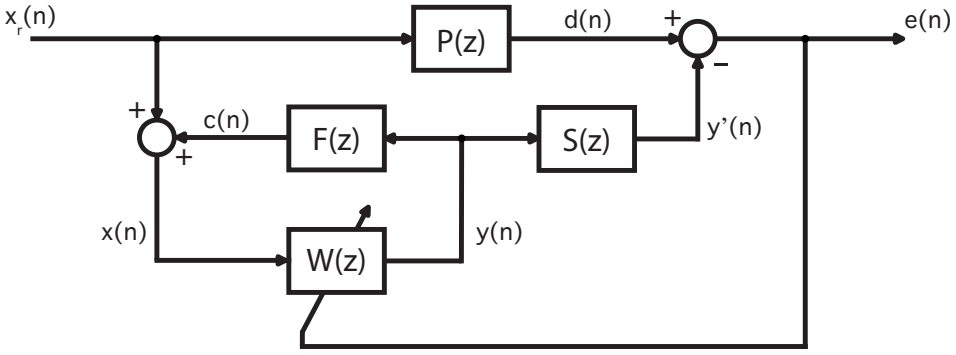

Figure 1.8: Block diagram of ANC system with feedback: $F(z)$ represents the transfer function from the loudspeaker to the reference microphone.

from the output of the adaptive filter to the reference sensor.

Instability due to $F(z)$ can occur if the open-loop phase lag reaches 180^o while the open-loop gain is greater than unity.

To ensure system stability we can use a simple algorithm known as feedback neutralization feedforward ANC approach. This approach uses a separate feedback cancellation filter $\widehat{F}(z)$ between the noise canceling signal $y(n)$ and the reference signal path. The transfer function $\widehat{F}(z)$ is meant to be an approximation of the acoustic feedback path $F(z)$ and, similarly to $\widehat{S}(z)$, it is estimated offline. With this solution the reference signal $x(n)$ can be expressed as

$$x(n) = x_r(n) + c(n) - \sum_{i=1}^{L} \widehat{f}_i \, y(n-i) \tag{1.15}$$

where $\widehat{f}_i$ is the i-th coefficient of $\widehat{F}(z)$ and $c(n)$ is the is the acoustic feedback component.

The structure of the feedback neutralization ANC system is shown in Figure 1.9. This electrical model of the feedback path is driven by the secondary signal, and its output is subtracted from the reference sensor signal. If $\widehat{F}(z)$ well approximates this acoustic path, then the feedback component of the reference microphone signal is canceled electronically subtracting the output of $\widehat{F}(z)$, thus leaving only the primary noise signal at the input to the adaptive filter.

Estimation of the acoustic paths

The system first performs the offline modeling to estimate the secondary path transfer function $S(z)$ from the canceling speaker to the error micro-

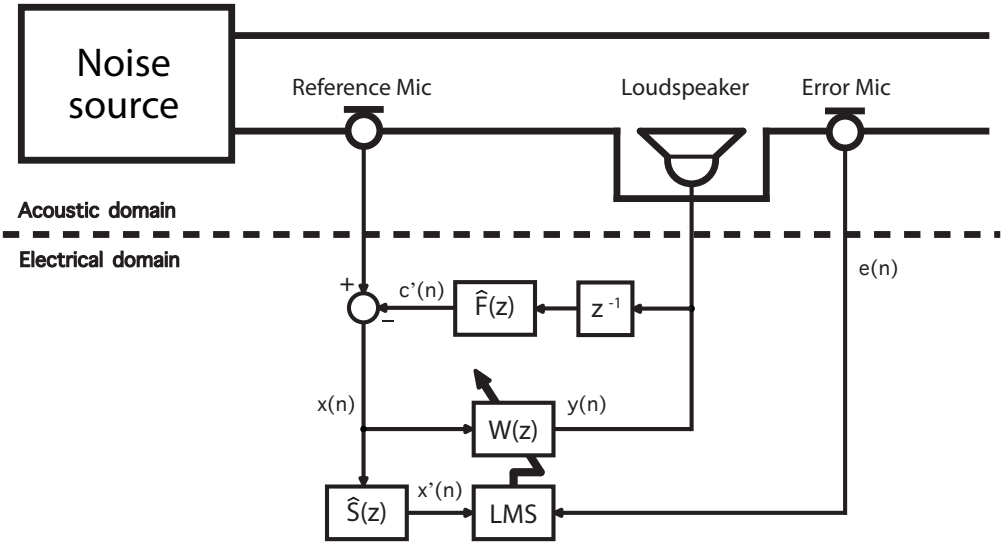

Figure 1.9: ANC system with feedback neutralization: the estimation $\widehat{F}(z)$ is introduced to eliminate the feedback between loudspeaker and reference microphone.

phone and the feedback path transfer function $F(z)$ from the canceling speaker to the input microphone. Assuming that the characteristics of the paths are time-invariant, the models can be obtained from an offline system identification process illustrated in Figure 1.10. During the identification, white noise is fed to the secondary source and the impulse response of the secondary and feedback paths is estimated using the LMS algorithm. Both paths are typically modelled as FIR filters.

The algorithm for the off-line modeling is summarized as follows:

1. Drive the canceling loudspeaker with a white noise signal $y(n)$, sending the same signal to the adaptive filters $\widehat{S}(z)$ and $\widehat{F}(z)$.

2. Compute the following error signals:

$$e_s(n) = x_s(n) - \sum_{i=0}^{N-1} \widehat{s}_i \, y(n-i) \tag{1.16}$$

$$e_f(n) = x_f(n) - \sum_{j=0}^{M-1} \widehat{f}_j \, y(n-j) \tag{1.17}$$

3. Update the coefficients of the adaptive filters $\widehat{S}(z)$ and $\widehat{F}(z)$ using the LMS equations

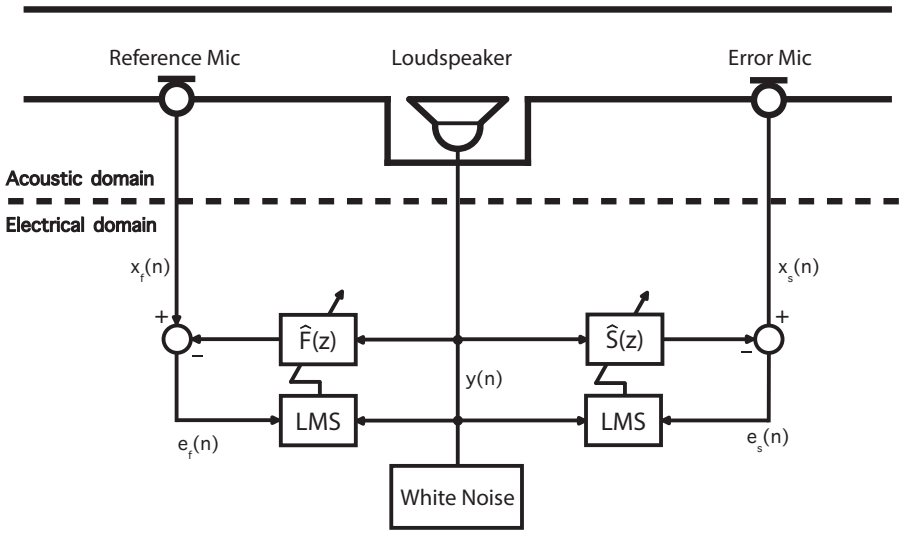

Figure 1.10: Off-line modeling of the secondary and feedback paths.

$$\widehat{s}_i(n+1) = \widehat{s}_i(n) + \mu\, e_s(n)\, y(n-i), \qquad i = 0, 1, \ldots, N-1 \tag{1.18}$$

$$\widehat{f}_j(n+1) = \widehat{f}_j(n) + \mu\, e_f(n)\, y(n-i), \qquad j = 0, 1, \ldots, M-1 \tag{1.19}$$

4. Repeat the process from step 1 until the error signals $e_s(n)$ and $e_f(n)$ are minimized and the models have converged, then save the coefficients of the adaptive filters.

In this procedure the step-size μ must satisfy the following stability condition:

$$0 < \mu < \frac{1}{L\, P_y} \tag{1.20}$$

where P_y is the power of the white noise signal, L is the length of the adaptive filter.

1.4 Narrowband feedforward ANC systems

Narrowband ANC systems are typically applied to machines with rotating mechanisms such as engines. The noise produced by these machines is periodic and contains multiple harmonic-related narrowband components. Moreover, the related noise is depending on the operational conditions.

In these applications, the reference microphone can be replaced by a non-acoustic sensor, such as a tachometer or an accelerometer, to synchronize an internally generated reference signal.

A basic block diagram of a narrowband ANC in a duct is illustrated in Figure 1.4b. This system uses the FxLMS algorithm to control harmonic sources. It consists of an adaptive filter excited by a single sinusoid or a sum of multiple sinusoids internally generated that have the same frequencies as the corresponding harmonic tones to be canceled. This technique prevents the undesired acoustic feedback and allows to use a lower order FIR filter compared to the broadband case because it is only necessary to model the acoustic plant transfer function in the neighbourhood of the harmonic tones. In this section we discuss the two main approaches for feedforward narrowband ANC:

- The first approach is based on the adaptive notch filter (ANF). A sinusoidal reference signal and two adaptive weights are used to cancel the narrowband noise. It allows easy control of bandwidth and has low computational complexity. A parallel version of ANF system is also discussed for the simple reason that in practical applications the noise usually contains multiple tones, at the fundamental and several harmonic frequencies.

- The second approach is the one proposed by Glover [10], where a sum of sinusoids is applied as a reference signal to an adaptive filter with length much higher than two. This technique will automatically create a notch for each sinusoid that will track changes in frequency, thereby providing a simple means for the elimination of a multiple-frequency sinusoidal interference.

1.4.1 Adaptive notch filter

A single frequency adaptive noise canceler has two adaptive weights and two reference inputs, a sine and a cosine wave with the same frequency as the narrowband noise to be canceled. A block diagram of this narrowband ANC system is shown in Figure 1.11.

The output of the system is

$$y(n) = a(n)\, x_a(n) + b(n)\, x_b(n) \tag{1.21}$$

where $a(n)$ and $b(n)$ are the adaptive weights and x_a and x_b are reference inputs,

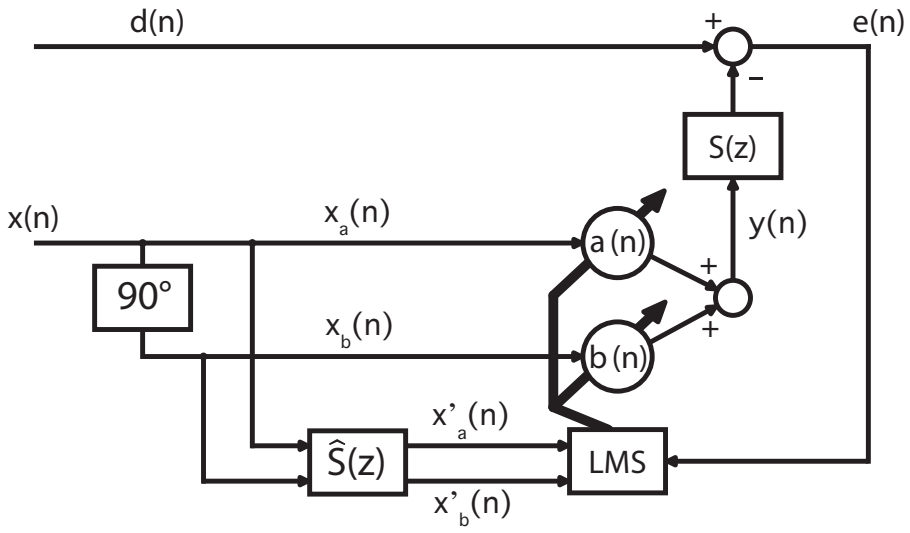

Figure 1.11: Block diagram of the single frequency Adaptive Notch Filter: the sinusoidal input signal $x(n)$ is acquired by a non-acoustic sensor or by a pre-designed lookup table. The filter coefficients $a(n)$ and $b(n)$ have the task of correcting the phase and the amplitude of $x(n)$ through a FxLMS algorithm.

$$x_a(n) = A\,\cos(m\,\omega_0\,n) \tag{1.22}$$

$$x_b(n) = A\,\sin(m\,\omega_0\,n) \tag{1.23}$$

where ω_0 is the fundamental frequency, m is the harmonic index, A is the amplitude of the reference signal, and n is the time index.

The weights are adapted using the FxLMS algorithm

$$a(n+1) = a(n) + \mu\,x'_a(n)\,e(n) \tag{1.24}$$

$$b(n+1) = b(n) + \mu\,x'_b(n)\,e(n) \tag{1.25}$$

where μ is the step size and x'_a and x'_b are the reference signals filtered by the secondary path model.

Based on the fundamental frequency, the reference signals can be provided by a sine wave generator. In the absence of a generator, a simple way to provide input sinusoidal signals is to use a lookup table containing

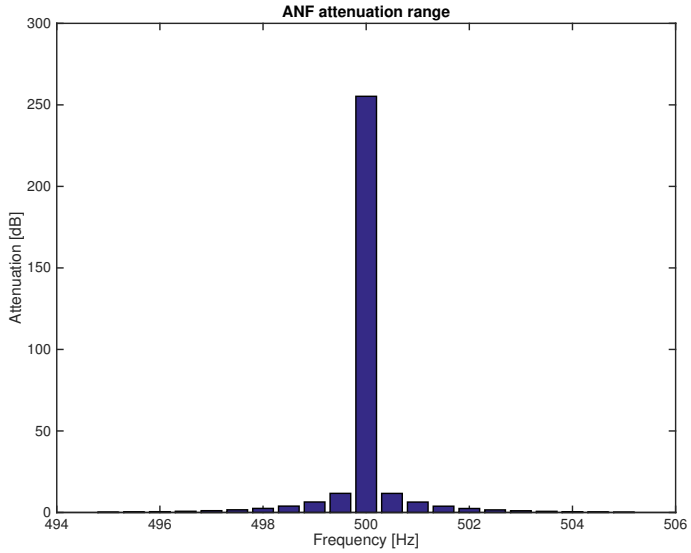

Figure 1.12: Degradation of the noise attenuation performance of an ANF system as a function of the frequency mismatch (nominal frequency= 500Hz).

one cycle of the wave at the desired frequency. Another way to generate the sinusoidal waveforms is to use a recursive oscillator.

The attenuation achieved by an ANF-based ANC system is really frequency-selective: if the system doesn't have a frequency tracking block or a non-acoustic sensor that can provide information on frequency variations, the algorithm can suppress only the frequency component for which it has been designed. An example of this case is presented in Figure 1.12, where the ANF is set to attenuate the 500 Hz component. Even a frequency shift of 0.5 Hz causes a difference in attenuation performance of over 200 dB, and increasing the distance the performances gets worse.

1.4.2 Multiple frequency ANF

In practical ANC systems, the noise usually contains tones at the fundamental frequency and at several harmonic frequencies. This kind of noise can be attenuated by a filter with multiple notches. The realization of multiple notches requires higher-order filters which can be realized by parallel or cascade connection of multiple ANF.

In the parallel form, M two-weight ANFs are connected in parallel to attenuate M sinusoidal components of the primary noise. The block

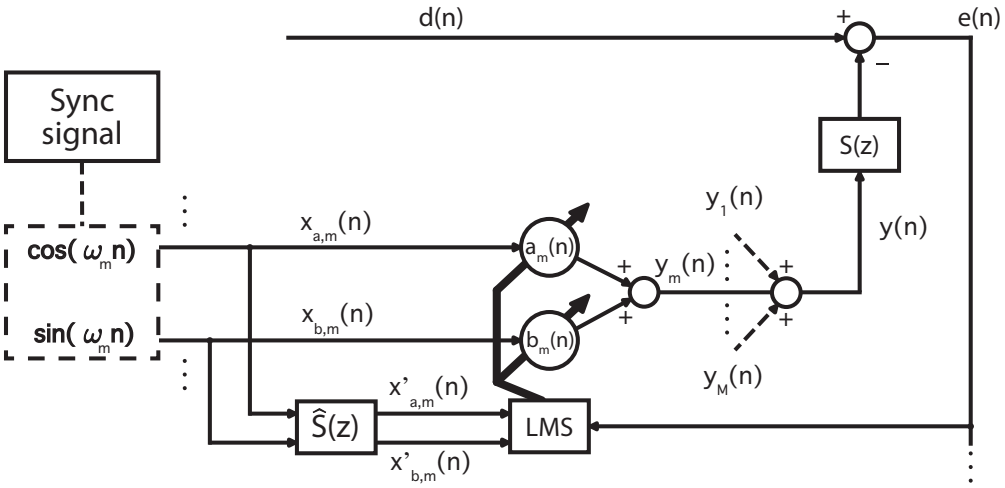

Figure 1.13: Block diagram of the parallel-form Adaptive Notch Filter (m-th channel).

diagram of the parallel ANF system is shown in Figure 1.13. The system consists of M two-tap adaptive filters $W_m(z)$, with $x_{a,m}$ and $x_{b,m}$ being sinusoids at the m-th harmonic frequency of the noise signal. The output of the m-th ANF is expressed as

$$y_m(n) = a_m(n)\, x_{a,m}(n) + b_m(n)\, x_{b,m}(n) \tag{1.26}$$

so that the output of the whole parallel-form ANF is

$$y(n) = \sum_{m=1}^{M} y_m(n) \tag{1.27}$$

Each reference input is filtered by the secondary-path model $\widehat{S}(z)$ which has a length of L_s. This implies intensive computation when both M and L_s are large. The update equation for the adaptive weights is the same as single-channel case

$$a_m(n+1) = a_m(n) + \mu\, x'_{a,m}(n)\, e(n) \tag{1.28}$$

$$b_m(n+1) = b_m(n) + \mu\, x'_{b,m}(n)\, e(n) \tag{1.29}$$

where $m = 1, \ldots, M$ is the channel index and $x'_{a,m}$ and $x'_{b,m}$ are the filtered reference signals.

A new narrowband ANC system structure has been proposed in [11] in order to reduce the computational cost of the system. Instead of filtering each component $x_{a,m}$ and $x_{b,m}$ with the estimate $\widehat{S}(z)$, the reference (cosine or sine) waves are combined, respectively, to form an input to an x-filtering block. The output of each x-filtering block is decomposed into filtered-x cosine or sine waves by a bandpass filter bank derived from notch filters. This method requires only two reference signal filtering blocks regardless of the number of targeted frequencies and performs equivalently to its counterpart, while requiring considerably fewer multiplications. The block diagram of this system is shown in Figure 1.14 where

$$BP_m(z) = \frac{(\rho - 1)c_m z^{-1} + (\rho^2 - 1)z^{-2}}{1 + \rho c_m z^{-1} + \rho^2 z^{-2}}, \tag{1.30}$$

where $c_m = -2\cos(\omega_m)$, and ρ is a pole attraction factor (or pole radius) defined in $[0, 1]$. The right choice of ρ is crucial, and depends on the spacing of the signal frequencies considered. If they are closely spaced, a ρ very close to 1 is selected to allow the bandpass filters to produce clean reference waves for the FxLMS. However, this may bring some delay to the system dynamics, because a bandpass filter with larger ρ has a larger time constant. In [11, 12] a modification to the proposed scheme is also proposed, to address the frequency mismatch (FM) issue.

1.4.3 Narrowband input applied to a broadband ANC

The application of a narrowband reference signal to a broadband ANC system, is an interesting case of study. The reference input $x(n)$ is a sum of M sinusoids expressed as

$$\begin{aligned} x(n) &= \sum_{m=1}^{M} A_m \cos(\omega_m n) \\ &= \sum_{m=1}^{M} A_m \cos\{[\omega + (m-1)\Delta\omega]n\} \end{aligned} \tag{1.31}$$

where $\Delta\omega$ is the frequency separation, A_m is amplitude of the m-th sinusoid at frequency $[\omega + (m-1)\,\Delta\omega]$, ω being the fundamental frequency.

When a sum of M sinusoids is applied to an adaptive filter $W(z)$, a notch will be formed over each sinusoid and tracks it if it changes in frequency. The filter length L_w is at least twice the total number of sinusoids so that $L_w \geq 2M$, because each frequency needs at least two real

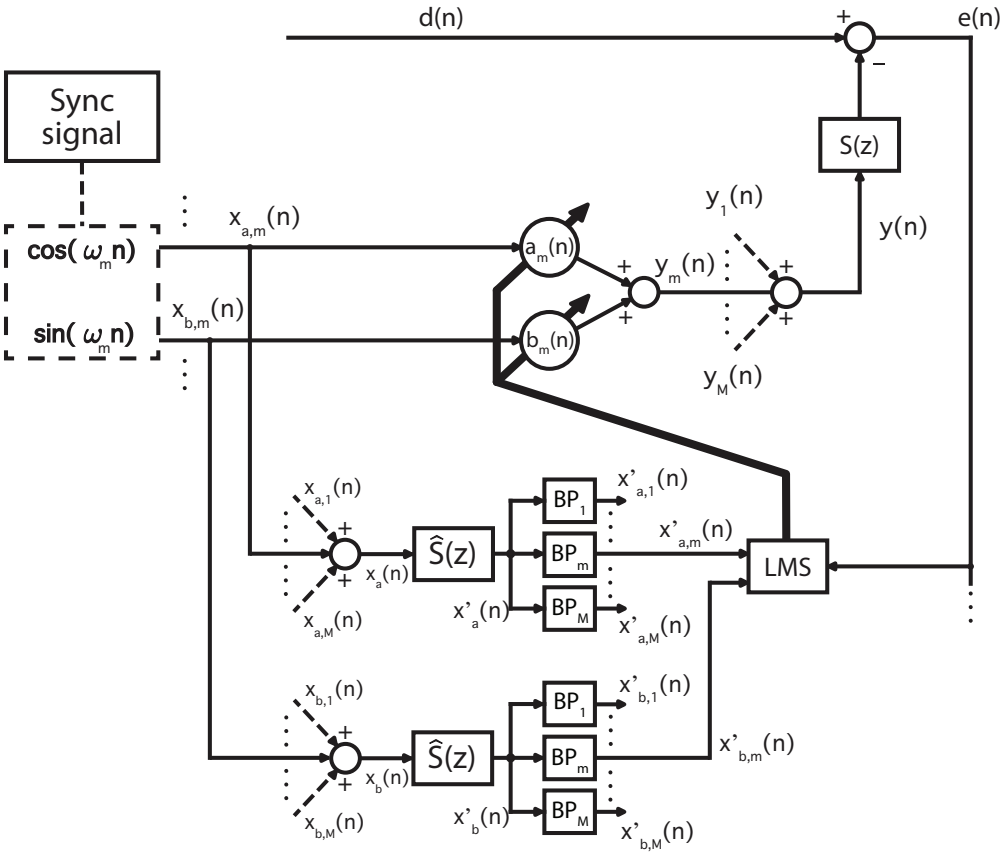

Figure 1.14: Efficient parallel narrowband ANC system (m-th channel): a summing node is added to convey the signals of all channels to a single update signal. After the filtering with the estimate $\widehat{S}(z)$, the band-pass filters $BP_m(z)$ decomposes again the signal in its main components.

weights to deal with the in-phase and the quadrature components. The length of the adaptive FIR filter is an important factor, a small filter length L_w is preferred to keep the computational burden small, but the canceling performance will be affected, limiting the maximum attenuation achievable. A larger filter length allows to achieve the maximum noise attenuation but results in slower convergence and higher excess error. Notice that the Equation (1.14) limits the maximum value of the stepsize μ allowed by the algorithm, and hence the convergence rate. Bigger L_w means smaller μ and vice versa. There is no rule for the choice of L_w, and a trade off between convergence rate and attenuation performance is needed. In general, the minimum order of the adaptive filter depends on the component with the smallest frequency in the reference signal. If F_s is the sample frequency and f_{min} is the frequency of the narrowband component at lowest frequency, a good choice for the filter length is $L_w = 2(F_s/f_{min})$. With real and more complex signals we could need a bigger L_w, for example when $\Delta\omega$ is small the frequencies of the sinusoids are close together and a higher-order adaptive filter is required to give good resolution between adjacent frequencies [13, 14].

Chapter 2

Theoretical background

One difficulty in implementing the FxLMS algorithm is that the secondary path $S(z)$ is unknown and an estimate $\widehat{S}(z)$ must be used. The inclusion of $\widehat{S}(z)$ is necessary for system stability, but it could degrade the performance by slowing the algorithm convergence. The possible issues deriving from the inclusion of $\widehat{S}(z)$ are

- frequency dependent magnitude of $\widehat{S}(z)$
- frequency dependent phase delay of $\widehat{S}(z)$
- errors in the transfer function estimation

In this chapter we analyze these problems and propose possible solutions. Simulations will be carried out using a 180-tap secondary path (see Figure 2.1a) and a reference input signal taken from [15], measured directly from the DVB-T cooling fans. An FFT of the reference signal is presented in Figure 2.1b (the analysis of this signal will be considered in Chapter 3). This signal is quasi-periodic and it has fundamental frequency $f_0 = 1136$Hz, it also has harmonic components and a white noise component allover the frequency range.

2.1 Convergence analysis

One of the limitations of the FxLMS algorithm is that its convergence exhibits a frequency dependent behavior. This can lead to a significant degradation in the overall performance of the system if the noise is time-varying. The frequency dependent behavior can be better understood by looking at the eigenvalues of the autocorrelation matrix $\mathbf{R}$ of the

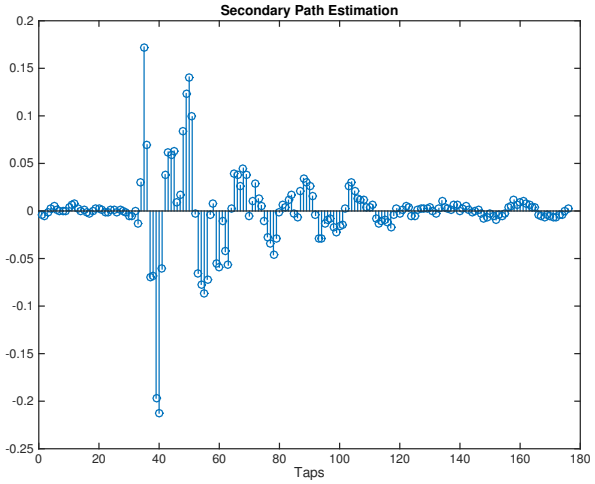

(a)

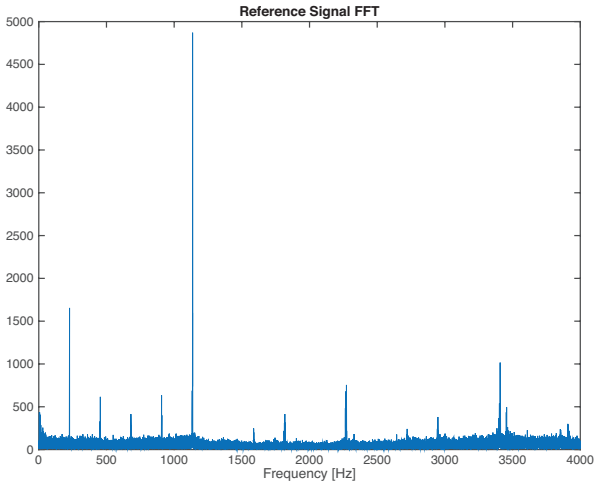

(b)

Figure 2.1: Examples of the filter and reference signal used in this Chapter.
(a): an example of a 180-Tap secondary path
(b): FFT of the DVB-T cooling fans noise in the frequency range of interest ($0 \div 4000$ Hz).

filtered-x signal, which is a function of $\widehat{S}(z)$ and $x(n)$. The eigenvalues of $\mathbf{R}$ are related to the dynamics, or time constants, of the modes of the system. Typically, a large spread is observed in the eigenvalues of this matrix, which corresponds to fast and slow modes of convergence.

The steepest descent method used for the LMS algorithm is based on the Newton's method, a basic iterative method for finding the minimum of the error cost function. The Newton's method is applied using the inverse of the hessian matrix at each iteration. The hessian matrix is equal to the autocorrelation matrix $\mathbf{R}$, thus the computation of $\mathbf{R}^{-1}$ is required at each iteration. The steepest descent method essentially approximates the hessian in the update equation with a constant step-size μ. This method follows strictly the negative gradient direction. It is generally slower than Newton's method but requires less computational effort. Studying the stability constraint of the LMS algorithm it is possible to establish a connection between the value of the step-size μ and the eigenvalues λ_i of the autocorrelation matrix $\mathbf{R}$. In particular, the convergence of the adaptive filter $W(z)$ to its optimal value requires that

$$|\,1-\mu\lambda_i\,| \,<\, 1\,, \qquad i=\,0,1,\ldots,L-1\,, \tag{2.1}$$

where L is the length of the adaptive filter. Therefore, the following constraint can be posed on μ:

$$0 \,<\, \mu \,<\, \frac{2}{\lambda_i}\,, \qquad i=\,0,1,\ldots,L-1\,. \tag{2.2}$$

Some considerations about the relationship between the eigenvalues and the step-size can be made:

- The slowest modes (corresponding to the smallest eigenvalues) dominate the overall convergence of the algorithm to the optimum, and are therefore related to the performance. In particular:
  - A small μ reduces the misadjustment error [1], but slows down the convergence of the error signal.
  - For stationary input and sufficiently small μ, the convergence time τ_{mse} is dependent on the eigenvalue spread ρ of the input autocorrelation matrix as $\mathbf{R}$

$$\tau_{mse} \leq \frac{\lambda_{max}}{\lambda_{min}}\, T_s = \rho\, T_s \qquad (sec) \tag{2.3}$$

[1] The misadjustment error is the increase in mean square error due to the LMS wandering near the optimum $W^o(z)$.

where T_s is the sampling period.

- The fastest modes (corresponding to the largest eigenvalues) have the fastest convergence and the greatest reduction potential but also determine a bound on the step size μ, associated to the stability requirement. In particular:

  - A larger μ is especially desirable for non-stationary noise as is leads to faster convergence and increased attenuation. In addition, when the real-time tracking is crucial a large μ is preferred, e.g. when the noise tone shifts in frequency faster.
  - A large μ increases the misadjustment error.

Generally μ is set as a compromise between fast convergence and acceptable misadjustment error.

The autocorrelation matrix of $\mathbf{x}'(n)$ is defined as

$$\mathbf{R} = \mathbf{E}[\mathbf{x}'(n)\,\mathbf{x}'(n)^T] \tag{2.4}$$

where $\mathbf{E}[\bullet]$ denotes the expected value of the operand.

Since the autocorrelation matrix is positive semidefinite, the eigenvalues are all real and non-negative, though some of them may be zero. The rank of the autocorrelation matrix gives the number of nonzero eigenvalues, that is twice the number of tones in the reference signal.

In general, it has been shown that the algorithm will converge and remain stable as long as the chosen μ satisfies the following equation:

$$0 < \mu < \frac{2}{\lambda_{max}} \tag{2.5}$$

where λ_{max} is the maximum eigenvalue of $\mathbf{R}$.

The selection of the step size is thus based on the maximum eigenvalue in the frequency range of interest, and when the algorithm is controlling a tone in a different frequency range convergence will be slower.

In practice, it is computationally demanding to obtain a real-time estimate of the autocorrelation matrix, so the optimal μ is often selected through experimentation. Several adaptive steps size $\mu(n)$ have been proposed in many studies (see [16, 17])

2.2 Estimation errors

The delay in the secondary path influences the dynamic response of the ANC system by reducing the maximum step size in the FxLMS algorithm.

Boucher in [18] discusses the effects of $\widehat{S}(z)$ phase errors on the optimum step size and on the convergence time.

Let

$$\beta = \mu\, A\, A_s \qquad , \tag{2.6}$$

where A and A_s are respectively, the magnitudes of the reference signal and the magnitudes of $\widehat{S}(z)$, at the frequency of interest. The transfer funcion $\widehat{S}(z)$ has complex conjugate poles at distance d from the origin, where

$$d = \sqrt{1 - \beta\, \cos(\Delta\varphi)} \qquad . \tag{2.7}$$

In this equation $\Delta\varphi$ is the phase difference between the actual secondary path transfer function $S(z)$ and the secondary path estimate $\widehat{S}(z)$. In the limit of slow adaption, β is assumed to be a small positive number, so the distance from the poles to the origin will be greater than 1 only if $\cos(\Delta\varphi)$ is negative.

This puts a stability limit for phase errors

$$\cos(\Delta\varphi) > 0 \qquad \Rightarrow \qquad -90^o < \Delta\varphi < +90^o \tag{2.8}$$

and the convergence time constant is slowed down by a factor of $1/\cos(\Delta\varphi)$.

This result suggests that convergence will slow as the phase difference approaches $\pm 90^o$ because the poles come closer to the unit circle. Conversely, errors less than $\pm 45^o$ hardly affect the performance of the algorithm.

The gain applied to the reference signal by filtering it with $\widehat{S}(z)$ does not affect the stability of the algorithm and is usually compensated for by modifying the step size μ

Magnitude estimation errors in the secondary path model can be compensated for by the choice of the step size μ, proportionally to the gain applied to the reference signal when filtered with $\widehat{S}(z)$ itself.

Overall, the FxLMS algorithm appears to be very tolerant of errors in the estimation of $\widehat{S}(z)$, so the response of the model does not have to exactly match that of the secondary path and it is often sufficient to use a relatively low-order filter.

2.3 Phase delay compensation

In the simplest case, the secondary path transfer function $S(z)$ can be modeled as a pure delay Δ, i.e. $\widehat{S}(z)$ is replaced by a delay block $z^{-\Delta}$.

The time delay can be estimated by an off-line modeling technique and then built into the controller. In general, the value of the delay is a function of the frequency.

The upper bound for the step size depends on the delay Δ and is in close agreement with Elliott's approximation given in (1.14). For this reason the delay should be keep small, decreasing the distance between the error sensor and the secondary source and/or reducing the delay in electrical components.

These frequency-dependent delays can be determined by taking the discrete Fourier transform of $\widehat{S}(z)$ and then calculating the delays from the phase values using the following expression:

$$\tau(\omega) = -\frac{\varphi(\omega)}{\omega} \quad , \tag{2.9}$$

where $\tau(\omega)$ is the time delay in seconds at frequency ω and $\varphi(\omega)$ is the phase of $\widehat{S}(z)$ in radians. The value of Δ at angular frequency ω_0 is then determined by

$$\Delta = \frac{\tau(\omega_0)}{T} \quad , \tag{2.10}$$

where T is the sampling period.

The introduction of a pure delay block implies that all frequency components, into the range of interest or not, are filtered in the same way. As a consequence, if the reference signal changes in frequency and/or it has components which require different values of the delay Δ, system instability can occur. Assuming that the secondary path has no large phase variations near the frequency of interest, and taking into account the theory presented in the last section, we can say that in this bandwidth the phase doesn't change in such a way to drive the system unstable. For this reason the application of a delay compensation is typically used with narrowband schemes, where the reference signal is usually self generated. An example of this application is the ANF scheme showed in Figure 2.2.

2.4 Eigenvalue equalization

It has been shown in [19] that the FxLMS algorithm reaches maximum efficiency when all the eigenvalues of matrix $\mathbf{R}$ are equal. If the variance

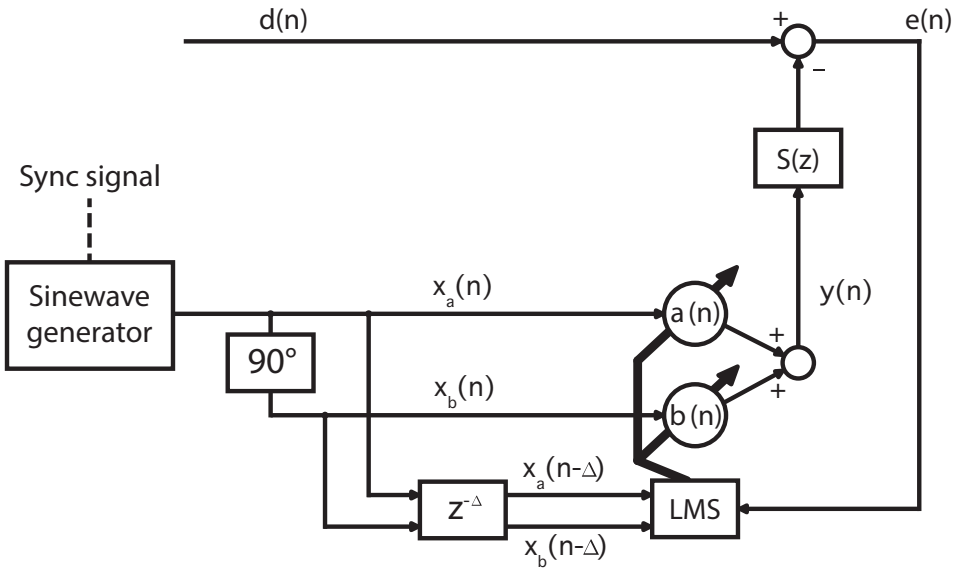

Figure 2.2: Example for delay compensation in a Narrowband ANF scheme.

in the eigenvalues of the autocorrelation matrix $\mathbf{R}$ is minimized (i.e. if the eigenvalue spread ρ approaches unity), a single step size μ could be used and it would be nearly optimal for the whole frequency range.

The autocorrelation matrix is directly dependent on the filtered-x signal. Thus, any attempt at equalizing the eigenvalues must be done by altering either $x(n)$ or $\widehat{S}(z)$, but in many practical applications the control over $x(n)$ is either difficult or undesirable, so we focus here on making changes to $\widehat{S}(z)$ only. The resulting algorithm is called the Eigenvalue Equalization FxLMS (EE-FxLMS) algorithm.

The eigenvalues of $\mathbf{R}$ and the magnitude of $\widehat{S}(z)$ are related so that the maximum eigenvalue occurs where the response of $\widehat{S}(z)$ is large. Manipulating the magnitude coefficients of $\widehat{S}(z)$, we are modifying the eigenvalue spread. Indeed, if the magnitude coefficients were flat over frequency, the eigenvalue spread should also be flat. So the goal of this algorithm is to replace the estimate of secondary path with a new FIR filter $\widehat{S}_{EE}(z)$ with different magnitude information and same phase response.

The eigenvalues equalization of $\widehat{S}(z)$ can be derived offline (no computational burden is added) in two different ways, depending on the characteristics of the reference signal $x(n)$:

- *The frequencies of interest in $x(n)$ are equally weighted*

  $\widehat{S}_{EE}(z)$ is implemented to also have an equal (flat) weighting over

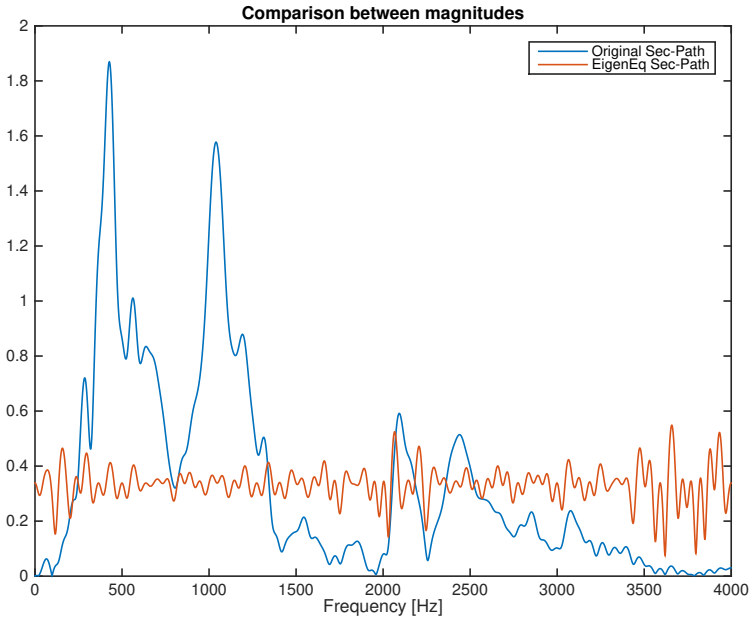

Figure 2.3: Magnitude comparison: original $\widehat{S}(z)$ (blue) and after the Eigenvalues Equalization (orange).

frequency. The process can be summarized as follows:

- Obtain the time domain impulse response $\widehat{\mathbf{s}}(n)$ through the offline system identification process as explained in Chapter 1.
- Take the fast Fourier transform (FFT) to obtain $\widehat{S}(j\omega)$.
- Divide each value in the FFT by its magnitude and then multiply by the mean value of the FFT

$$\widehat{S}_{EE}(j\omega) = \frac{\widehat{S}(j\omega)}{|\widehat{S}(j\omega)|}\, mean(|\widehat{S}(j\omega)|) \tag{2.11}$$

  .
- Compute the inverse FFT to obtain the $\widehat{\mathbf{s}}_{\mathbf{EE}}(n)$.

The changes in magnitude, phase and coefficient amplitudes are illustrated in Figures 2.3, 2.4 and 2.5. The magnitude is essentially flat compared to the original version. The two phases are almost identical, except for small variations that do not affect the correct operation of the FxLMS algorithm.

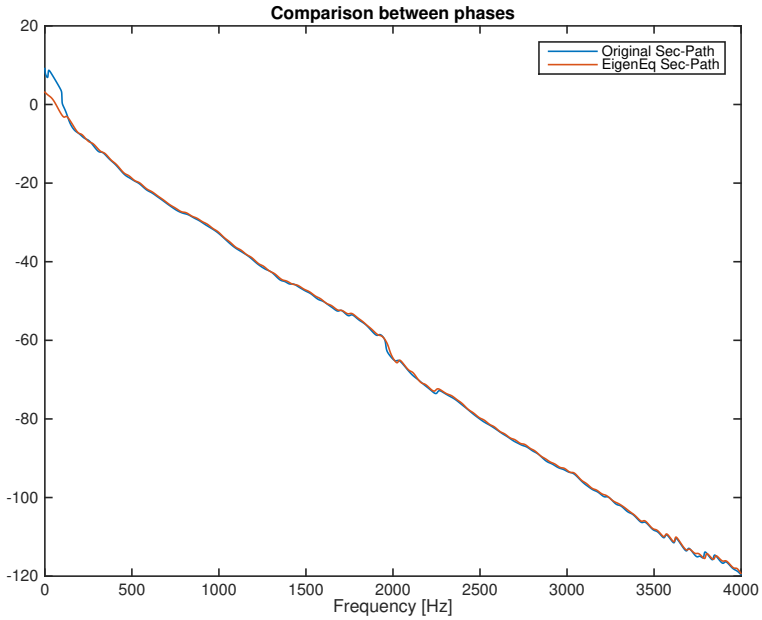

Figure 2.4: Phase comparison: original secondary path (blue) and after the Eigenvalues Equalization (orange).

- *The frequencies of interest in $x(n)$ are unequally weighted*

  In this case the magnitude coefficients of $\widehat{S}_{EE}(z)$ at each frequency bin must compensate for the unequal weighting of each tone in $x(n)$ so that the eigenvalue spread becomes essentially flat over frequency. The process can be summarized as follows:

  - Obtain the time domain impulse response $\widehat{\mathbf{s}}(n)$ through the offline system identification process as explained in Chapter 1.
  - Take the Fast Fourier Transform (FFT) to obtain $\widehat{S}(j\omega)$ and separate it into the magnitude and phase components.
  - Compute the FFT $X(j\omega)$ of the reference signal $x(n)$.
  - Find the magnitude coefficients of $X(j\omega)$ at the frequencies of interest.
  - Create a vector of magnitude coefficients that is equal to $1/|X(j\omega)|$.
  - The new magnitude coefficients are combined with the original phase response to create a new single vector of complex coefficients.

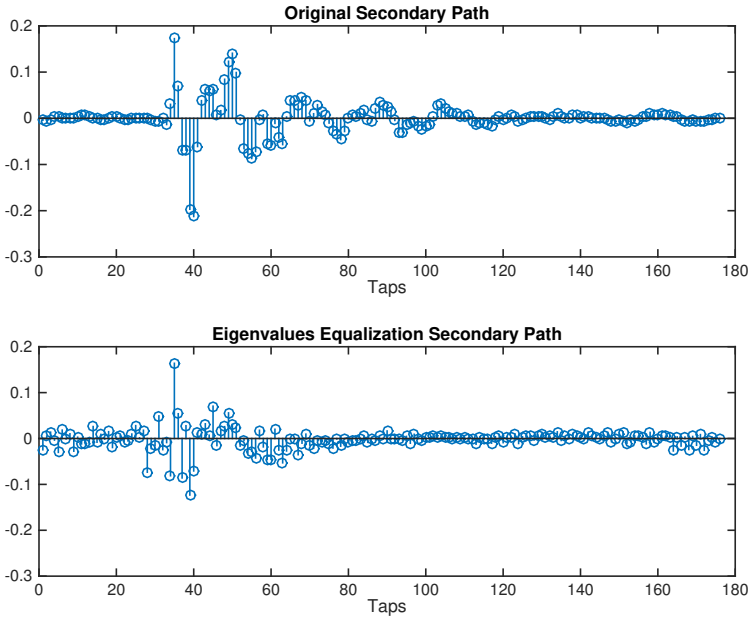

Figure 2.5: Filter coefficient comparison between the original $\widehat{S}(z)$ taps and the Eigenvalues Equalization version.

– Compute the inverse FFT to obtain the $\widehat{\mathbf{s}}_{\mathbf{EE}}(n)$.

The changes in the magnitude of the frequency response function and the coefficients of the impulse response can be seen in Figures 2.6, 2.7. The phase is the same already showed in Figure 2.4.

These changes imply that the $\widehat{S}(z)$ used to provide the filtered-x signal is no longer a good estimate of the true secondary path. The errors introduced in the magnitude of the secondary path estimate only affect the eigenvalues and hence the rates of convergence of the algorithm, but do not affect stability.

The new $\widehat{S}_{EE}(z)$ can then be used in the FxLMS algorithm for filtering the reference signal.

A comparison between the EE-FxLMS method and the standard FxLMS control is taken into account for a problem with 33 tones (each separated from the other by 25 Hz in the frequency range of [200÷1000] Hz). For each method convergence times are calculated relatively to the interested frequency, and simulations have been carried out using the largest stepsize μ possible by the stability constraint. The performances of the EE-FxLMS

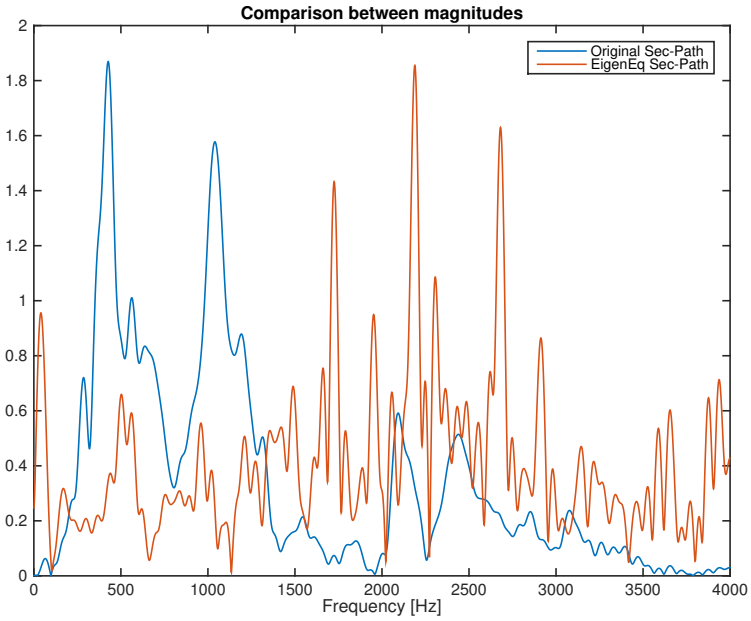

Figure 2.6: Magnitude comparison: original $\widehat{S}(j\omega)$ (blue) and after the Eigenvalues Equalization (orange). The EE-version is based only on the inverse magnitude of the reference signal. Thus, the minimum value of $|\widehat{S}_{EE}(j\omega)|$ is at the fundamental frequency $f_0 = 1136$Hz.

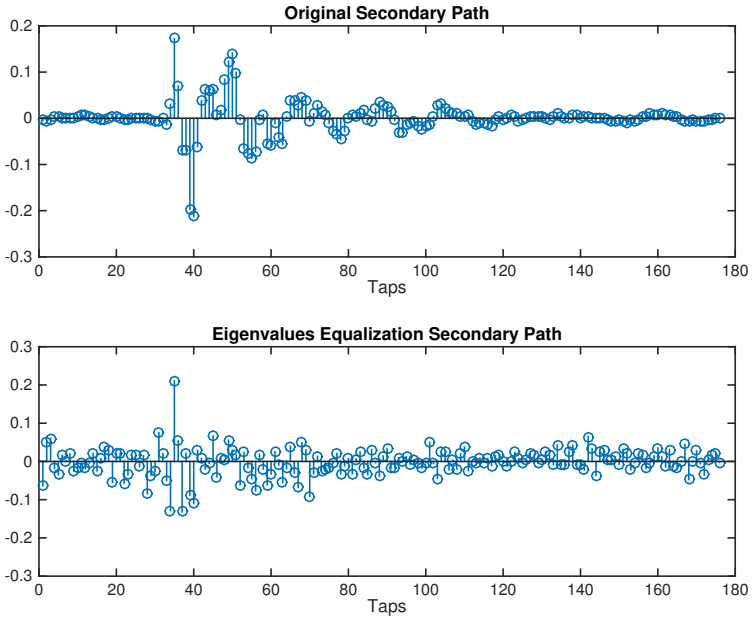

Figure 2.7: Filter coefficient comparison between the original $\widehat{S}(z)$ taps and the Eigenvalues Equalization version based on the reference signal.

are illustrated in Figure 2.8. It is easy to see that the EE-FxLMS works better than the plain FxLMS.

These results confirm what was said until now, i.e. that a single step size μ could be used and it would be nearly optimal for the whole frequency range.

In the literature there are other modified FxLMS-type algorithms that have been developed to overcome the issues caused by the secondary path. Most of them employ another filter $H(z)$ in cascade to the estimate $\widehat{S}(z)$ or filter the error signal (FeLMS, Filtered-error LMS). One example of such methods is the FxFeLMS algorithm (Filtered-x/Filtered-e LMS) proposed by Sujbert [20] to overcome the drawbacks of the standard FxLMS algorithm. Sujbert showed that in order to overcome the above-mentioned disadvantages due to the dynamics of the magnitude response of the secondary path, a filter $H(z)$ can be inserted into both the reference signal path and the error signal path. Then, the magnitude response of the cascade of $\widehat{S}(z)$ and $H(z)$ becomes flat. The analysis and the simulation results carried out in [20, 21, 22] demonstrated the effectiveness of the proposed algorithm and its improvement in terms of convergence speed compared to FxLMS algorithm. These methods however may significantly

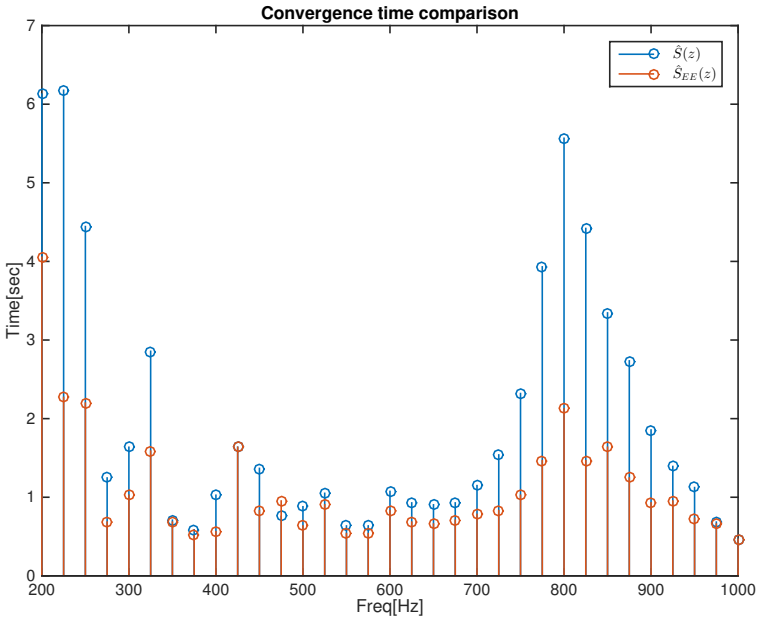

Figure 2.8: Comparison between convergence times using the original $\widehat{S}(z)$ (blue) and the Eigenvalues Equalization version (orange). Results refer to a noise with 33 tones, each separated from the others by 25 Hz in the frequency range of [200÷1000] Hz.

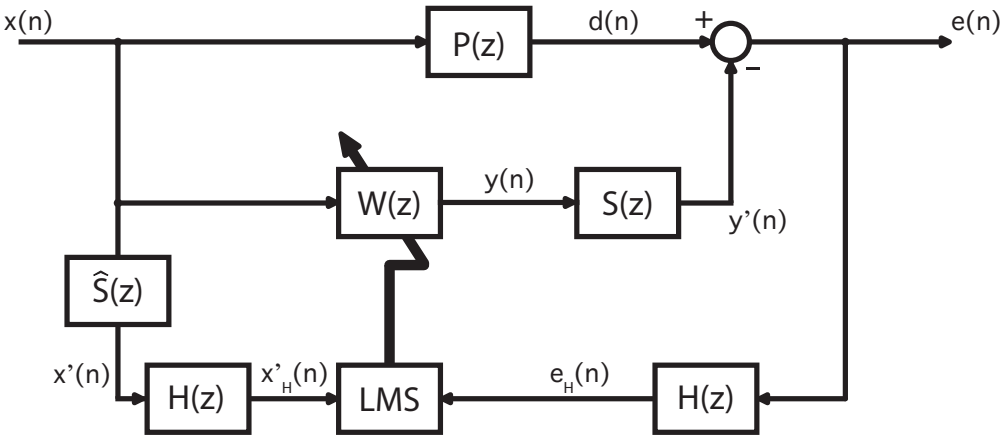

Figure 2.9: Block diagram of an ANC system with the FxFeLMS algorithm.

increase the computational cost compared to the EE-FxLMS, because other filtering blocks are required. The FxFeLMS block diagram is presented in Figure 2.9.

2.5 Leaky FxLMS

The estimation errors of $\widehat{S}(z)$ increase when the order of the FIR filter used for the estimation is small. In this case the phase response is difficult to model and large phase errors occur around the resonances of the secondary path. High noise levels associated with low frequency resonances may cause nonlinear distortion by overloading the secondary source, especially when the frequency of this primary noise changes. Large phase errors affect the operation of the FxLMS algorithm, deteriorating the performance.

In order to increase the robustness of the FxLMS algorithm, a leakage factor can be introduced to limit the output of the adaptive filter. The leakage has the effect of modifying the correlation matrix $\mathbf{R}$. All eigenvalues are positive even if some of the original input eigenvalues are zero. This guarantees a unique solution and a bounded time constant for all modes. The price of leakage is an increased complexity of the weight update equation and the introduction of a bias into the solution.

The update equation of the leaky FxLMS algorithm can be expressed as:

$$\mathbf{w}(n+1) = \nu\,\mathbf{w}(n) + \mu\,\mathbf{x}'(n)\,e(n) \tag{2.12}$$

where ν is the leakage factor with $0 \ll \nu \leq 1$. It should be kept larger than $1 - \mu$ in order to maintain an acceptable level of performance.

The leaky FxLMS algorithm can also reduce the numerical error in the finite precision implementation and limit the output power of the loudspeaker to avoid nonlinear distortion [23]. However, the usage of the leakage factor may decrease the preformance of the algorithm in other situations, and an adaptive leakage factor is preferred to avoid this problem, using leakage when large phase shifts occur and no leakage when phase shifts are small. An adaptive leakage algorithm is discussed in [24] but will not be considered in this work because of the increased complexity of the overall ANC system. A simple constant-leakage algorithm is instead used if needed.

Chapter 3

Signal analysis

In this chapter we analyze the signal emitted by the DBV-T device. A time and frequency analysis of the acquired signals will be carried out.

3.1 Signal analysis

Fans perform a necessary cooling function for many machines but create noise as a negative byproduct. This noise depends on the number of fan blades and the rotation speed of the fans. In particular, we denote as Blade Passage Frequency (BPF) the main frequency produced by a single fan. This frequency will be the fundamental frequency of the emitted noise. Additionally, at multiples of the BPF, there are tonal noise peaks in the spectrum, the harmonics of the BPF. The tonal noise is representative of the "hum" that is associated with a fan in operation. In addition to the tonal noise content, the spectrum also shows broadband noise, which is associated with the "whoosh" sound of the fan.

Various passive noise control methods have been implemented, which mainly consist of changing the geometry of the fan housing and blades. In our project it is not allowed to modify the structure of the DBV-T device. Therefore, we have to use an ANC solution which is structurally not invasive. Figure 3.1 illustrates the fans under analysis. They have a diameter of 8 cm and their centers are 10 cm distant. The fan grid was removed only to show the fans position and to emphasize that the access to this area is very difficult. Thus, even if alterations were possible, they would be very difficult to realize.

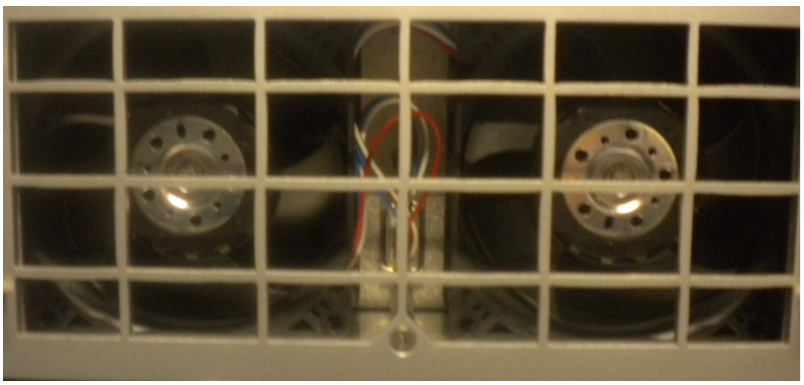

Figure 3.1: Details of the refrigerant fans in the DBV-T device without the protective grid.

3.2 Spectral analysis and beat frequency

Often times, when a single cooling fan is not adequate to cool a device, multiple cooling fans are used, as in our case. These fan arrays are often built with identical model fans. However, even if the fans are supposed to rotate at the same speed in phase accordance, this does not happen in practice, because differences in manufacturing cause a slight difference in the BPF of each fan, even when the same voltage is applied to the fans. The difference creates a beat frequency that can be annoying. This results from the superposition of two closely spaced waves that interfere with each other to create low and high amplitude oscillations in the time signature. The time series of two sinusoids closely spaced in frequency which are added together is shown in Figure 3.2 to illustrate the beating phenomenon.

The two fans under analysis are assumed as a single source and not as a two source array, this choice being mainly dictated by hardware limitations for the ANC implementation. Accordingly, only one reference microphone is employed. The signal under analysis is the sum of the two individual fan signals, acquired in the middle. The measurements here presented were acquired in a semi-anechoic room at the Sound and Music Computing Laboratory (SMC Lab) of Politecnico di Milano - Polo Territoriale di Como (details on the acquisition phase are described in [15]).

Figure 3.3 presents a filtered version of the signal emitted by the DBV-T's fans. A band-pass filtering was applied near the fundamental frequency f_0, in the range of $[f_0 - 30, f_0 + 30]$ Hz, where f_0 is approximately 1136 Hz. It is easy to see that a beating phenomenon exists. The beat frequency and its resulting changes in amplitude can be appreciated in Figure 3.4. Two

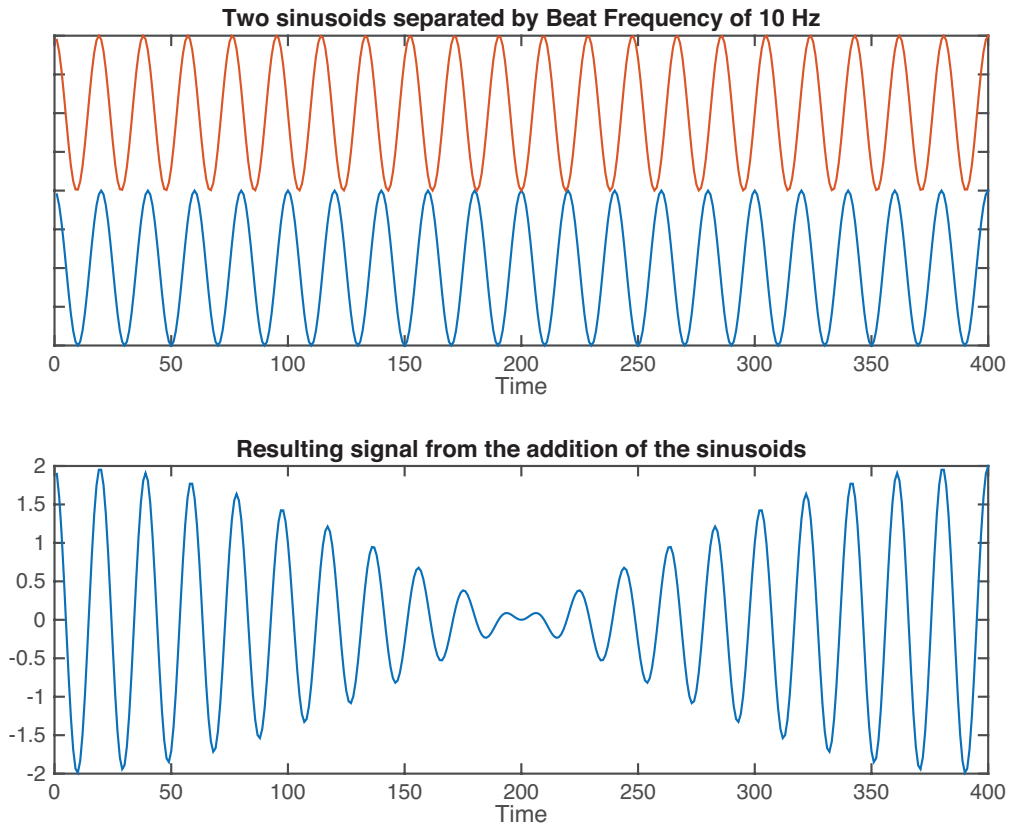

Figure 3.2: Graphic representation of the beat phenomenon: the upper subplot shows two sinusoids of equal amplitude but with slightly different frequency, (the blue sinusoid has frequency $f_b = 200$Hz, the orange sinusoid has a frequency $f_o = 210$Hz). The bottom subplot shows the sum of these two sinusoids.

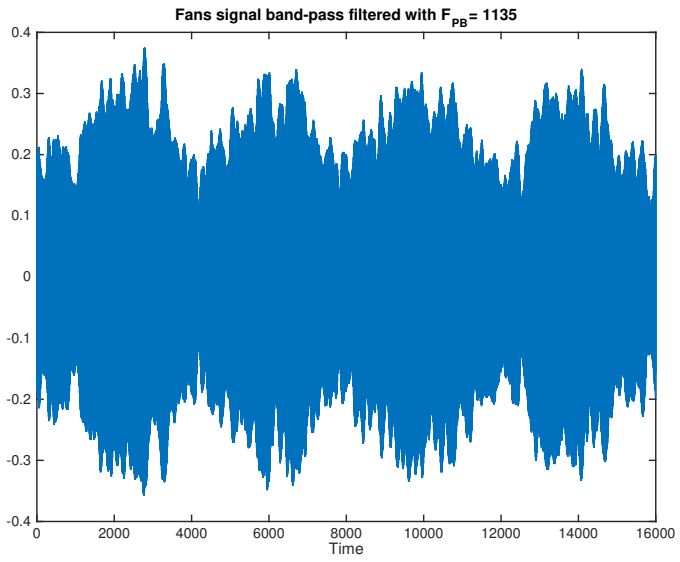

Figure 3.3: Temporal behavior of the reference signal around the fundamental frequency $F_0 = 1136$Hz.

tonal components are apparent in the spectrogram, that can be associated to the two fans. The two frequencies vary vary over time and are separated approximately by 5Hz. The one on the left ($f_l \sim 1134$ Hz) has lower magnitude than the one on the right ($f_r \sim 1137$ Hz).

Figure 3.5 shows the overall spectrum of the signal. The main component is at the fundamental frequency of 1136 Hz, while the rest of the power is mainly distributed between the first harmonic (2270 Hz), the second harmonic (3408 Hz) and the four sub-harmonics (227, 454, 681 and 908 Hz). The value on the y-axis changes depending on the distance between the microphone and the source, but the relation between the harmonics is always the same. The presence of a little quantity of background noise is due to the air produced by the fans, which can be removed only by switching off the device.

Figures 3.6a and 3.6b show respectively the left fan and the right fan spectra, from an acquisition made close to each fan (about 3 cm). Unlike the signal previously presented in Figure 3.5, this acquisition was not made in a semi-anechoic room with professional measurement microphones, but in a normal room subject to sound reflections. It was also acquired with the same low-cost microphones used in the ANC system. This is the reason why the background noise is not so flat. As we can see from these images the right fan generates more power than the left one. This reflects the fact

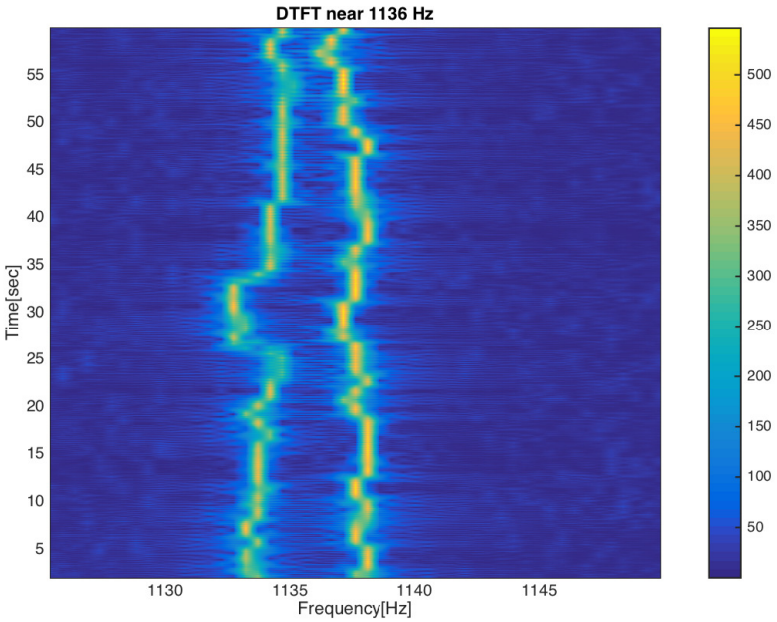

Figure 3.4: Spectrogram of the fan signal near the fundamental frequency, i.e. in the frequency range of $[1125, 1150]$ Hz.

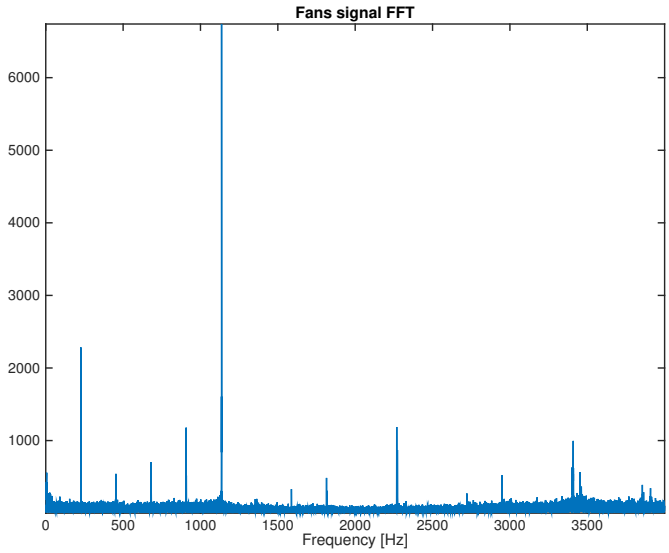

Figure 3.5: Magnitude of the DBV-T noise signal.

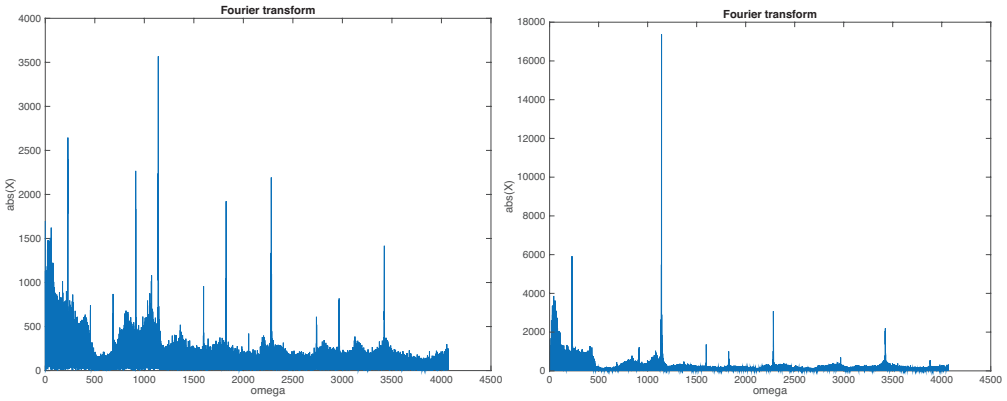

(a) Left fan spectrum **(b)** Right fan spectrum

Figure 3.6: Individual spectrum analysis of the fans.

that structural differences exist between the two fans.

3.3 Flow noise

As we can observe in Figure 3.6 the air flow can produce flow noise components at low frequencies (below 300 Hz), as result from pressurization or depressurization effects (depending on the rotational direction of the fans) of the air passing over the surface of the microphone. Flow noise and turbulent pressure fluctuations at the microphones can limit cancellation effectiveness. Thus, the reference signal may contain unwanted frequency components. In particular, an unwanted component in the reference signal implies an unnecessary anti-noise component in the canceling loudspeaker output. This problem can be solved both in a practical way, by taking proper precautions on the microphone positioning, or via software with the correct system choices. Both solutions will be discussed in the sequel.

Chapter 4

The proposed ANC method

In this chapter two new Feedforward ANC schemes are presented, namely a hybrid system (broadband + narrowband) and a narrowband scheme with an error-filter block. Both are employed in the ANC method proposed in this work and presented next. The ANC system proposed here is an ad-hoc method to cancel the noise produced by the DBV-T machinery.

From the signal analysis carried out in the last Chapter 3, we can make the following observations regarding the implementation of the ANC system:

- Different BPFs for the two fans cause the appearance of a beat frequency in the reference signal. In principle, two reference sensors would be necessary for a narrowband ANC system, but our hardware instrumentation supports only one. As mentioned before, the two fans will be assumed as a unique source.

- Non-acoustic sensors are not allowed by the project specifications. This implies that a pure narrowband ANC system cannot be implemented, because of the frequency shifts in the reference signal (observable in Figure 3.4). Implementing a pre-designed narrowband ANC system to delete the component at the fundamental frequency is not recommended. Indeed, the performance of an ANF system not equipped with a frequency tracking block is very low, as already shown in Figure 1.12.

- Flow noise can introduce unwanted components in the antinoise signal, degrading the system performance. In the absence of improvements with practical solutions (based essentially on a good microphone placement), we have two choices:

  - neglect the reference signal components subject to flow noise, eliminating them with a high-pass or a band-stop filter, focusing on the remaining components;
  - use a pre-designed narrowband ANC system, e.g. an ANF solution with a lookup-table in input, to cancel the flow noise components without the need of a reference signal.

Keeping in mind the issues listed above, our ANC system can take advantage of two recent ANC schemes presented in the sequel.

4.1 Hybrid ANC method

A new feedforward hybrid ANC system has been proposed by Xiao and Wang in [25] which is capable of reducing a noise signal containing both broadband and narrowband components.

In their work Xiao and Wang carry out numerous simulations and remark that the performance of the standard FxLMS system may degrade in a serious way when the targeted noise consists of both broadband noise and low-frequency sinusoidal components. In this scenario the narrowband system does not have adequate power, as it only takes care of the sinusoidal components determined in advance, leaving the broadband component untouched. The broadband system is also not effective, as it was originally designed to suppress broadband noise.

The simple and very effective idea explored in [25] is to split up the reference signal in two parts:

- a signal with only the low-frequency narrowband component(s) to use as input to a narrowband system;
- a signal that represents the original reference signal where the previously discussed narrowband components have been removed. This signal is used as input to a broadband system.

The block diagram of this sytem is showed in Figure 4.1. This new system consists of a hybrid narrowband-broadband feedforward solution with three subsystems:

- **An adaptive Fourier analyzer** (also called sinusoidal noise canceller, SNC) that is essentially an ANF (or more ANFs in parallel) driven by two sinusoidal signals at the same frequency in quadrature. The sinusoidal noise canceler takes the input signal $x_r(n)$ from the

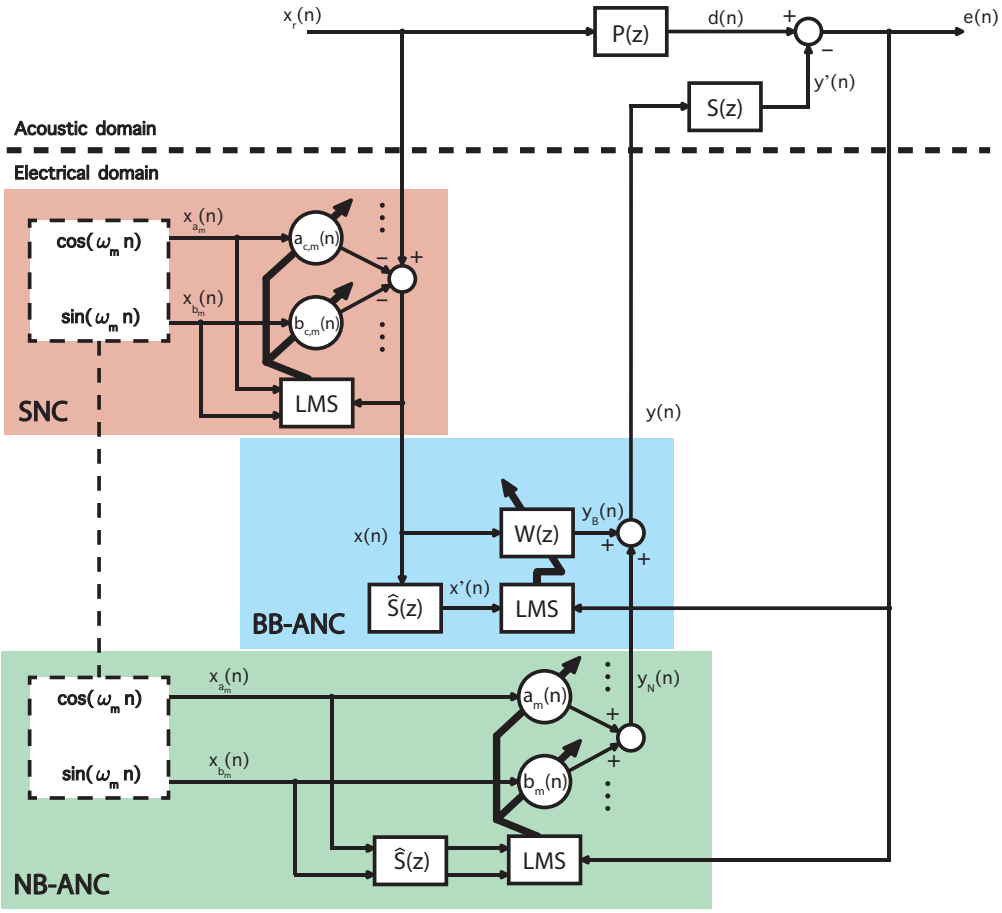

Figure 4.1: Hybrid feedforward ANC scheme: the system consists of three subsystems, a SNC (red) that 'cleans' the reference signal from selected sinusoidal components, a broadband FxLMS-based active noise canceler (blue) and a second SNC (green) that takes into account the secondary path and eliminates the sinusoidal components neglected by the broadband subsystem.

reference microphone and removes the chosen sinusoidal components. The resulting output of the SNC is given by

$$x(n) = x_r(n) - \sum_{m=1}^{M} [\, a_{c,m}(n)\, x_{a_m}(n) + b_{c,m}(n)\, x_{b_m}(n) \,] \tag{4.1}$$

where M is the number of frequency components to remove, $a_{c,m}(n)$ and $b_{c,m}(n)$ are the SNC coefficients, $x_{a_m}(n)$ and $x_{b_m}(n)$ are equal to

$$x_{a_m}(n) = \cos(\omega_m\, n) \qquad x_{b_m}(n) = \sin(\omega_m\, n) \qquad . \tag{4.2}$$

Signal $x(n)$ is then used as reference signal for the broadband ANC subsystem.

The update equation for the SNC coefficients is given by

$$\begin{aligned} a_{c,m}(n+1) &= a_{c,m}(n) + \mu_c(n)\, x(n)\, x_{a_m}(n) \\ b_{c,m}(n+1) &= b_{c,m}(n) + \mu_c(n)\, x(n)\, x_{b_m}(n) \end{aligned} \tag{4.3}$$

where $\mu(n)$ is a variable step-size defined as:

$$\mu_c(n) = \alpha\, \mu_c(n-1) + (1-\alpha)\, \mu_{c,min}(n-1), \quad \mu_c(0) = \mu_{c,max} \tag{4.4}$$

where α is a forgetting factor with typical value $0 \ll \alpha \leq 1$. $\mu_{c,max}$ is the maximum or initial value of the step size, while $\mu_{c,min}$ is the minimum or steady-state value. $\mu_{c,max}$ is set to a large value such that the SNC converges fast enough in the early stages of adaptation. $\mu_{c,min}$ is set small to guarantee the steady-state performance of the SNC.

- **A broadband ANC subsystem** with an adaptive FIR filter based on the FxLMS update equation, as already discussed in Chapter 1. The output $y_B(n)$ of this subsystem is related to the broadband signal component and it will add up to the output signal $y_N(n)$ of the narrowband subsystem so that

$$y(n) = y_B(n) + y_N(n) \tag{4.5}$$

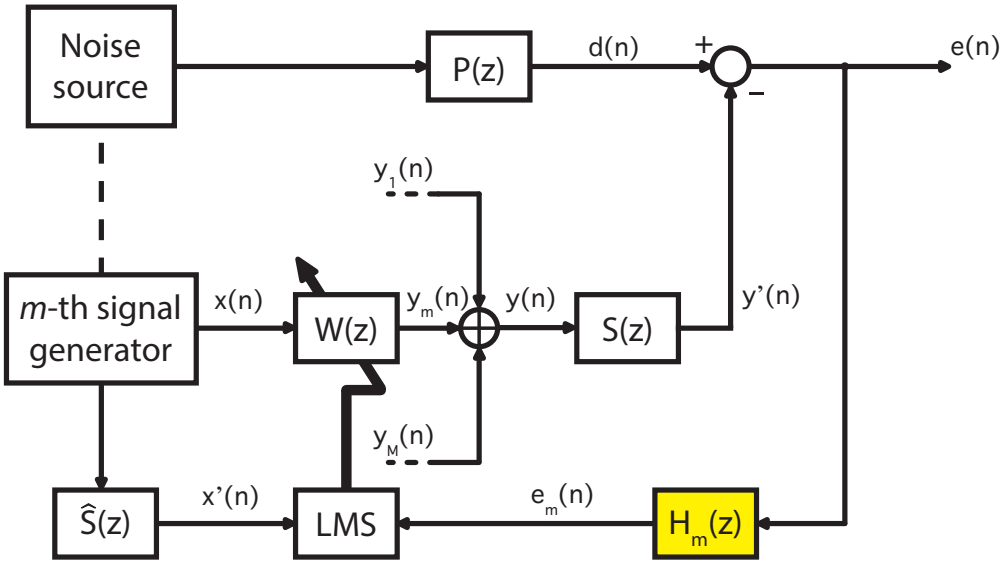

Figure 4.2: Parallel filtered-error narrowband FxLMS ANC scheme: the highlighted block $H_m(z)$ represents the m-th band-pass filter, used to make the update equation error-selective in each m-th system in parallel.

- **A narrowband ANC subsystem** that is essentially equal to the SNC system, the only difference being that it is taking into account the secondary path transfer function in the update equation.

4.2 Filtered-error parallel narrowband ANC

In a standard broadband ANC usually the filter coefficients are updated with a non-filtered error because the adaptive FIR filter has the task of suppressing all the frequency components. But in the narrowband ANC case each filter (usually a two-weight adaptive filter) in the filter bank has to deal with a single specific frequency, so the convergence speed and thus the noise reduction of every adaptive filter will be degraded because the error signal has a much richer frequency content. A filtered-error method has been proposed by Chang and Kuo [26] to overcome this problem of conventional parallel-form narrowband ANC systems. They proposed a complete parallel narrowband ANC system using individual error signals to update the corresponding adaptive filters. They employ a bank of 2^{nd}-order IIR band-pass filters connected in parallel to split the error signal into the corresponding channels. These band-pass filters are delayless at the center frequency to avoid introducing extra delay in the secondary path, so

that the convergence rate of the ANC system is not affected. A modified cost function is defined to derive the FxLMS algorithm for this complete parallel narrowband ANC system.

The complete filtered-error parallel narrowband ANC system block scheme is presented in Figure 4.2. In this scheme $H_m(z)$ represents the band-pass filter used to filter the error signal. Its transfer function is expressed as

$$H_m(z) = \frac{(1-p_m^2)(\frac{q_m z}{1+p_m^2} - 1)}{z^2 - q_m z + p_m^2} \tag{4.6}$$

where $0 \ll p_m < 1$ determines the bandwidth of the filter, and q_m controls the center frequency. The bandwidth parameter p_m is usually set close to one to achieve a narrow bandwidth, while the center frequency of the m-th band-pass filter is tuned to the frequency of the m-th harmonic and is equal to

$$q_m = (1+p_m^2)\cos\left(\frac{2\pi f_m}{f_s}\right) \tag{4.7}$$

where f_m is the frequency value of the m-th harmonic and f_s is the sample frequency.

With this solution, an increase of the individual maximum step size is possible for each single adaptive filter in the ANC filter bank, without losing stability.

4.3 The proposed method

The method here proposed is mainly based on the idea of Xiao and Wang, i.e. it is a hybrid system (narrowband - broadband) designed to optimize the cancellation of the noise produced by the fans of the DBV-T equipment. The initial idea was to use the SNC block to remove the flow noise component from the reference signal, so that the input signal to the broadband block does not contain components that can degrade the performance of the ANC system. The NB-ANC block has the task of suppressing those narrowband components that fall within the frequency range subject to flow noise, i.e. in our case the sinusoids near 227 Hz. Since these low-frequency components represents only a portion of the total noise power, we will use a filtered error to update the coefficients of the narrowband subsystem, through a band-pass filter of the type proposed in section 4.2 centered at 227 Hz.

Removing all the flow noise components with an SNC filter-bank is however computationally too costly for our hardware. One solution is to replace the initial SNC block with a high-pass filter $H_{HP}(z)$ having a cutoff frequency that ensures a reference signal without flow noise in input to the broadband subsystem. This filter may cause the loss of some sub-harmonic components that should actually be present in the input signal $x(n)$ of the broadband subsystem for proper noise cancellation. Indeed, these components are present both in the signal $x_r(n)$ acquired by the reference microphone, and in the disturbance signal $d(n)$ that we want to attenuate at the error microphone. Thus, employing just the broadband subsystem with the filtered input $x(n)$ would result in a partial cancellation of the noise signal at the error microphone. The parallel narrowband subsystem overcomes this problem, by handling only these sub-harmonic components. The antinoise signal will be the sum of the outputs of both subsystems, thus containing all the necessary frequency components for proper noise cancellation. In the case of the signal emitted by the DVB-T fans, the component to be deleted with the narrowband subsystem is only one and it is at 227 Hz. The drawback of this solution is the addition of a delay in the control chain, due to the introduction of the high-pass filter.

The block diagram of the whole hybrid ANC system is shown in Figure 4.3, where:

$\mathbf{H_{HP}(z)}$ is the high-pass filter for the reference signal, with cutoff frequency between 300 and 400Hz, where the flow noise no longer affects the reference signal. It is modelled as a 2^{nd}-order IIR filter.

$\mathbf{H_{BP}(z)}$ is the band-pass filter used to filter the error signal which provides the input to the narrowband subsystem. The transfer function of $H_{HP}(z)$ and its implementation have been discussed in the preceding subsection. Observing that there are no other major power components close to 227Hz, one does not necessarily need a narrow bandwidth.

$\mathbf{A_s}$ and $\mathbf{z^{-\Delta}}$ are respectively the inverse magnitude of the secondary path estimate $\widehat{S}(z)$ at the frequency of interest, in our case 227Hz, and the corresponding delay compensation. In this way we can reduce the computational burden, avoiding the additional filter between the two input signals to the narrowband subsystem and the secondary path estimation $\widehat{S}(z)$.

$\widehat{\mathbf{S}}(\mathbf{z})$ is the secondary path estimate. It is estimated offline and processed to obtain the Eigenvalue Equalization version. As discussed in

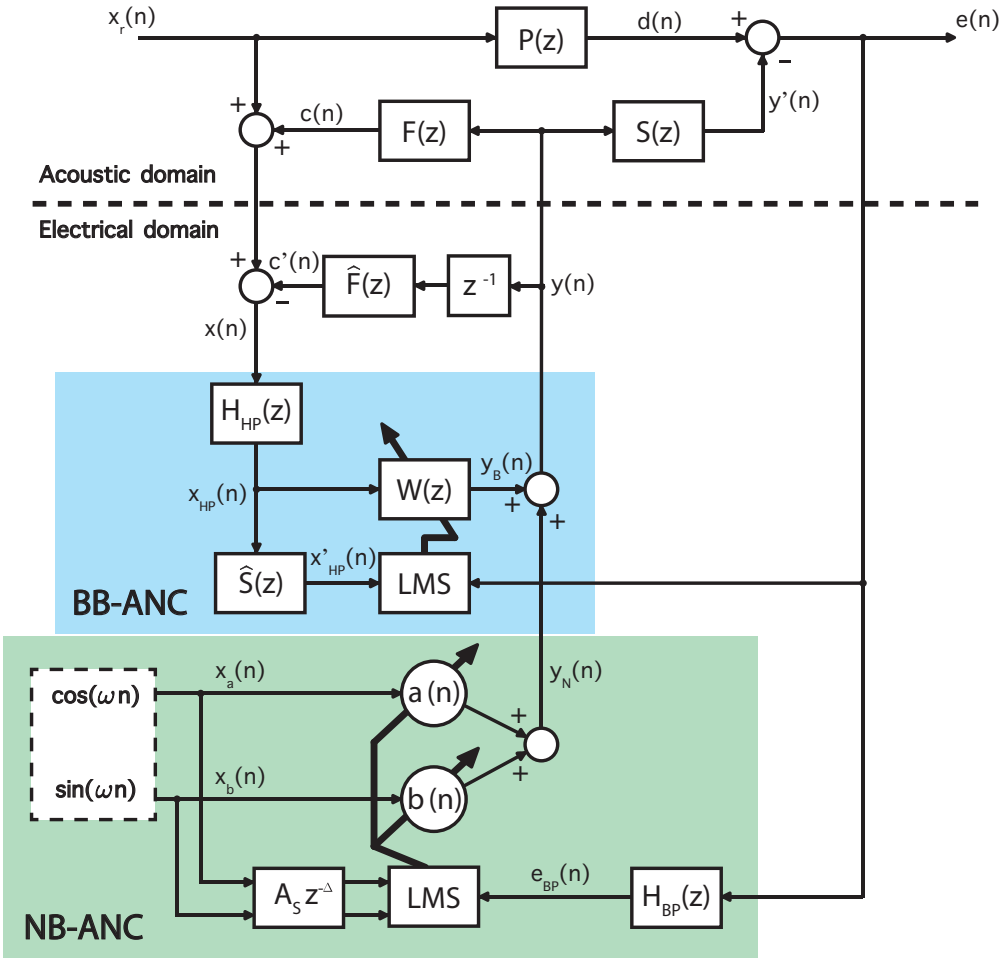

Figure 4.3: Block diagram of the proposed hybrid method: the broadband ANC subsystem (blue) filters the input signal with a high-pass filter $H_{HP}(z)$ in order to eliminate the flow noise components. The narrowband ANC subsystem (green) handles the cancellation of the narrowband component at 227 Hz. This component is not present in the input signal x(n) entering the broadband subsystem, due to the highpass filtering applied to obtain that signal. Hence, the broadband subsystem is not capable of attenuating this narrowband component, which motivates the introduction of the narrowband subsystem to correct the antinoise signal. The band-pass filter $H_{BP}(z)$ is included to make the update equation of the narrowband subsystem error-selective.

Chapter 6, to decrease the computational complexity of the whole system, $S(z)$ and $F(z)$ are modelled with FIR filters of order higher than the ones used in the online phase.

If we use the EE-FxLMS algorithm we don't need any adaptive step size $\mu_B(n)$ for the update equation of the broadband subsystem. Accordingly the adaptive FIR filter can be updated with the following formula

$$\mathbf{w}(n+1) = \mathbf{w}(n) + \mu_B \, \mathbf{x_{HP}}(n) \, e(n) \tag{4.8}$$

where $x_{HP}(n) = H_{HP}(z) \, x(n)$ and $x(n)$ is the resulting reference signal after the feedback compensation. For the narrowband subsystem the update equation of the two adaptive coefficients is the following

$$\begin{aligned} a(n+1) &= a(n) + \mu_N \, A_S \, x_a(n-\Delta) \, e_{BP}(n) \quad , \\ b(n+1) &= b(n) + \mu_N \, A_S \, x_b(n-\Delta) \, e_{BP}(n) \quad . \end{aligned} \tag{4.9}$$

Since μ_N and A_S are two constants, we can replace the product $\mu_N A_S$ with a single step size parameter.

The right combination of the presented blocks is critical for the proper functioning of the system, and even the absence of one component could compromise the final performance. The absence of one or both of the $H_{HP}(z)$ and $\widehat{F}(z)$ filters can lead to system instability. In particular, the omission of the high-pass filter $H_{HP}(z)$ causes the flow noise component to appear at the input of the broadband subsystem. Then, the system will attempt to remove this low frequency component resulting from the reference signal. As can be seen in the spectrogram of Figure 4.4, the antinoise output $y(n)$ contains the component relative to flow noise. In the worst case, the coefficients of the adaptive filter $W(z)$ overflow in the attempt to remove this component, and drive the system towards instability, as shown between the instants $t = 9$ and $t = 10$ in Figure 4.4.

Conversely, the absence of the NB-ANC subsystem, the BB-ANC subsystem and/or the EE-FxLMS approach do not affect the stability of the system, but may degrade its performance in terms of noise attenuation and convergence rate.

The use of delay compensation in the narrowband subsystem avoids two convolution operations. Indeed, using two lookup tables for the sine and cosine signals one just has to identify the right samples to update the two adaptive coefficients. Overall, with our method the computational complexity is not greatly increased compared to a classic broadband system

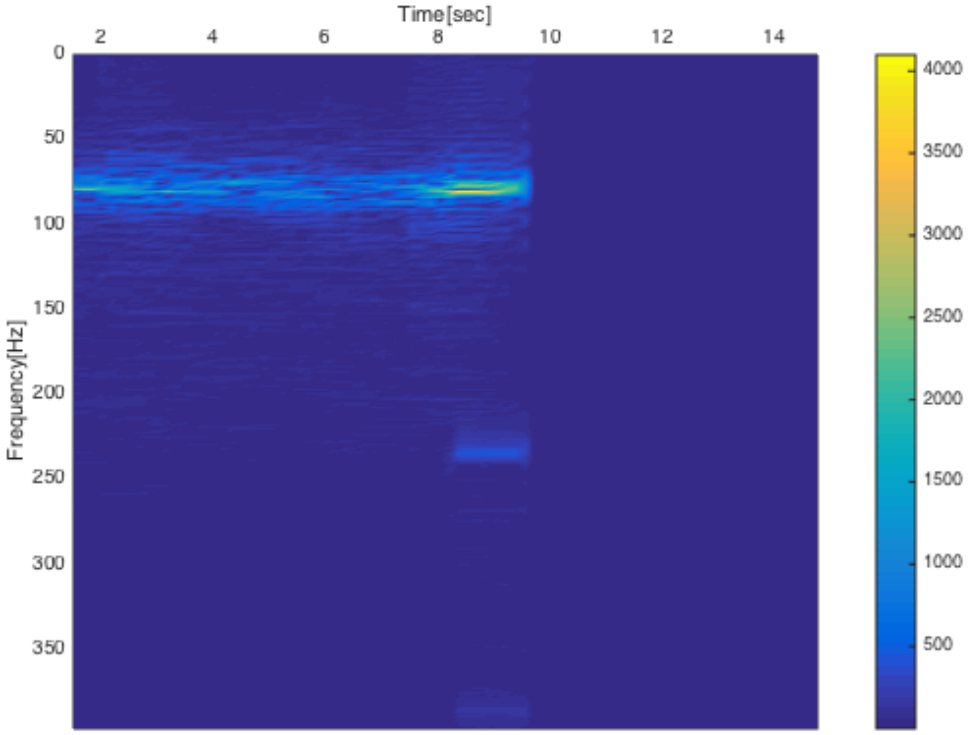

Figure 4.4: Spectrogram of the antinoise output $y(n)$ in the case of system instability due to flow noise.

Table 4.1: Cost of the proposed method in terms of addition and multiplication for each operation.

Operation	Addition	Multiplication
$c'(n) = \widehat{F}(z)\, y(z)$	$N_{\widehat{F}}$	$N_{\widehat{F}}$
$x(n) = [x_r(n) + c(n)] - c'(n)$	1	0
$x_{HP}(n) = H_{HP}(z)\, x(n)$	5	5
$y_B(n) = W(z)\, x_{HP}(n)$	N_W	N_W
$x'_{HP}(n) = \widehat{S}(z)\, x_{HP}(n)$	$N_{\widehat{S}}$	$N_{\widehat{S}}$
$w(n+1) = w(n) + \mu_B\, x'_{HP}(n)\, e(n)$	N_w	N_w
$y_N(n) = a(n)\, x_a(n) + b(n)\, x_b(n)$	1	2
$e_{BP}(n) = H_{BP}(z)\, e(n)$	5	5
$a(n+1) = a(n) + \mu_N\, x_a(n-\Delta)\, e_{BP}(n)$	1	2
$b(n+1) = b(n) + \mu_N\, x_b(n-\Delta)\, e_{BP}(n)$	1	2

FxLMS. The filtering operations with the IIR filters $H_{HP}(z)$ and $H_{BP}(z)$ involve 5 additions and 5 multiplications each, while the whole narrowband subsystem adds 2 multiplications and 1 sum for the output equation, 4 multiplications and 2 sums to upgrade both the filter coefficients. The overall cost is dominated by the broadband FxLMS subsystem which depends on parameters N_w, $N_{\widehat{S}}$ and $N_{\widehat{F}}$ which are typically much larger.

Table 4.1 lists the number of operations carried out for each operation, where N_W is the number of the adaptive FIR filter coefficients, $N_{\widehat{S}}$ and $N_{\widehat{F}}$ are the number of taps of $\widehat{S}(z)$ and $\widehat{F}(z)$ respectively.

Taking as a reference signal the one considered in Chapter 3, the simulations show that our method can successfully remove both the com-

ponents not affected by flow noise and those contained in the range of frequencies affected by flow noise. The two subsystems work in parallel without any interference, the only weakness begin the limitation given by the narrowband subsystem. Any important components eliminated with the high-pass filter $H_{HP}(z)$ cannot be deleted if not taken into account through a previous analysis stage. However, since the majority of power is concentrated around the 1135Hz this problem does not affect the final performance.

Chapter 5

Hardware implementation

In the previous chapters, after discussing the necessary theoretical background, a novel ANC method has been outlined. In this chapter, instead, the actual implementation of this method will be discussed, describing the technical instrumentation used to set up the control system. The hardware must allow software flexibility as well as fully automatic operation of the complete active noise control system. Self-calibration and self-modeling are important system functions. The implementation of the audio signal chain is considered, illustrating its elements and the connections used to interface them. The hardware and software instrumentation for signal measurements will be illustrated. The calibration procedures are presented with microphone and loudspeaker placement tips. Lastly, some considerations on the theoretical constraints will be taken into account for real time operational correctness.

5.1 The digital signal processor

The DSP is a dedicated processor for the processing of digital signals, optimized to perform extremely efficient sequences of instructions, such as sums and multiplications. A DSP device is then used to perform all the mathematical operations required by the ANC algorithm.

In the project a STM32F407VGT6 microcontroller by STMicroelectronics [27] has been used. This device belongs to the STM32F4 series, designed for high performance and ultra fast data transfers. It provides the following benefits: a 32-bit ARM Cortex-M4F core, 1 MB Flash, 192 KB RAM, up to 168 MHz operating frequency and a single-precision floating point unit. It also allows a boosted execution of control algorithms, code efficiency and elimination of scaling and saturation.

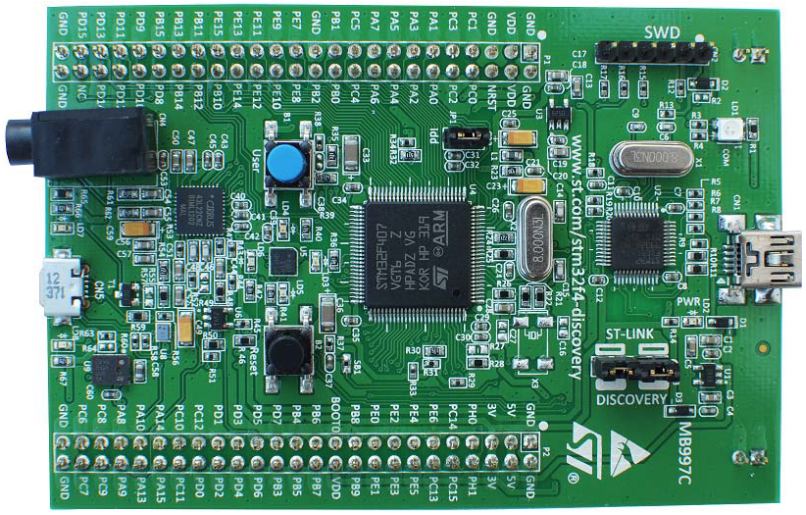

Figure 5.1: STM32F4 DISCOVERY evaluation board.

This microcontroller is embedded in the STM32F4DISCOVERY evaluation board [28] showed in Figure 5.1, a low-cost and easy-to-use development kit to quickly evaluate and start a development with an STM32F4 MCU. It includes useful features for the ANC application: an ST-LINK/V2 embedded debug tool interface, a Cirrus Logic CS43L22 audio DAC with integrated class D speaker driver, LEDs and pushbuttons.

The STM32F4DISCOVERY evaluation board is relatively cheap compared to some other DSP boards, and the Atollic TRUEStudio software used for programming the DSP processor is available free of charge.

5.2 The audio signal chain

A signal chain describe a series of signal-conditioning electronic components that receive an audio signal input every system cycle, with the output of one portion of the chain supplying input to the next. Signal chains are often used in signal processing applications to apply system controls based on the analysis of real-time phenomena. In ANC applications an audio signal chain is used and its elements, ordered with respect to the signal flow, are the following: the microphones, the microphones pre-amplifiers, the analog-to-digital converter (ADC), the digital signal processor (DSP), the digital-to-analog converter (DAC), the loudspeaker pre-amplifier, the canceling loudspeaker. The audio signal chain of this thesis project is illustrated in Figure 5.2. The ANC systems use real time signal processing to implement adaptive filtering that requires extensive computations. Thus,

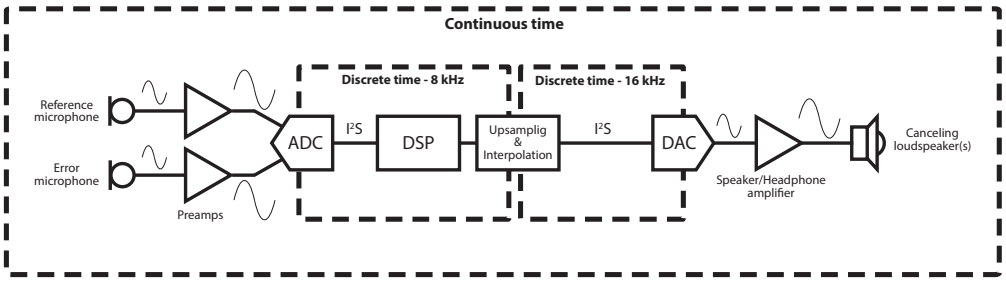

Figure 5.2: Audio signal chain.

the core of the audio signal chain is the DSP device.

The analog-to-digital converter

Digital systems operate with discrete time and amplitude signals that are acquired from analog signals through a sampling process. The ADC provides the discrete-time input signals to the DSP, converting the analog signals obtained from the reference microphone and the error microphone. An external PCM1808-Q1 ADC by Texas Instruments [29] is used in this project: a high-performance and low-cost stereo analog-to-digital converter with single-ended analog voltage input.

The ADC and the DSP communicate through the Integrated Interchip Sound (I^2S) protocol [30], an electrical serial bus interface standard, used for connecting digital audio devices together. This audio data interface format is left-justified and it provides, for each input signal, a 24-bit data to the DSP. Thus, the DSP has to convert the incoming 24-bit data (left aligned on a 32-bit signed integer frame) to a 32-bit single-precision floating-point format. Among all the options available for the choice of the ADC audio sampling frequency, the smallest value has been chosen, i.e. $f_s = 8$kHz. Thus, all the calculations of one cycle must be completed in $125\,\mu s$. This value allows the ANC system to operate up to 4kHz, although in the case under analysis the reference signal will never have significant noise components over 2kHz. In general, ANC systems are effective in eliminating noise components below 1kHz, while passive methods are preferable for higher frequencies. The I^2S protocol acts as a multiplexer in output of the ADC, so the DSP must perform data demultiplexing.

The digital-to-analog converter

The DAC device is interfaced with the DSP in an equal and opposite way respect to what has just been described for the ADC. The DSP

must provide the DAC 24-bit data, left aligned on a 32-bit signed integer frame. Therefore, a previous conversion stage is needed before being able to interface with I^2S bus.

The DAC device used in the project is embedded in the evaluation board, a CS43L22 digital-to-analog converter by Cirrus Logic [31]. It is a highly integrated, low power stereo DAC with a Class D stereo/mono speaker amplifier. The CS43L22 offers many features suitable for low power, portable system applications.

Using a working frequency of 8kHz, distortions can occur as the frequency of the DAC output signal increases, providing errors in sinusoid generation already at 1900Hz. Thus, even before the data conversion, an upsampling stage followed by an interpolation stage are required in order to raise the working frequency from 8kHz to 16kHz, with an upsample factor of 2. In this way, the DAC output signal is without distortions in the frequency range interested by the ANC application.

The microphones

The most common sensors for ANC applications are microphones. The microphone frequency response is not a critical factor, as any lack of flatness in amplitude or phase can be estimated by the system identification algorithms and compensated by the adaptive filter. Moreover, the microphones are selected to satisfy requirements of low cost, low impedance, large signal-to-noise ratio, nondirectivity, and high sensitivity. In this project, microphones have been used both as reference and error sensors.

The analog signal acquired by the microphones is weak and cannot be directly fed to the ADC. A previous signal conditioning stage is required to amplify both the microphone signals. In order to comply with the technical specifications of the ADC, a preamplifier is needed to interface the microphones. The gain of the preamplifier should be set in such a way that the amplified signal is never above 3.23V, the maximum input voltage of ADC. Moreover, the preamplifier has to guarantee a protection mechanism so that signals above a certain threshold saturate, which prevents overloading the ADC.

To take advantage of the dynamics of the input signal, the gain of each preamplifier can be manually changed through a trimmer. This calibration phase is recommended offline, adjusting the gain so that the signal is amplified to a maximum of 90% with respect to the saturation threshold (this choice takes into account any future peak in the amplitude caused by the operation of the ANC system).

Figure 5.3: FourPointSurround^{TM} Speaker System.

The canceling loudspeaker

The loudspeakers used in this project are made by Cambridge SoundWorks. They are part of the FourPointSurround^{TM} Speaker System [32] shown in Figure 5.3, that consists of a powered subwoofer, four satellite loudspeakers and a volume control. All the satellite loudspeakers are magnetically shielded, relatively small in size (diameter = 7cm) and have a directivity sound directional pattern. The loudspeaker must generate a sound pressure level higher than the noise source pressure level. The frequency response range of the satellite loudspeakers is approximately 70Hz $\div$ 20kHz. They are one channel driven into a 4 ohm load with less than 1% total harmonic distortion at 1kHz. For these reasons they have been chosen as canceling sources and in the test-bed case also as noise sources.

The interface between the DAC and the loudspeakers is represented by the powered subwoofer. It is a self-contained speaker/headphones amplifier configuration in which the characteristics of the amplifier are optimally matched for the surround system, all encased in the same enclosure. Thus, the subwoofer is used only as an amplifier for the antinoise signal $y(n)$ in output from the DAC.

The calibration of the amplifier gain is carried out in the offline phase, after having adequately placed microphones and loudspeaker(s). The DSP

(a) Front view **(b)** Back view

Figure 5.4: PicoScope2000 digital oscilloscope.

has been programmed so as to perform a check on the incoming data. If the absolute value of a datum from a microphone is greater than 0.98 (the unit is the maximum sampled value, corresponding to the saturation threshold), a designated LED is turned on in order to warn the user. The speaker gain is set once the microphone preamplifier is calibrated, relying on the random noise signal used in the system identification phase, which is normalized. In particular, the gain value must be set as high as possible without hitting the threshold.

5.3 Signal acquisition

In order to evaluate the performance of the ANC system presented in this thesis, suitable mechanisms for the acquisition of audio signals and internal DSP data are required. Three analog signals can be acquired: the reference signal, the error signal and the canceling signal which drives the loudspeaker. All three are obtained by an oscilloscope after the preamplifier stage.

The oscilloscope used for this purpose is a PicoScope2000 [33] shown in Figure 5.4, an USB oscilloscope by Pico Technology, with 2 input channels,

1 output channel and a bandwith of 25 MHz. It has a spectrum analyzer, a function generator, an arbitrary waveform generator and a protocol decoder. An easy PC interface is available, that can display the acquired signals and save them in a data format compatible with Matlab. At most two signals can be acquired simultaneously, and the length of the temporal window that can be saved depends on the oscilloscope's internal memory, and consequently on the choice of the sampling frequency. With a sampling frequency of 12 kHz, the signals can be acquired (and saved) for almost 90 seconds, which is a good time to evaluate the performance and effectiveness of the ANC system under analysis

The STM Studio software (by STMicroelectronics) is used for the acquisition of digital signals. STM Studio helps debug and diagnose STM32 applications while they are running by reading and displaying their internal variables in real-time. It interfaces with STM32 MCUs via the standard ST-LINK development tools and it is a non-intrusive tool, preserving the real-time behavior of applications. Thus, it perfectly complements traditional debugging tools to fine tune applications that cannot be stopped. By contrast, its limitation is a capture period of 200 ms, which is relatively low compared to the ANC system frequency (8 kHz), but still allows the monitoring of variables which vary more slowly.

5.4 Some considerations on the physical ANC system

The physical factors that limit the performance of ANC systems, such as sample frequency, filter length, causality, temporal and spatial matching are discussed in this section as part of the implementation of ANC systems [5].

Causality

The DSP task is to estimate precisely any delay and amplitude change that occurs as the unwanted noise travels from the input microphone to the loudspeaker. Thus, the controller must complete the entire signal processing task before the primary noise arrives at the loudspeaker. This acoustic delay is denoted as

$$\delta_A = \frac{L}{c_0} \quad , \tag{5.1}$$

where L is the distance from the input microphone to the canceling

speaker and $c_0 = 343.2\,m/s$ is the speed of sound in air. The electrical delay δ_E instead can be expressed as the sum between the total delay of the electronic devices and the group delay of the digital filter $W(z)$. To ensure that the adaptive filter has a causal response, the inequality $\delta_A > \delta_E$ must be satisfied.

This causality condition sets the minimum distance from the input microphone to the output speaker:

$$L_{min} > c_0\,\delta_E \quad . \tag{5.2}$$

If the electrical delay is longer than the acoustic delay, the response of the controller is noncausal. To reduce the electrical delay, a higher sampling frequency f_s is required for a given length. Periodic noises are a special case where causality is not required and shorter systems are possible.

Sampling frequency and filter length

Real-time digital signal processing requires that the processing time t_{DSP} be less than the sampling period T_s, i.e.:

$$t_{DSP} < T = \frac{1}{f_s} \quad , \tag{5.3}$$

where f_s is the sampling frequency. The maximum distance L_{max} between the reference microphone and the loudspeaker can be expressed in terms of taps of the filter $W(z)$:

$$L_{max} = \frac{N\,c_0}{f_s} \quad , \tag{5.4}$$

where N is the filter length. This means that L_{max} is the maximum distance that an N-tap adaptive filter can model. It is necessary that the filter be long enough to account for the physical distances within the acoustic paths. The required filter length is reduced by the addition of passive damping material and the number of coefficients required also depends on the sampling rate.

Thus the filter length N, the sampling frequency f_s and the distance L between the reference microphone and the loudspeakers are three extremely important parameters related to each other:

- The distance L should be large enough to meet the causality constraint. At the same time it must be small enough to avoid using too many taps for the adaptive filter $W(z)$.

- The filter length N has to be long enough to guarantee a good modeling of the acoustic path, but it must also be small enough not to increase the computational burden and degrade the system performance. As already mentioned in Chapter 1, N also depends on the reference signal.

- The sampling frequency f_s must respect the Nyquist sampling theorem, i.e. it has to be at least twice the maximum frequency of interest. However, a larger f_s implies a smaller processing time t_{DSP}.

Sensor and actuator placement

The placement of the sensors and actuators is a fundamental issue in the ANC system. Indeed, a wrong choice in the placement of the devices could completely compromise the performance. Some practical considerations can be made in this respect:

- The reference microphone position should allow the acquisition of a signal strictly correlated to the one to be attenuated.

- In some special cases, a proper placement of the error microphone produces a global canceling effect. This is true in the case of a duct, where the sound is conveyed and propagates mainly on one axis. In the free-field case the zones of reduced sound pressure are often extremely localised near the error sensor, so that it is often difficult to perceive any difference between the primary and controlled sound pressures at an observer location remote from the sensors.

The duct case

Heating, ventilating, and air conditioning (HVAC) systems are typical practical cases in which the ANC is applied to a duct [34, 35, 36]. The rigid walls of the duct act as acoustic insulation to the external environment. Thus, ideally the noise can reach the external environment only through the ends of the duct. Assuming that the noise source is placed at one of two ends, the producted disturbance is conveyed by the duct, only propagating along one axis, and it follows that the sound field is essentially one-dimensional. A duct closed at one end produces only odd harmonics and its resonance frequency depends on the length L and the diameter d as follow

$$f = \frac{n\, c_0}{4\,(L + 0.4\, d)} \quad , \tag{5.5}$$

where c_0 is the speed of sound and n is a positive odd number. In a closed duct, nodes and antinodes always appear if the duct is resonating [37]. Nodes are a series of locations at equally spaced intervals where the wave amplitude is zero, they always appear at the closed end. Nodes are spaced in intervals of half a wavelength λ, where $\lambda = c_0/f$. Antinodes are locations where the amplitude is maximum and are located in midway between each pair of nodes.

Additional considerations regarding the arrangement of the sensors and actuators can be made for the duct case:

- The microphones should not be placed at the nodes (points of little or no sound magnitude).
- If the ANC system components are located inside a HVAC duct, they should be placed on the duct wall to prevent the inhibition of the airflow. This also reduces the flow noise, which can limit the cancellation effectiveness.
- If the error microphone is placed outside and close to the end of the duct, the effect of flow noise can be further reduced. It also removes the possibility of the error microphone being at an acoustic node in the duct.
- Moving the control sources outside the duct significantly reduces the method employeeacoustic feedback problem.

Chapter 6

Software implementation

Computationally, the most demanding part of the FxLMS algorithm is the filtering of the signals. In a standard FxLMS scheme with feedback neutralization, three filtering operations are involved: the filtering of the reference signal $x(n)$ with the adaptive filter $W(z)$ and the estimate of the secondary path $\widehat{S}(z)$, the filtering of the antinoise signal $y(n)$ with the estimate of the feedback path $\widehat{F}(z)$. The ANC scheme proposed in this thesis (Chapter 4) also adds a narrowband ANC block, a band-pass filter and a high-pass filter. If the system is well designed only few operations are added. Thus, in order to reduce the computational burden, some simplified methods for computing the filtered signals are discussed in this chapter. All the vector-based mathematical operations implemented on the DSP code are defined in the CMSIS [1] DSP software library [38], a suite of common signal processing functions optimized for the Cortex-M processor based devices.

6.1 Lookup tables and delay compensation

In the standard implementation of a FxLMS-based ANC system, each signal to be filtered is stored in a buffer denoted as

$$\mathbf{x}(n) = [x(n)\,,\, x(n-1)\,,\, x(n-2)\,,\, \cdots\,,\, x(n-N)] \quad , \tag{6.1}$$

where N is the order of the corresponding FIR filter. All the buffers are updated at each time step by shifting the samples rightwards and inserting the new samples in the leftmost positions.

[1] Cortex Microcontroller Software Interface Standard

The delay compensation in a narrowband ANC system avoids the filtering of the reference signal with the estimate $\widehat{S}(z)$. Since the reference signal is a sine wave with constant amplitude and frequency, a lookup table can be used. The lookup table must contain the samples covering a period of the sinewave. Directly generating the sinusoidal inputs using the mathematical library is a costly operation for the DSP, and therefore not recommended. It is preferable to increase the memory usage, which leaves more time for the signal processing task.

For each adaptive notch filter, two lookup tables are needed as input, one for the sine values and one for the cosine values. The replacement of the estimate $\widehat{S}(z)$ with a pure delay block $z^{-\Delta}$ allows a faster update of the filter coefficients, selecting the sample $x(n-\Delta)$ from the lookup table. If the value of Δ is greater than the length of the lookup table, the corresponding index Δ_{mod} must be found as follows

$$\Delta_{mod} = mod\left(n-\Delta\,,\, round\left(\frac{f_s}{f_{ref}}\right)\right)+1 \qquad , \tag{6.2}$$

where $round(\bullet)$ is a function that rounds the input value to the nearest integer, $mod(\bullet,\bullet)$ is the modulo operation function and f_{ref} is the frequency of the reference sine wave stored in the lookup table.

Therefore, the combined use of lookup tables and compensation delay in an adaptive notch filter can avoid two shifting operations and two filtering operations, minimizing the computational cost.

Notice that in practice Δ must be an integer value to select the sample $x(n-\Delta)$ from the lookup table. Thus, unless an interpolation method is employed, equation 2.10 must be modified as follows:

$$\Delta = round\left(\frac{\tau(\omega_0)}{T}\right) \qquad . \tag{6.3}$$

Stability issues can occur if the rounding factor leads to a phase shift greater than $\pm 90^o$ with respect to the secondary path transfer function. This happens if the frequency f_{ref} of the reference sine wave is such that

$$f_{ref} > \frac{f_s}{4} \qquad . \tag{6.4}$$

In this case the sampling of the sine wave does not allow enough resolution to use the delay compensation approach. However, this problem does not occur in this thesis project, since the narrowband subsystem is driven with sinusoids which have much smaller frequency compared to the sampling rate.

6.2 Reduced-order path estimation

In this project the estimation of the secondary path $\widehat{S}(z)$ and the estimation of the feedbak path $\widehat{F}(z)$ are identified only in the offline phase. If the length of the filters is considerably large, the filtering operation becomes one of the most costly tasks that the DSP has to perform. So, the only way to decrease this computational load is to reduce of the FIR filter length.

$\widehat{S}(z)$ and $\widehat{F}(z)$ are identified using 180 taps for each, the maximum length allowed by the DSP computing power. These models have too many taps to be used online, but they are useful to obtain lower-order filters, preserving almost the same magnitude and phase characteristics.

Defining $\widehat{H}(z)$ as a N-order acoustic path estimation

$$\widehat{H}(z) = [\,\widehat{h}_1\,,\,\widehat{h}_2\,,\,\ldots\,,\,\widehat{h}_N\,] \qquad , \tag{6.5}$$

identified offline with $N = 180$ taps (overestimated), a k-order filter $\widehat{H}_k(z)$ can be created as a copy of the first k taps of the filter $\widehat{H}(z)$, as follows

$$\widehat{H}_k(z) = [\,\widehat{h}_1\,,\,\widehat{h}_2\,,\,\ldots\,,\,\widehat{h}_k\,] \qquad with\, k < N\,. \tag{6.6}$$

The crucial point in this procedure is the choice of the value k. As previously discussed in Chapter 2, for a proper functioning of the ANC system, the estimates of the acoustic paths have to ensure a phase shift smaller than $\pm 90^o$. Thus, the choice of the index k is based on the phase difference between $\widehat{H}(z)$ and its partial copy $\widehat{H}_k(z)$. Let $\Delta Phase(k)$ denote the square of the phase difference between $\widehat{H}(z)$ and the reduced version $\widehat{H}_k(z)$:

$$\Delta Phase(k) = \left(\angle\widehat{H}(j\omega) \,-\, \angle\widehat{H}_k(j\omega)\right)^2 \qquad . \tag{6.7}$$

Then, the optimal k minimizes this function. Since k should not be large as N, a constraint must be imposed during this searching phase, for example $k < N/2$.

Taking as acoustic path estimation the same presented in Chapter 2, a reduction from 180 taps to 71 taps can be applied (see Figure 6.1). The magnitude and phase comparisons are illustrated in Figure 6.2 and 6.3 respectively. Notice that this order reduction keeps the phase of the filter almost unchanged, and the magnitude is slightly smoothed. This degree of approximation in the magnitude does not create problems for the correct operation of the ANC system.

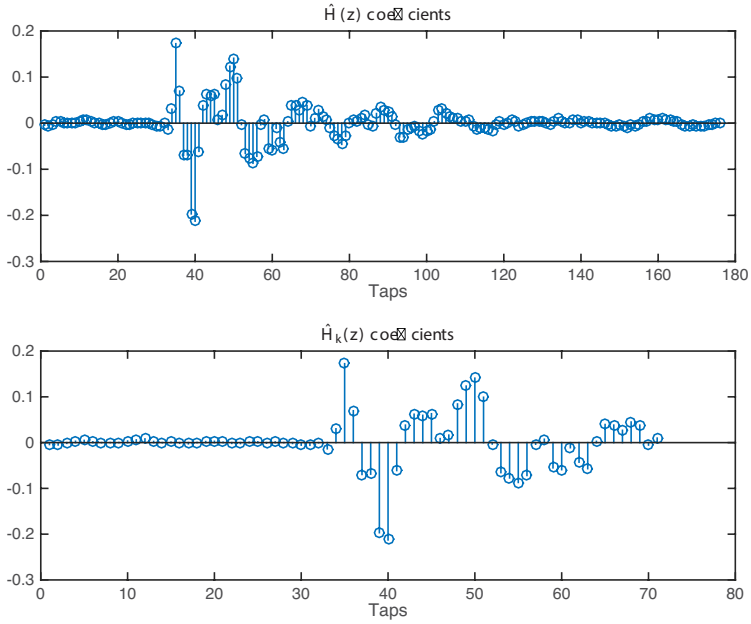

Figure 6.1: Filter coefficients comparison between the 180-taps estimation $\widehat{H}(z)$ and its reduced version $\widehat{H}_k(z)$.

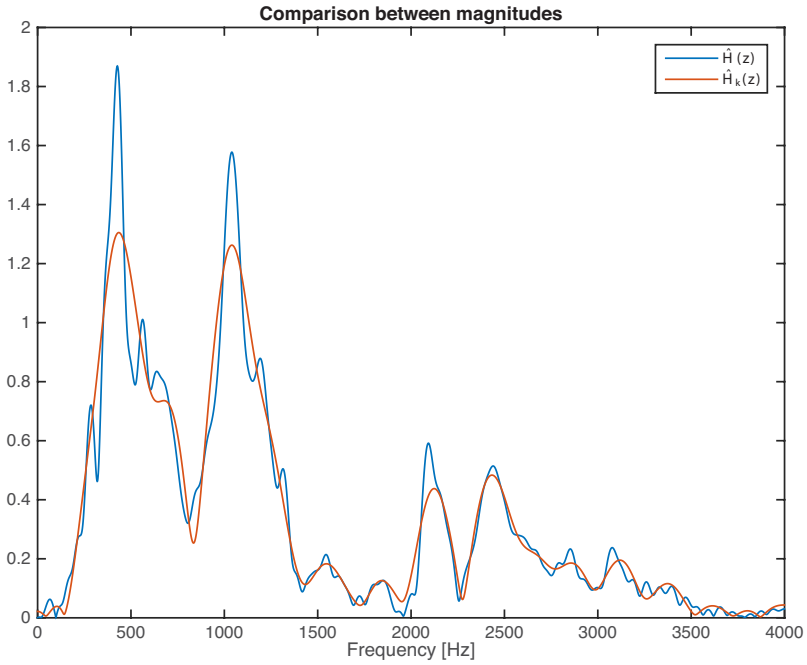

Figure 6.2: Magnitude comparison between the 180-taps estimation $\widehat{H}(z)$ (blue) and its reduced version $\widehat{H}_k(z)$ (orange).

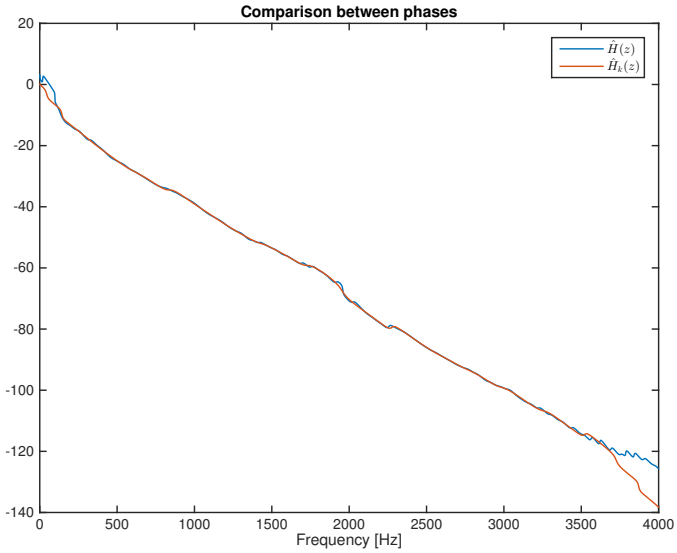

Figure 6.3: Phase comparison between the 180-taps estimation $\widehat{H}(z)$ (blue) and its reduced version $\widehat{H}_k(z)$ (orange).

Usually, the first coefficients of the FIR filter have a much smaller amplitude than the subsequent ones. This is due, in the identification phase, to the electrical devices delay and the acoustic delay between loudspeaker and microphone. The involved coefficients can be replaced by a pure delay block, further reducing the length of the estimated filter, and hence the cost of the related filtering task. The same phase minimization method described before can be used for such operation. Defining d as the number of coefficients to be set to zero, its optimal value minimizes the function

$$\Delta Phase(d,k) = \left(\angle\widehat{H}(j\omega) - \angle\widehat{H}_{d,k}(j\omega)\right)^2 \quad , \tag{6.8}$$

where $\widehat{H}_{d,k}(j\omega)$ is the frequency response of the digital filter $\widehat{H}_{d,k}(z)$ such that

$$\widehat{H}_{d,k}(z) = [\,\mathbf{0}_d\,,\,\widehat{h}_{d+1}\,,\,\ldots\,,\,\widehat{h}_k\,] \quad , \tag{6.9}$$

with $\mathbf{0}_d$ as zero vector of length d. Thus, the resulting filter can be thought as a pure delay block z^{-d} followed by an exact copy of n coefficients of $\widehat{H}(z)$, where $n = k - d$.

Figure 6.4 illustrates the filter $\widehat{H}_{d,k}(z)$ compared to the original secondary path estimation $\widehat{H}(z)$. Figures 6.5 and 6.6 compare the magnitudes

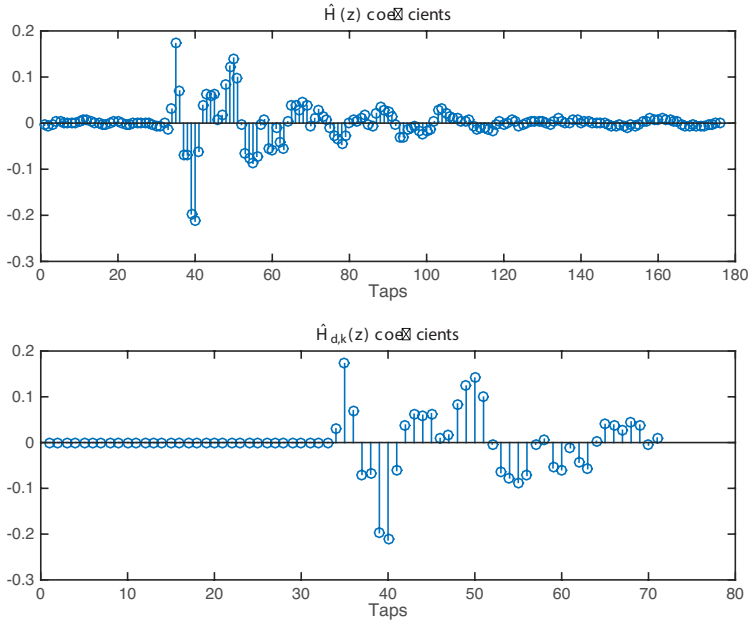

Figure 6.4: Filter coefficients comparison between the 180-taps estimation $\widehat{H}(z)$ (blue) and its reduced version $\widehat{H}_{d,k}(z)$ (orange).

and the phases. Again, the approximations do not compromise the correct operation of the ANC system. In the example just presented, the use of $\widehat{H}_{d,k}(z)$ dramatically reduces the number of taps involved in the filtering task, from the initial 180 to 37 taps.

The use of the pure delay block is impossible if the Eigenvalue Equalization is applied to the filter $\widehat{H}_{d,k}(z)$ because it flattens the magnitude of all the coefficients. Thus in practice, the estimation of the secondary path used in the proposed ANC system is the EE-version of the reduced-order filter $\widehat{S}_k(z)$ derived from the overestimated $\widehat{S}(z)$, while the pure delay version $\widehat{F}_{d,k}(z)$ is used as estimation of the feedback path, always based on the corresponding overestimation $\widehat{F}(z)$.

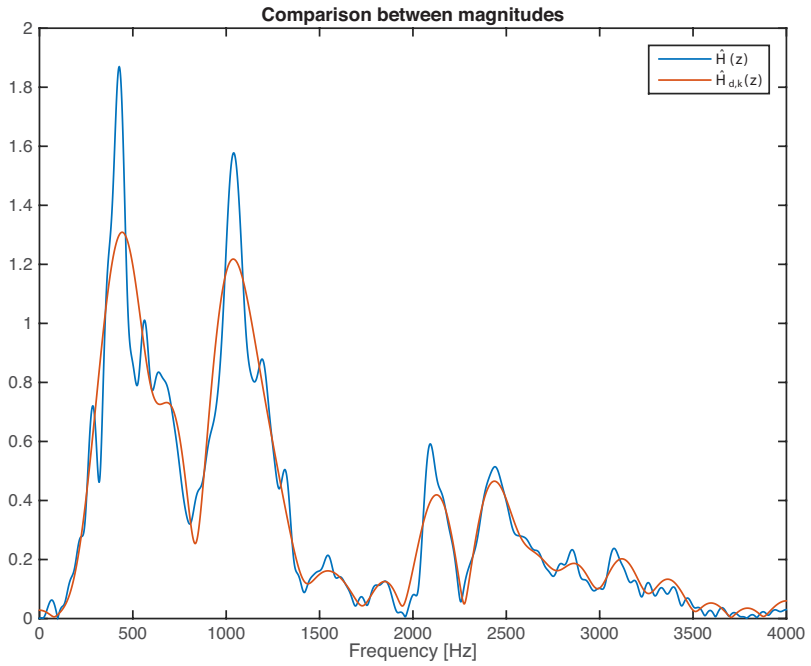

Figure 6.5: Magnitude comparison between the 180-taps estimation $\widehat{H}(z)$ (blue) and its reduced version $\widehat{H}_{d,k}(z)$ (orange).

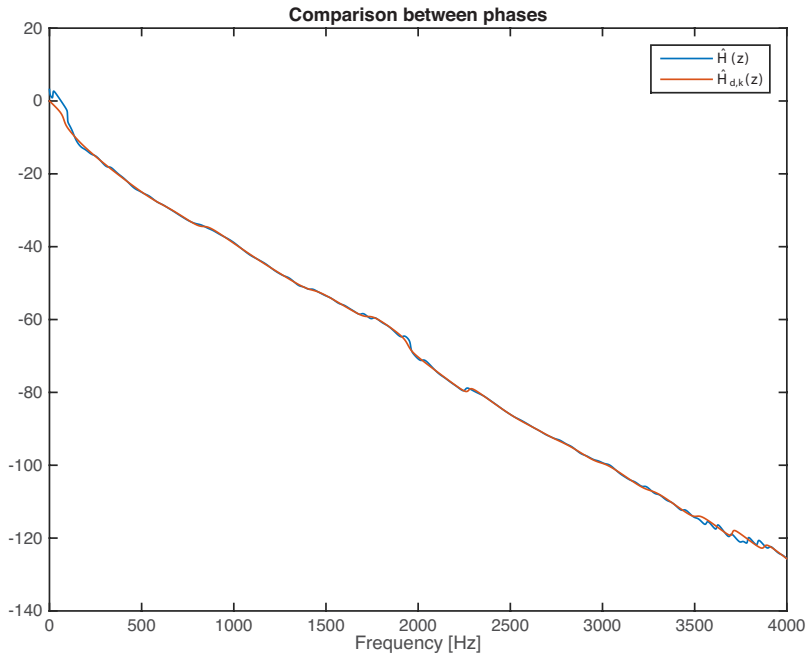

Figure 6.6: Phase comparison between the 180-taps estimation $\widehat{H}(z)$ (blue) and its reduced version $\widehat{H}_{d,k}(z)$ (orange).

Chapter 7

Test beds

In this chapter some experimental tests carried out on test beds will be presented, which simulate the application of the ANC in HVAC systems. In particular, two ducts with a square cross-section and different characteristics have been used. Starting from the simplest case, the goal is to achieve the closest possible solution for an ANC application on the DVB-T device. After a brief description of the ANC system initialization procedure, three type of tests will be presented, with different by its physical structures.

7.1 Initial test setup procedure

Before the testing phase, the following offline procedures must be carried out: the positioning of the sensors and actuators, the calibration of the preamplifiers and the identification of the acoustic paths. The sequence of steps to be performed is always the same, the only variations are relative to the software code loaded on the DSP board, depending on the algorithm to be used. In particular, the offline procedure steps are as follows:

1. Make all the hardware connections, observing the audio control chain presented in Chapter 5. Connect the speaker power amplifier to the laptop if the noise signal is generated in an artificial way.

2. Place the microphones and loudspeaker(s). For this step it is recommended (but not mandatory) to take into account the discussion in Chapter 5 regarding the positioning of sensors and actuators.

3. Upload on the evaluation board the code for the identification of the acoustic paths. The random noise signal used for this procedure must be self-generated by the DSP.

4. The calibration of the microphone preamplifiers: this procedure should be done based on the noise signal to be attenuated. The preamplifier gain must be such as to avoid saturation.

5. The calibration of the loudspeaker(s) amplifier. As already suggested in Chapter 5, the maximum possible gain for the loudspeaker(s) depends on the saturation threshold of the signal acquired by the microphones. The self-generated random noise signal is used as reference for this calibration because it is normalized.

6. Perform the identification of the acoustic paths separately, not simultaneously (10 seconds for each path are sufficient). In this way, it is possible to focus all the computational power of the DSP on one estimate per time, maximizing the number of taps of each $\widehat{S}(z)$ and $\widehat{F}(z)$. During this phase, no external noise sources must be present in the surrounding environment. Ideally, the microphones must be able to acquire only the random noise signal generated by the DSP through the cancelling loudspeaker.

7. Import from the DSP the data related to the estimates of the acoustic paths, process them with Matlab in order to obtain a reduced-order FIR filter for each one, as discussed in Chapter 6. All actions regarding the Eigenvalue Equalization and the delay compensation must be carried out in this step if they are used in the online algorithm.

8. Upload on the evaluation board the code relative to the online phase, including all the data calculated at the previous step.

7.2 Case 1 - ANC system inside the duct

The test bed used in this first case isolates the ANC system from outside sound interferences, by means of a wooden duct made from plywood, as shown in Figure 7.1. The duct has a square cross section d of 11 cm and a total length L of 80 cm. The branched shape of this duct has been designed to partially reduce the acoustic feedback at the reference microphone. In fact, the cancelling loudspeaker is located in the outgoing branch, the loudspeaker used as noise source is instead located on the farthest end of the duct. The microphones are positioned on the duct wall, 13 cm (reference mic) and 70 cm (error mic) away from the noise source.

In theory, an estimate of the resonance frequencies of this duct can be found applying equation 5.5. Thus, the first resulting resonance frequencies

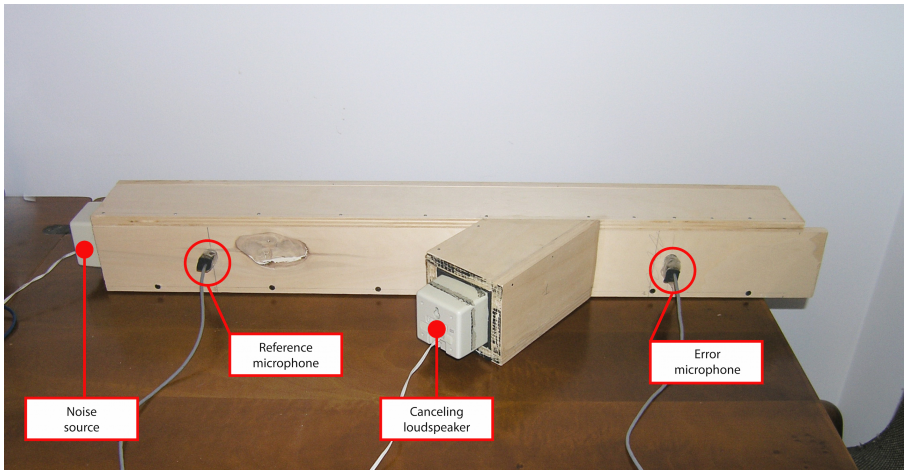

Figure 7.1: Case 1: wooden duct with all the sensors and actuators of the ANC system located internally.

are 102 Hz, 306 Hz and 509 Hz. These results are approximations since the equation 5.5 is based on ducts with circular cross section and without ramifications, but they are partially confirmed by the estimates of the acoustic paths. In Figure 7.2 the magnitude plots relative to the estimates $\widehat{S}(z)$ and $\widehat{F}(z)$ are shown and peaks are present in the proximity of the aforementioned frequencies.

7.2.1 The EE-FxLMS validation

This implementation was used for the validation of the EE-FXLMS algorithm. A comparison between the standard-FxLMS and the EE-FxLMS was carried out, testing 33 tones included in the frequency range of 200÷1000 Hz, each spaced 25 Hz from the others. The aim is the comparison of the convergence performance between the two algorithms. For each one, tests were performed in identical system conditions after finding the maximum step-size μ that ensures stability in the entire frequency range under analysis. The same filter lengths are used in both cases: $N_{\widehat{S}}$ =70, $N_{\widehat{F}}$ =91 (41 taps for the pure delay block and 50 taps of non-zero coefficients), N_W =96. The step-size selected for the standard-FxLMS is μ_{FxLMS} =0.001, while μ_{EE} =0.01 was chosen for the EE-FxLMS.

The results of these tests are shown in Figure 7.3. The EE-FxLMS algorithm has better convergence time as the frequency of the tones increases, confirming what discussed in Chapter 2. To ensure system stability, a small value of μ_{FxLMS} is needed where the frequency response of $\widehat{S}(z)$ is very high (in this case around 550 Hz). This ensure system stability but

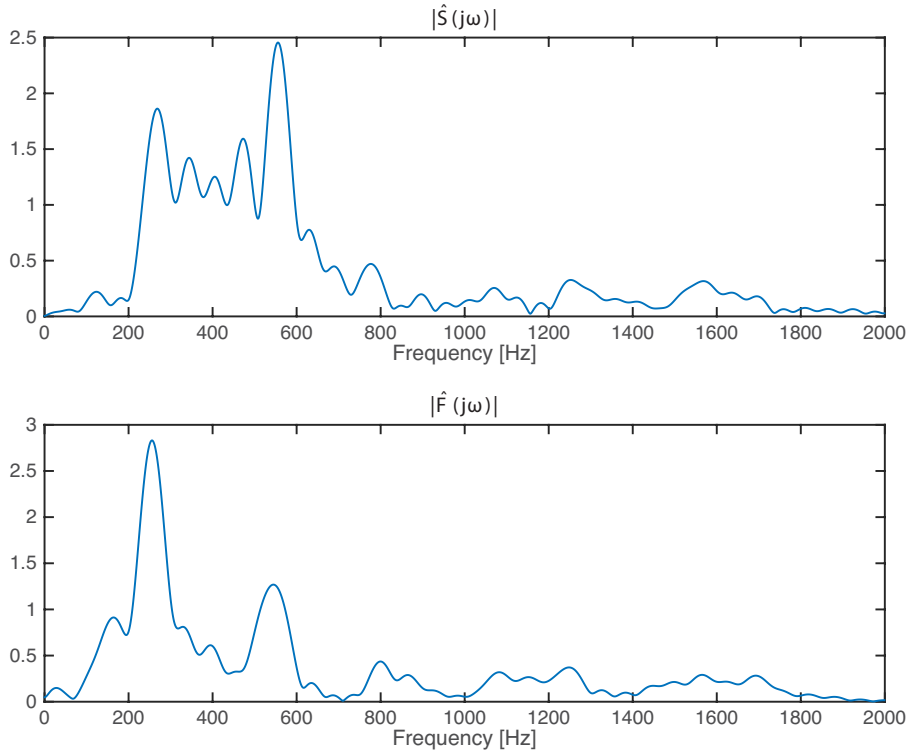

Figure 7.2: Case 1: impulse response magnitudes of the FIR filters $\widehat{S}(z)$ (top) and $\widehat{F}(z)$ (bottom).

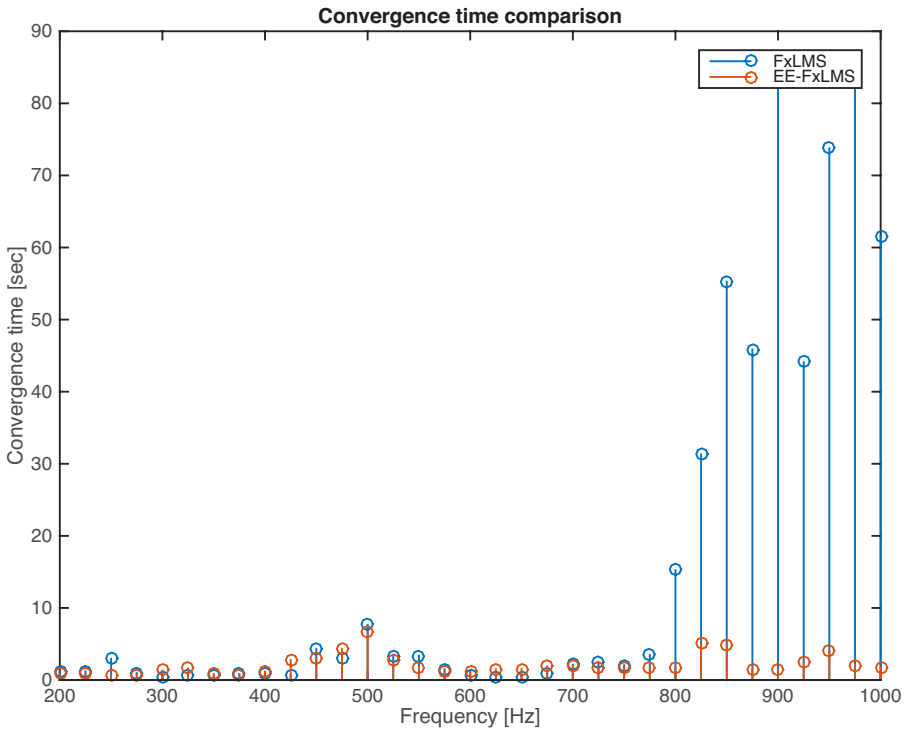

Figure 7.3: Case 1: convergence times comparison between the standard-FxLMS algorithm and the EE-FxLMS algorithm.

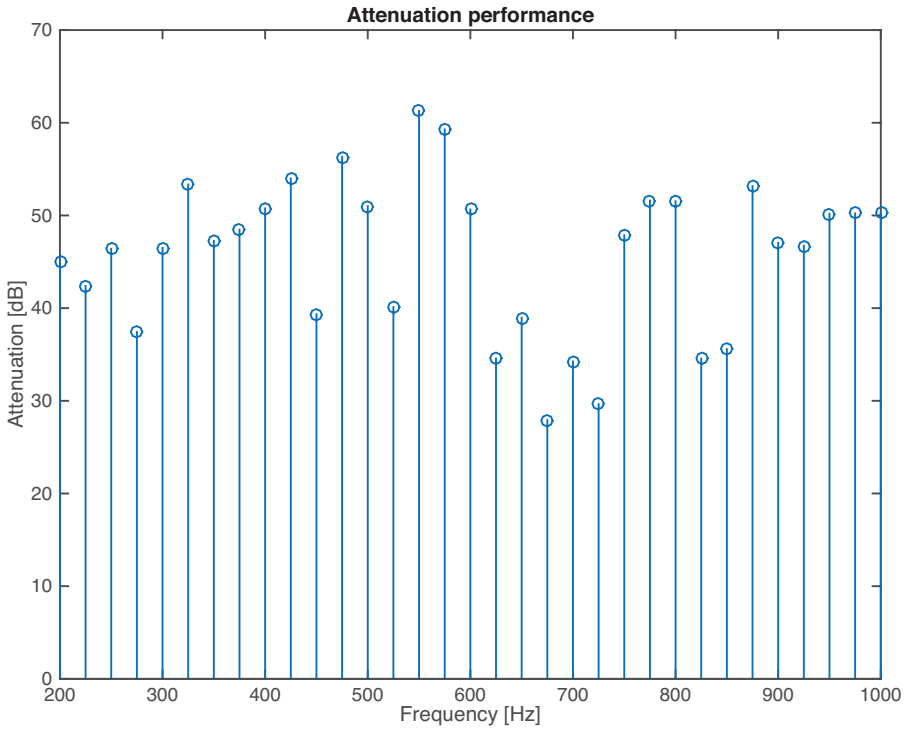

Figure 7.4: Case 1: attenuation performances achieved using the EE-FxLMS algorithm.

results in a slower convergence for noise components at other frequencies.

7.2.2 Attenuation performances

For both methods the attenuation performance is very similar, and is reported in Figure 7.4. The attenuation values are relative to the error microphone. An important aspect in the ANC systems is the cancellation perceived from a different observing location with respect to the error microphone. A strong attenuation near the error microphone does not necessarily mean an overall noise attenuation. As will be shown later, sometimes the noise cancellation in a specific area involves an amplification in other zones. To evaluate this aspect as well, the noise perceived at the workstation has been recorded using the laptop's built-in microphone, located approximately 1 meter away from the control area. In Figure 7.5 the RMS trends in dB of the signals picked up by the error microphone and the laptop microphone are shown. A sinusoid of frequency 500 Hz was chosen as noise signal. An attenuation of 50 dB is achieved at the error microphone and a reduction of nearly 35 dB is perceptible at the laptop microphone,

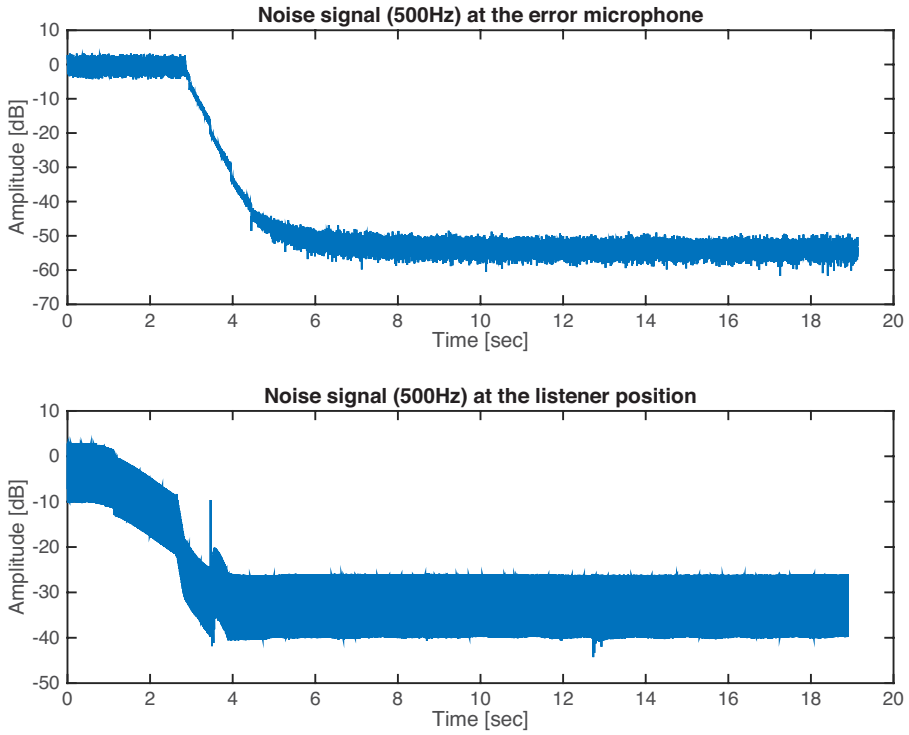

Figure 7.5: Case 1: comparison between the residual noise acquired at the error microphone and the one acquired at the workstation with the laptop's built-in microphone.

and therefore appreciable in all the surrounding environment. Thus, in this Case 1, for each tone a cancellation at the error microphone goes along with a reduction in the surrounding environment. Being the error microphone and the cancelling loudspeaker into the duct, and being the duct open only on one side, the noise cancellation is performed internally, before the open end. Therefore, if the residual error is low, the perceived noise outside the duct will be equally low.

As a last test performed with this structure, the method proposed in Chapter 4 is applied to the DVB-T fans noise signal acquired in [15]. The result of this test is shown in Figure 7.6 through a power spectrum and a RMS time trend of the error signal, before and after switching on the ANC. The attenuation of approximately 5 dB is relatively low compared to the tests previously performed, and represents the cancellation of the main frequency components, while the background noise cannot be eliminated. The main frequency components are typically easy to detect perceptually, and when the ANC operates only the background noise is recognizable.

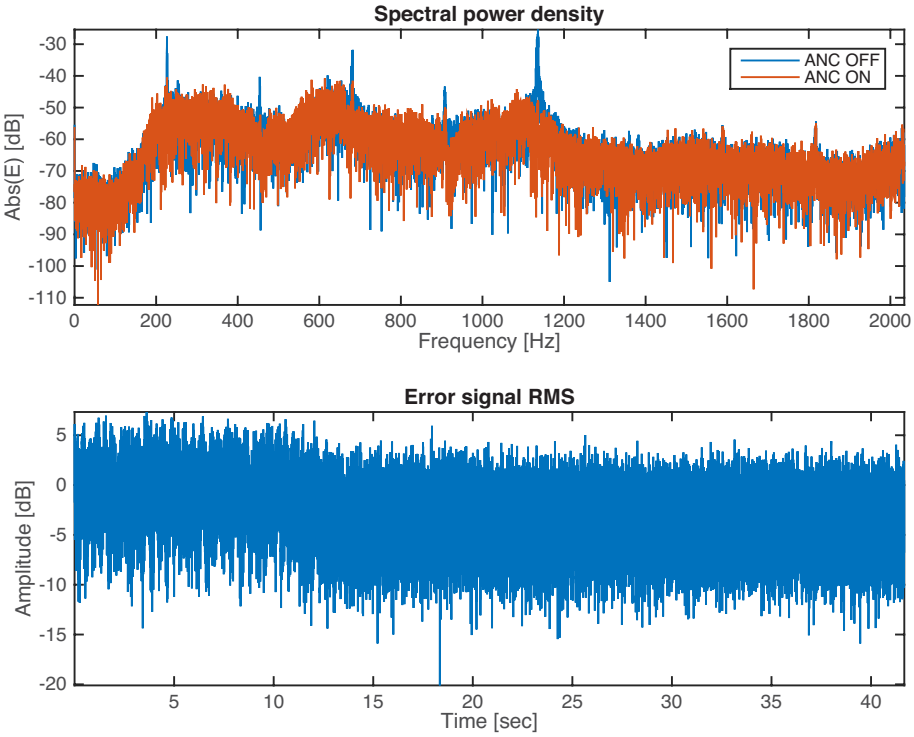

Figure 7.6: Case 1: attenuation performance at the error microphone using the proposed method applied to the DVB-T fans noise signal.

7.2.3 Pros and cons

The compactness of this structure allows a test standardization because sensors and actuator are internal to the duct, fixed and protected from external disturbances. The estimates of the acoustic paths are therefore hardly varying while the ANC operates. Its particular branched shape allows to reduce feedback to the reference microphone and an overall cancellation can be achieved, extended to regions beyond the error microphone.

The negative aspects of this structure concern its size and the acoustic nodes. In the DVB-T case, the use of this cumbersome duct to convey and then cancel the noise is not practical. The ANC methods should allow a reduction of the used space compared to the passive methods. Furthermore, the structure is subject to resonances. If the microphones are positioned in the vicinity of an acoustic node the performances could get worse.

7.3 Case 2 - ANC system outside the duct

Contrary to the previous case, the test bed presented in this section allows many variations and arrangements of sensors and actuators. The structure is always based on a wooden duct with the same square cross-section d =11 cm, but shorter length L =40 cm. It allows a fixed arrangement only for the noise source and the reference microphone. In particular, the loudspeaker used as noise source is positioned in one of the two ends of the duct and the reference microphone is 12 cm away from it. Instead, the error microphone and the cancelling loudspeaker(s) can be positioned freely out of the duct. Several arrangements have been tested, the most important ones of which will be explained here.

Also in this case, the calculation of the resonance frequencies is supported by practical results. Equation 5.5 estimates that the first resonances of this duct occur at 194 Hz, 581 Hz and 968 Hz. Observing the frequency responses of $\widehat{S}(z)$ and $\widehat{F}(z)$ in Figure 7.7, it is possible to observe magnitude peaks near the aforementioned frequencies.

7.3.1 Configurations

Among all the possible loudspeaker/error-mic configurations, three of them have been studied in detail. All the implementative solutions that will be presented here have one common point: the position of the error microphone. It has been positioned immediately at the end of the duct, on the edge of the duct wall to take into account, and hence avoid, the

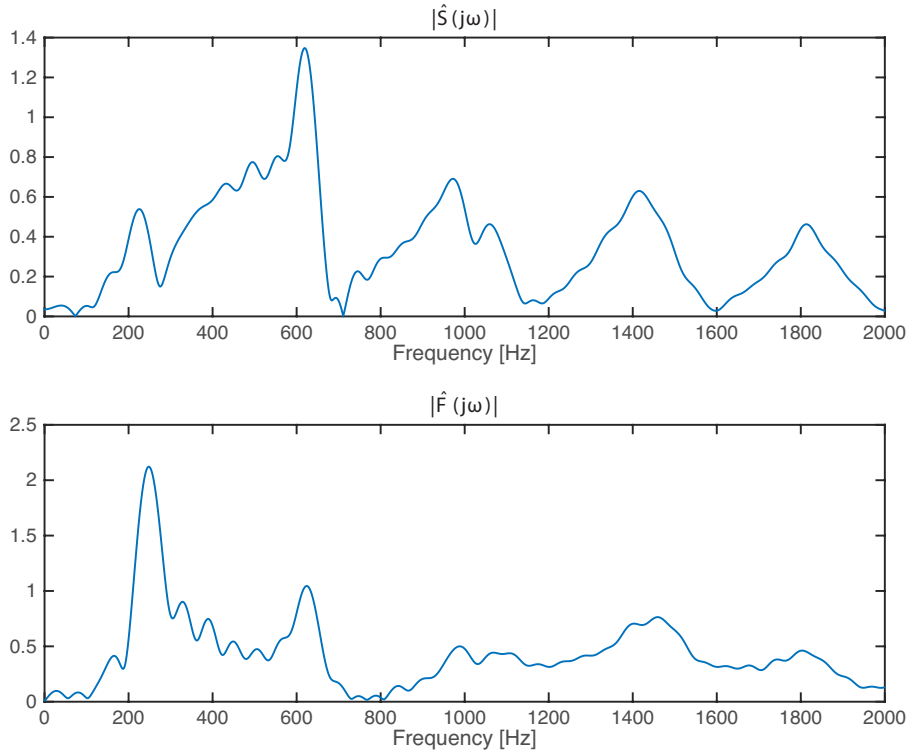

Figure 7.7: Case 2: impulse response magnitudes of the FIR filters $\widehat{S}(z)$ (top) and $\widehat{F}(z)$ (bottom).

hypothetical air flow effect. The location of the cancelling loudspeaker is different in the three implementations:

- Loudspeaker oriented towards the inside of the duct (Figure 7.8a).
- Loudspeaker oriented perpendicularly with respect to the duct (Figure 7.8c).
- Loudspeaker positioned in parallel and before the end of the duct (Figure 7.8e).

These three configurations have been considered because, despite their simplicity, they achieve the best results and are applicable to the DVB-T problem. For each of these three configurations, two versions were tested, one with a single cancelling loudspeaker, one using two loudspeakers, both driven by the same anti-noise signal, as shown in Figure 7.8b, 7.8d and 7.8f. Thus a total of six setups have been tested, all of them with the same number of taps per filter ($N_{\widehat{S}} = 60$, $N_{\widehat{F}} = 62$ and $N_W = 108$) and the same value of the step-size $\mu = 0.01$.

Figures 7.9 and 7.10 show, through magnitude and phase respectively, that the frequency response of $\widehat{S}(z)$ and $\widehat{F}(z)$ is very similar in all the three configurations. Compared to the other cases, an externally oriented loudspeaker results in a lower frequency response for the feedback path. Thus, in terms of system stability and convergence rate, the choice of a positioning rather than another has no significant effects.

7.3.2 Attenuation performances

The performance analysis of this physical structure was carried out in the same manner of Case 1. For each proposed setup, a study of the attenuation performance at the error microphone was carried out applying the EE-FxLMS algorithm to 33 tones within the frequency range of $200 \div 1000$ Hz. The results obtained from every loudspeaker arrangement are very similar to each other. In fact, among the different tests, small random variations of maximum 5 dB occur for some tones. The results of each configuration are shown in Figure 7.11.

Also in this case the results obtained are good, with a reduction of at least 35 dB for almost all the tones. But compared to Case 1, performances are lower by approximately 10 dB, which is probably related to the physical structure used for the tests. The application of the ANC system internally to the duct (Case 1) allows the noise cancellation before the open end. In this way, the signal picked up by the error microphone has no power losses

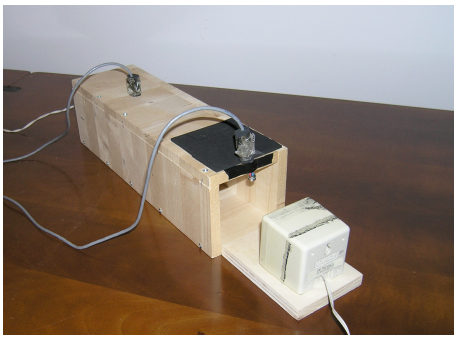

(a) Single cancelling loudspeaker internally oriented

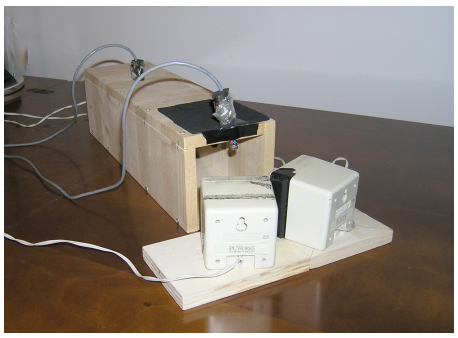

(b) Double cancelling loudspeaker internally oriented

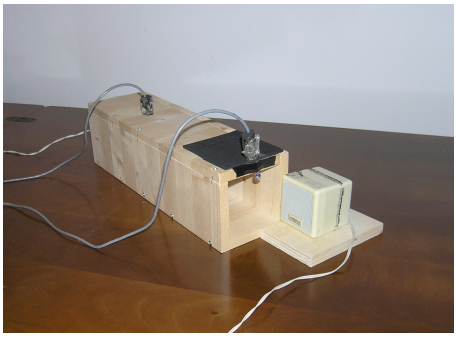

(c) Single cancelling loudspeaker perpendicularly oriented

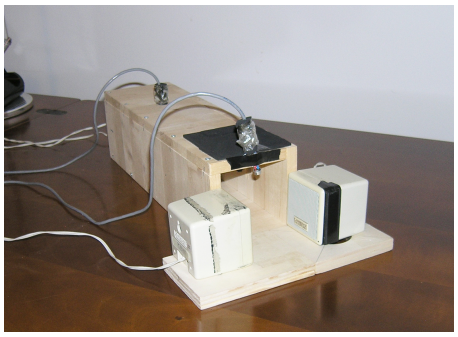

(d) Double cancelling loudspeaker perpendicularly oriented

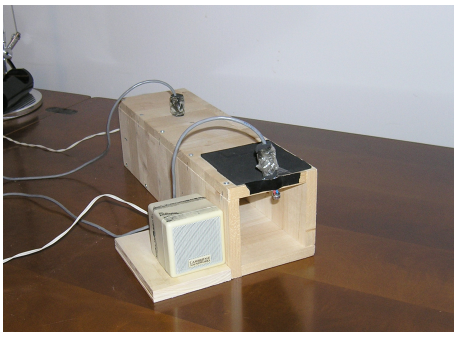

(e) Single cancelling loudspeaker externally oriented

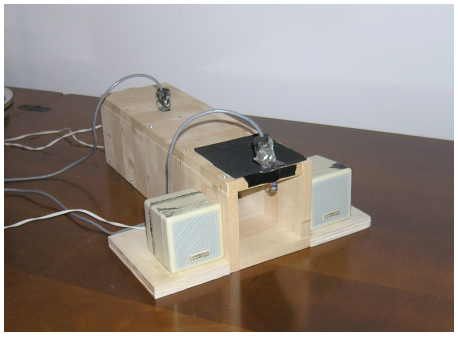

(f) Double cancelling loudspeaker externally oriented

Figure 7.8: Case 2: wooden duct with all the sensors and actuators of the ANC system located internally.

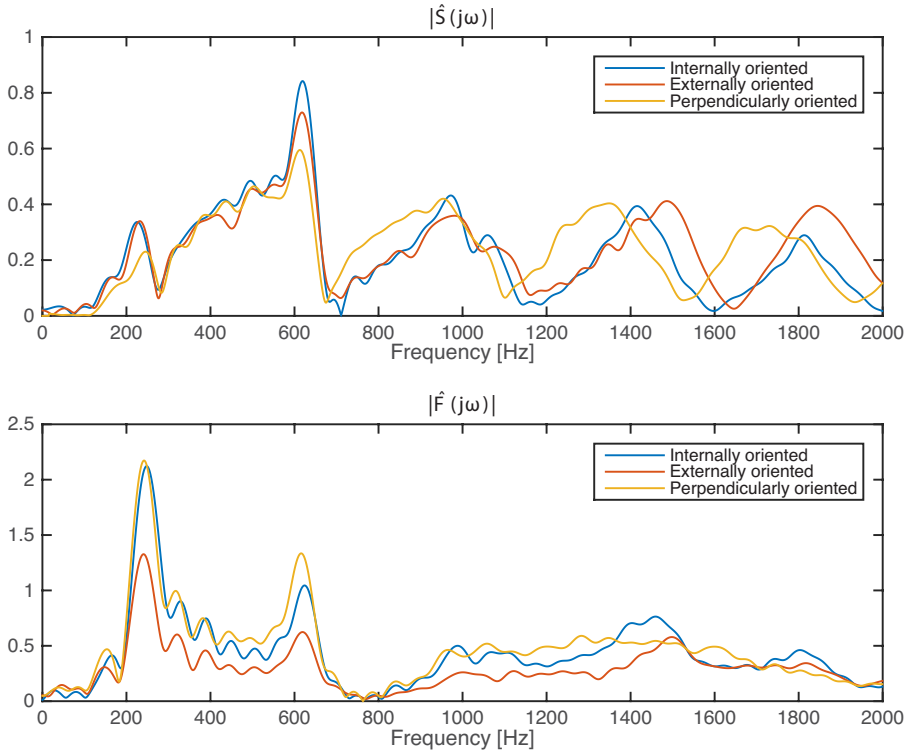

Figure 7.9: Case 2: magnitude comparison between the frequency response of $\widehat{S}(z)$ and $\widehat{F}(z)$ identified using three different loudspeaker configurations.

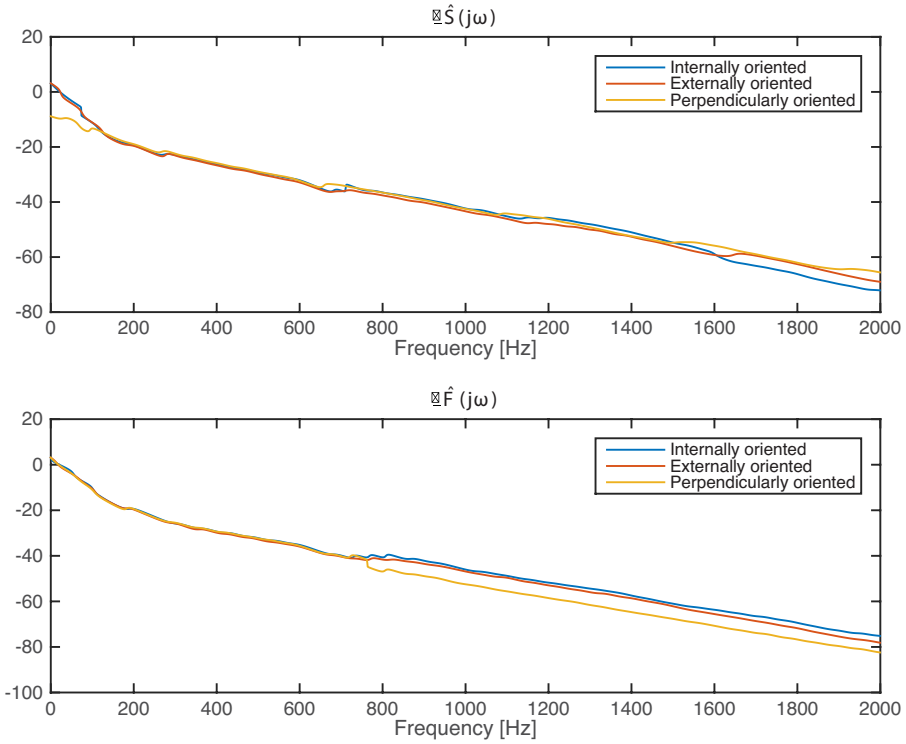

Figure 7.10: Case 2: phase comparison between the frequency response of $\widehat{S}(z)$ and $\widehat{F}(z)$ identified using three different loudspeaker configurations.

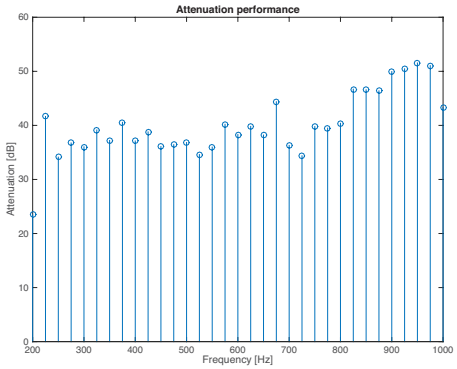

(a) Single cancelling loudspeaker internally oriented

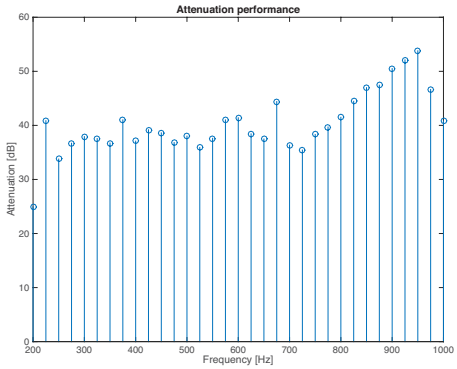

(b) Double cancelling loudspeaker internally oriented

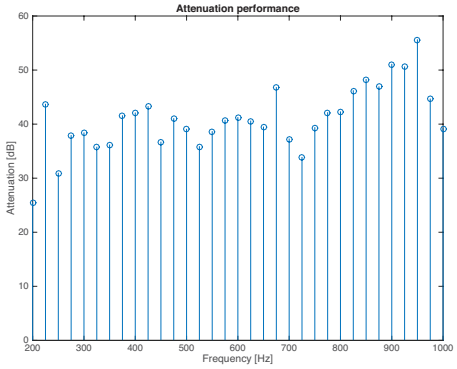

(c) Single cancelling loudspeaker perpendicularly oriented

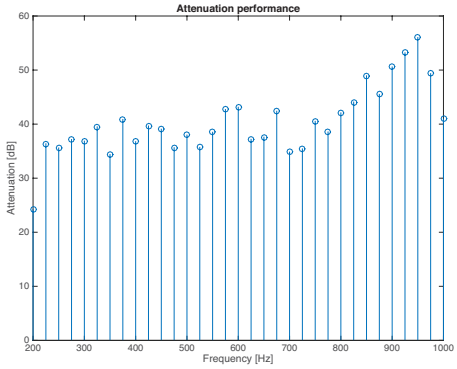

(d) Double cancelling loudspeaker perpendicularly oriented

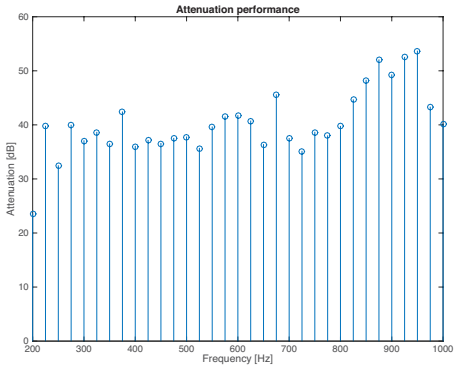

(e) Single cancelling loudspeaker externally oriented

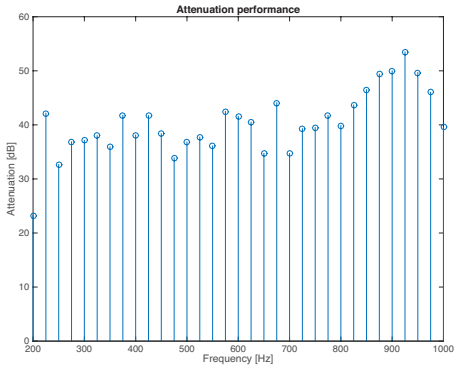

(f) Double cancelling loudspeaker externally oriented

Figure 7.11: Case 2: attenuation perfomances at the error microphone.

due to the propagation (ideally). Instead, the setups used here force the ANC system to operate externally. The signal acquired by the external error microphone is subject to power loss, hence the attenuation is limited.

Despite these optimistic results, not every loudspeaker configuration leads to a noise reduction in the surrounding environment. In fact, different effects are obtained with different choices in the speakers arrangement. Amplification or reduction of the perceived noise can occur although the residual error at the error microphone is reduced by more than 35 dB. The attenuation perceived at the workstation is evaluated using a sinewave of frequency 500 Hz as noise signal. Figure 7.12 shows the result of this test, comparing the attenuation performance of the six setups using the laptop microphone. An amplification of 2-5 dB is perceived, when using one or two loudspeakers oriented externally to the duct. With the four remaining setups the noise reduction is appreciable even away from the error microphone, and the best performances are reached by orienting the actuator internally to the duct. Greater attenuation (or amplification) is achieved using two loudspeakers, compared to the corresponding configurations with a single loudspeaker.

As a last test, the attenuation performance of the proposed method is analysed by applying it to the signal acquired by the DVB-T fans. Once again, the results are very similar between the different configurations, a reduction of 5 dB being reached by each one. Figure 7.13 illustrates the power spectrum and the RMS value in dB of the signal acquired by the error microphone. Being the results of the six tests comparable, only one of them is illustrated here.

7.3.3 Pros and cons

The advantages and disadvantages regarding the presented configurations will be described below.

Internally oriented structure

- Pros: greater attenuation perceived;
- Cons: the speaker is an obstacle for a hypothetical air flow.

Perpendicularly oriented structure

- Pros: the speaker does not preclude the incoming or outgoing air flow from the duct;
- Cons: the attenuation perceived in the surrounding environment is not optimal.

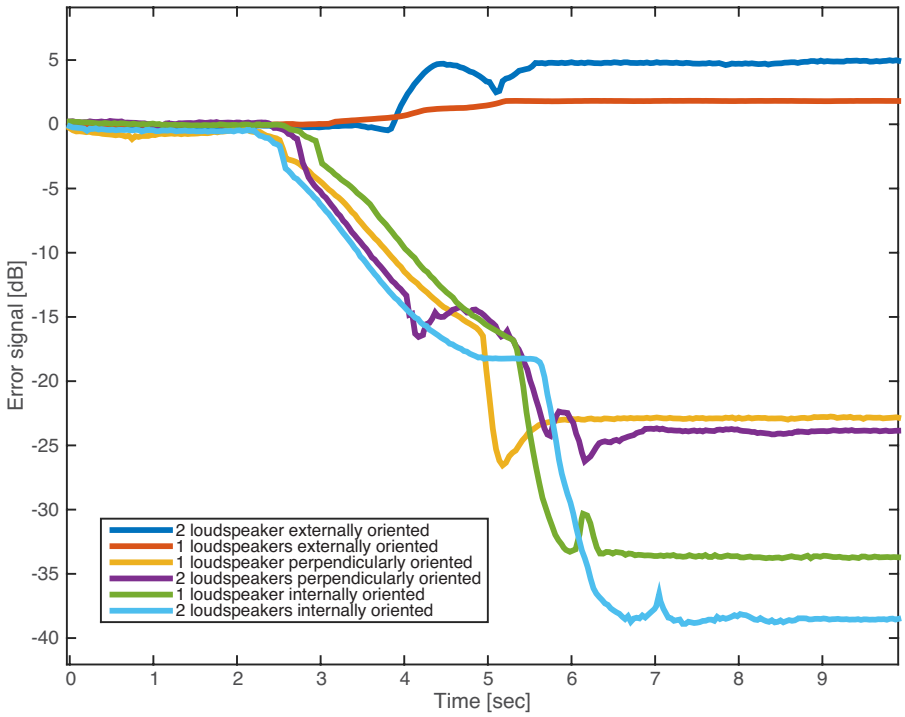

Figure 7.12: Case 2: comparison between the residual noise acquired at the workstation with the laptop's built-in microphone using six different loudspeaker configurations.

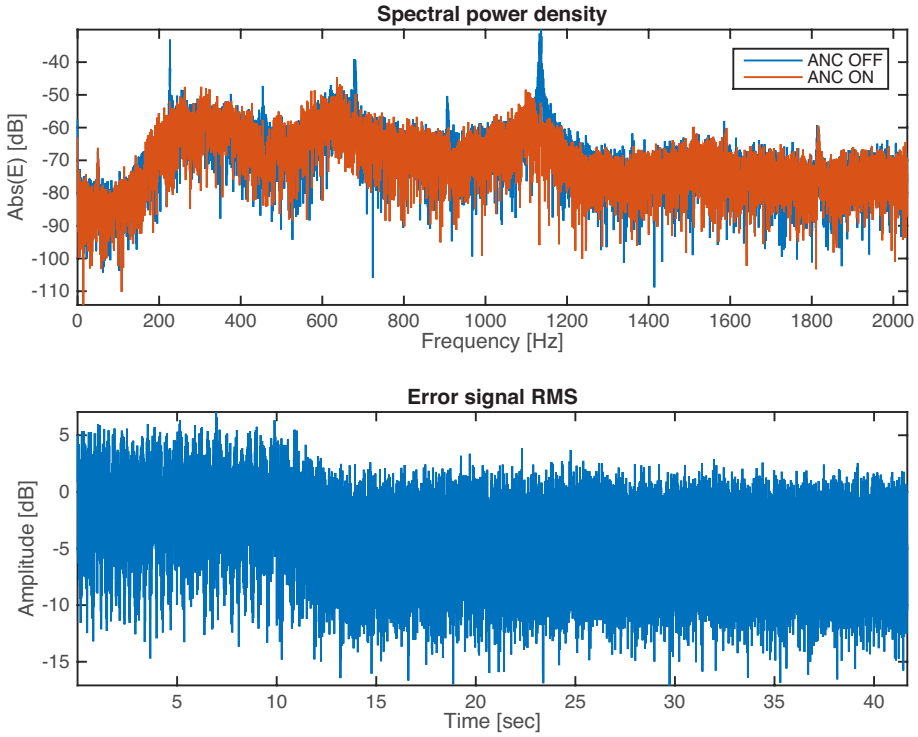

Figure 7.13: Case 2: attenuation performance at the error microphone using the proposed method applied to the DVB-T fans noise signal.

Externally oriented structure

- Pros: the speaker does not preclude the incoming or outgoing air flow from the duct and a smaller feedback component is present to the reference microphone;
- Cons: the attenuation in the vicinity of the error microphone does not involve reduction of noise in the surrounding environment, but amplification occurs.

Therefore, the best configuration applicable to the DVB-T case is the one with the loudspeaker oriented perpendicular to the duct. The ANC system should not prevent the proper functioning of the DVB-T system, by limiting the airflow required for the cooling purpose. For this reason, it is preferable to have a lower environmental attenuation without risking damages to the DVB-T device.

7.4 Case 3 - ANC system without the duct

In this last case, an analysis of the ANC system will be carried out without any duct. This setting is very close to the DVB-T case, since the two fans can be seen as a single noise source in the open field. Sensors and actuators are thus subjected to the external disturbances, uncorrelated with the fans noise. As can be observed in Figure 7.14, a loudspeaker is used as the noise source, the reference microphone is positioned close to the noise source in order to acquire only the signal emitted from it. The cancellation is carried out through one or two loudspeakers, directed towards the noise source and approximately 10 cm away from it. The error microphone is positioned close to the anti-noise source.

Figure 7.15 and 7.16 show respectively the magnitude and the phase of the frequency responses of the estimates $\widehat{S}(z)$ and $\widehat{F}(z)$. For each acoustic path estimate two plots are presented, regarding the use of one or two cancelling loudspeaker. The magnitude does not exhibit peaks related to resonances, due to the absence of a duct.

Three tests were carried out, as before. The first uses the EE-FxLMS algorithm to analyse the cancellation performance of 33 tones, the second evaluates the attenuation in the surrounding environment and the last applies the method proposed in this thesis to cancel the noise produced by the DVB-T fans. The tests were performed using an adaptive filter of length $N_W = 96$ and a step-size equal to $\mu = 0.01$. After being reduced in order, the length of the acoustic path estimates are $N_{\widehat{S}} = 88$ and $N_{\widehat{F}} = 74$.

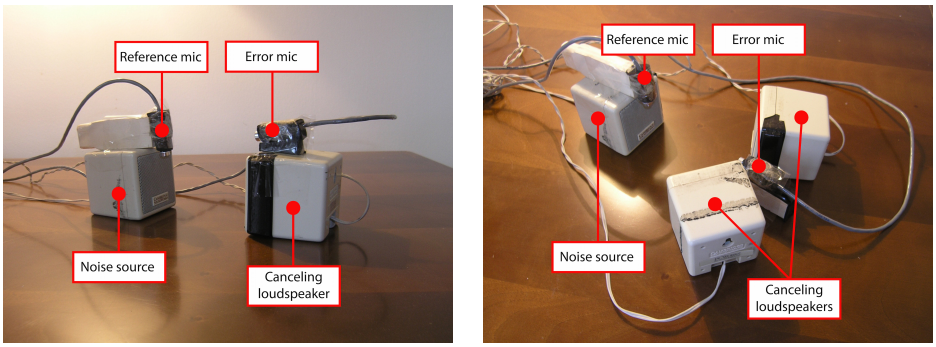

(a) Single cancelling loudspeaker setup **(b)** Double cancelling loudspeaker setup

Figure 7.14: Case 3: ANC system in the free field using one or two cancelling sources.

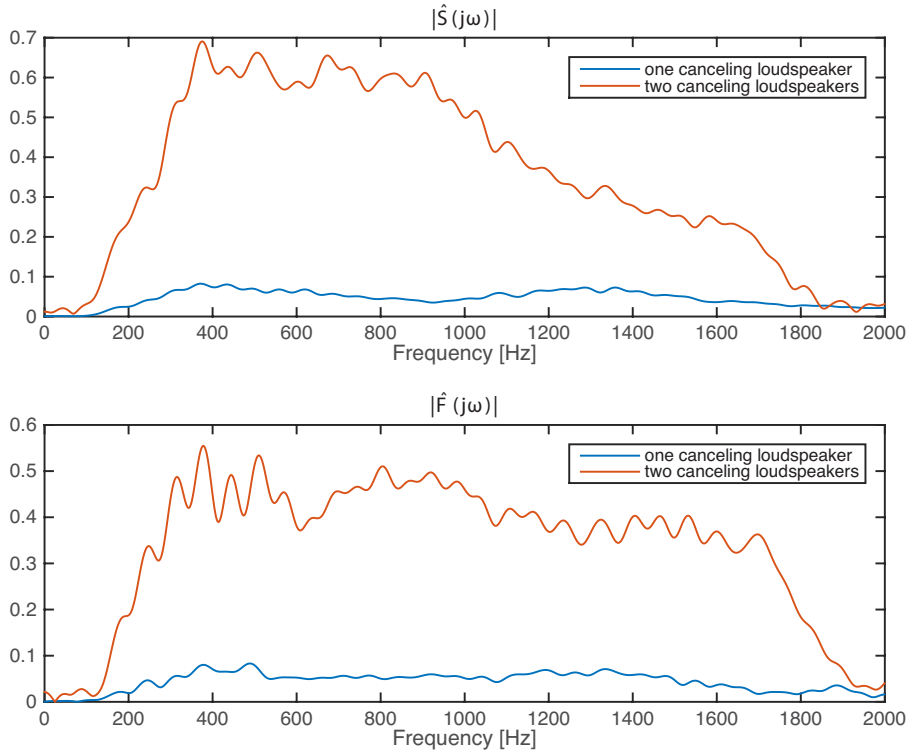

Figure 7.15: Case 3: magnitude comparison between the frequency response of $\widehat{S}(z)$ and $\widehat{F}(z)$ identified using one or two loudspeakers.

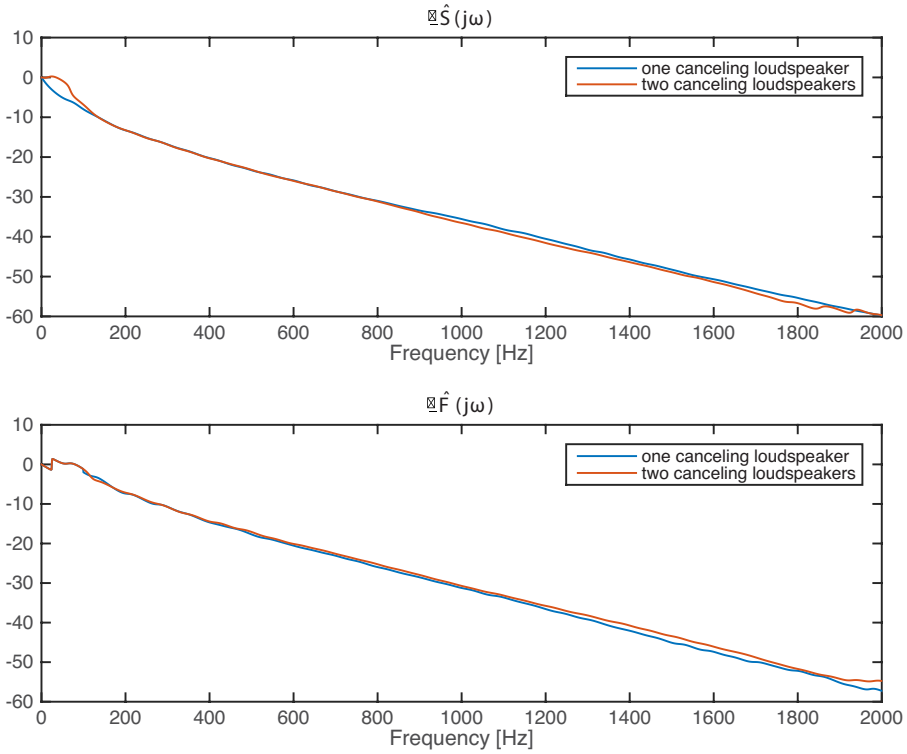

Figure 7.16: Case 3: phase comparison between the frequency response of $\widehat{S}(z)$ and $\widehat{F}(z)$ identified using one or two loudspeakers.

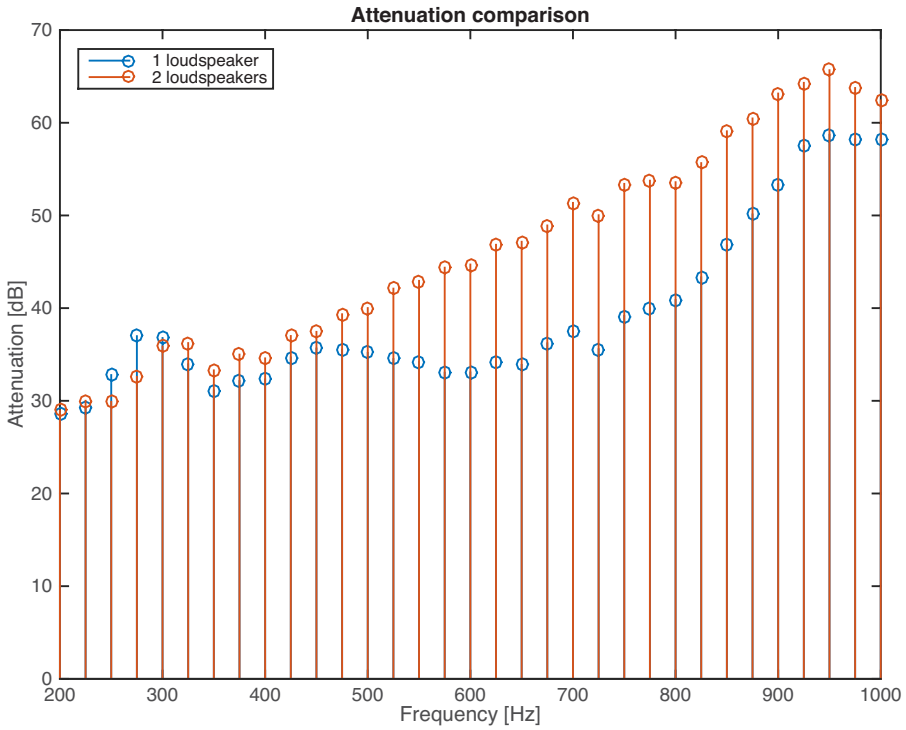

Figure 7.17: Case 3: comparison between the attenuation performances at the error microphone using one or two loudspeakers.

7.4.1 Attenuation performances

The results obtained from the test with tones are shown in Figure 7.17. The noise attenuation gradually grows as the frequency of the tones increases, starting from 30 dB at 200 Hz, up to approximately 60 dB at 1000 Hz. This frequency dependent behaviour is probably related to sound wave dispersion in space. For equal initial power, the lower frequency waves are subject to greater dispersion than those at higher frequency. Then, the signal acquired at the error microphone is reduced even before the ANC operates. This probably didn't happen in previous cases because of the duct structures, which conveyed the sound wave toward a single direction. Also the use of one or two cancelling loudspeakers results in a frequency dependent attenuation. As the frequency of the tones increases, the best performance is achieved by using two actuators instead of one.

Tests on the perceived noise at the working position were performed always with a tone of 500 Hz and using both loudspeaker configurations. The residual noise at the laptop microphone is shown in Figure 7.18 using the RMS measure in dB. Using two loudspeakers results in a greater

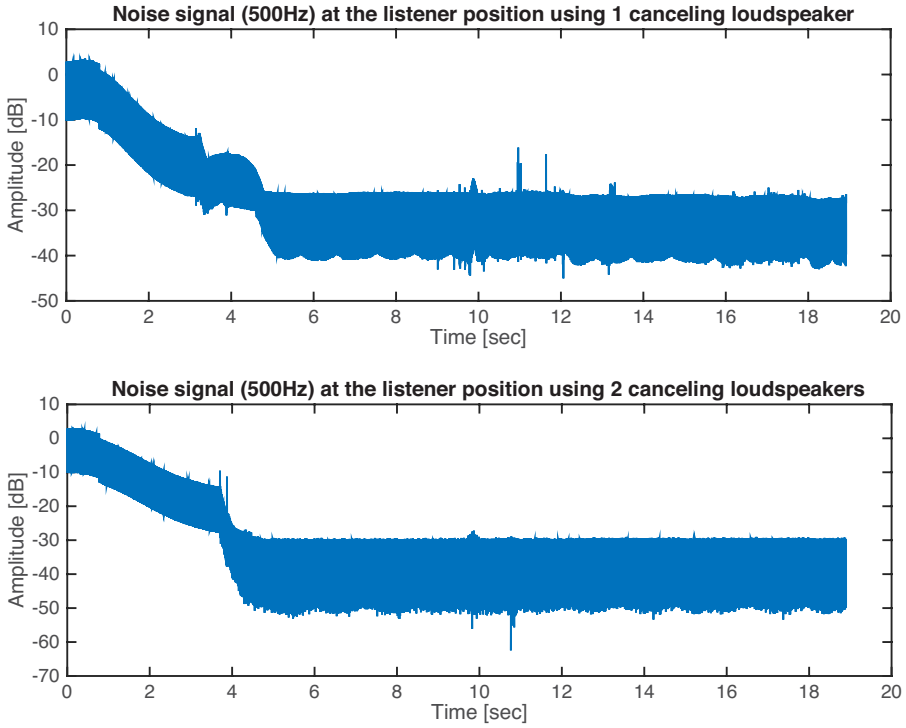

Figure 7.18: Case 3: comparison between the attenuation performances at the workstation using one or two loudspeakers.

attenuation (40 dB, compared to 35 dB with a single actuator).

In the test with the signal emitted by the DVB-T fans, the attenuation is very similar to the previous cases. A maximum reduction of 5 dB is achieved by using two cancelling loudspeakers, as shown in Figure 7.20. A lower performance is achieved with a single actuator, a reduction of only 3 dB as shown in Figure 7.19.

7.4.2 Pros and cons

In this last case the implemented ANC system has the advantage of not using a duct, which can be cumbersome for a real world application. In the case of the DVB-T device it would suffice to apply the microphones and cancelling loudspeaker near the fans region, saving on space and costs. In contrast, the lack of a duct leads to a more homogeneous sound propagation in space and therefore greater difficulty or even impossibility of an overall noise cancellation with a single-channel ANC system.

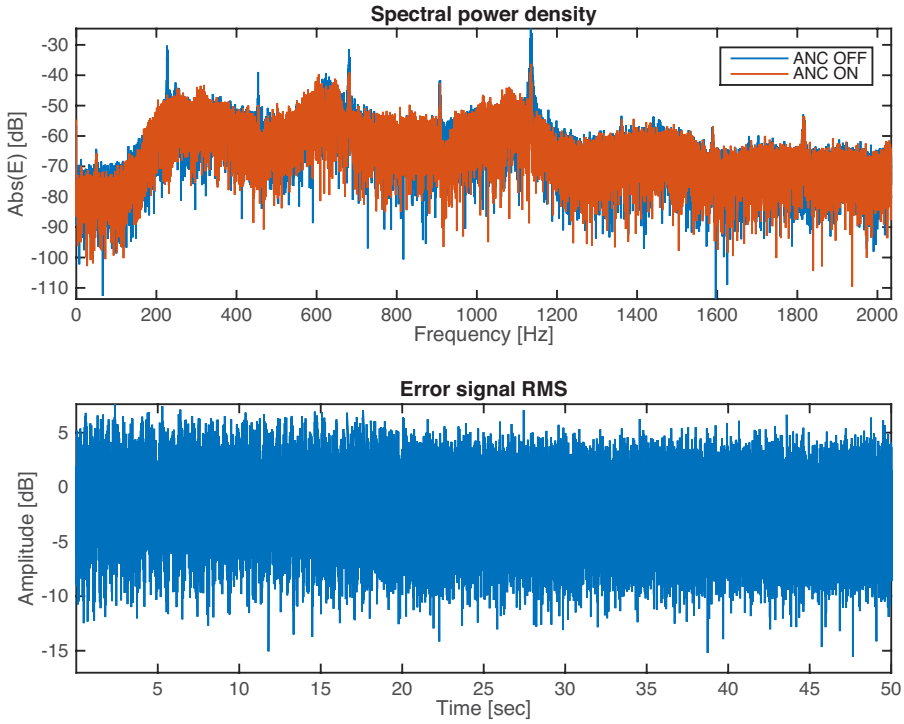

Figure 7.19: Case 3: attenuation performance at the error microphone using one loudspeaker. The proposed method is applied to the DVB-T fans noise signal.

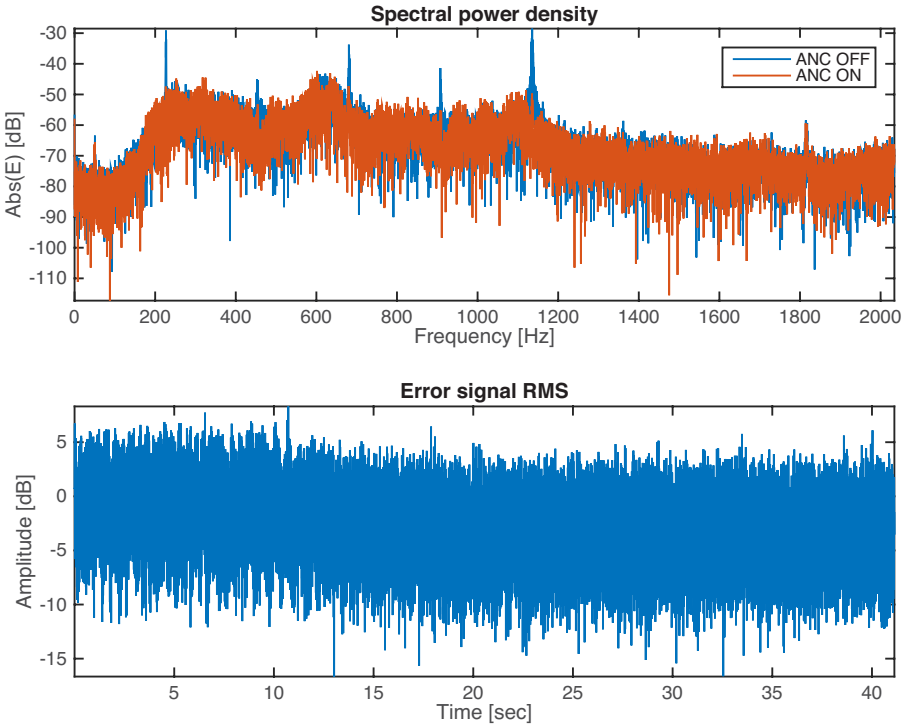

Figure 7.20: Case 3: attenuation performance at the error microphone using two loudspeakers. The proposed method is applied to the DVB-T fans noise signal.

Chapter 8

Results with the DBV-T

This last chapter presents the results obtained by applying the proposed method to the DVB-T device. Two approaches are presented with the aim of canceling the noise produced from the cooling fans. The first is characterized by the use of a wooden duct, applied to the protective grid of the fans. The second approach implements the ANC in the open field, without the use of auxiliary structures. The tests presented here were conducted in a room subject to reverberation and sound refraction, a similar environment compared to the one in which the DVB-T device usually operates.

8.1 Test with the duct

A rectangular wooden duct has been applied to the protective grid of the fans, with the aim to contain the noise and isolate the ANC system from external disturbances. The dimensions of the duct are the following:

- Length= 30 cm;
- Height= 8 cm;
- Width= 17 cm.

The sensors are positioned centrally, close to the duct walls to limit the effect of the flow noise. The reference microphone and the error microphone are placed respectively at 5 cm and 17 cm away from the grid. The loudspeakers are positioned 14 cm apart, facing each other, on the edge of the walls to allow the air flow, as shown in Figure 8.1.

With this structure, the equation 5.5 can not be applied to estimate the resonance frequencies because of its rectangular shape. However, the

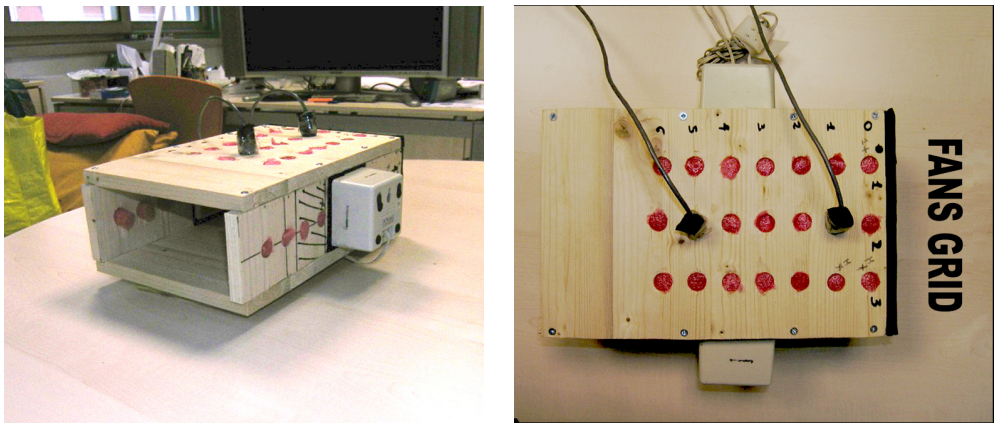

(a) (b)

Figure 8.1: Detail of the duct applied to the DVB-T device.

frequency response of the acoustic paths estimates can give an idea of the duct resonances. Observing Figure 8.2, a peak related to the resonance frequency is present at 300 Hz.

The application of this structure (Figure 8.4) conditions the noise produced and modifies the natural propagation. The resulting noise signal is not the same of Figure 3.5 studied so far, and has a stronger component at the fundamental frequency ($f_0 = 1135$ Hz), as shown in Figure 8.3.

The test was carried out using the method proposed in Chapter 4. The length of the adaptive filter $W(z)$ and of the estimates of the acoustic paths are respectively $N_W = 102$, $N_{\widehat{S}} = 75$ and $N_{\widehat{F}} = 55$. The results obtained from the application of the proposed ANC method are shown in Figure 8.5. The attenuation on the error microphone is approximately 5 dB, but it is not possible to perceive a reduction of noise in the surrounding environment. The reason is that the DVB-T machinery does not generate noise only from a precise point. There are at least two noise sources, the first represented by the cooling fans, the second corresponding to the vent for the outlet of the air flow created by the fans. This second noise source is positioned at the opposite side with respect to the fans, as shown in Figure 8.7. The rear side of the device presents a very similar noise signal respect the one produced by the fans, with a bigger component of background noise due to flow noise (see Figure 8.6). Moreover, the sound diffraction of the room contributes to reduce the apparent attenuation. Recordings made with the internal microphone of the laptop confirm this statement, as no noise reduction is appreciable from the working position.

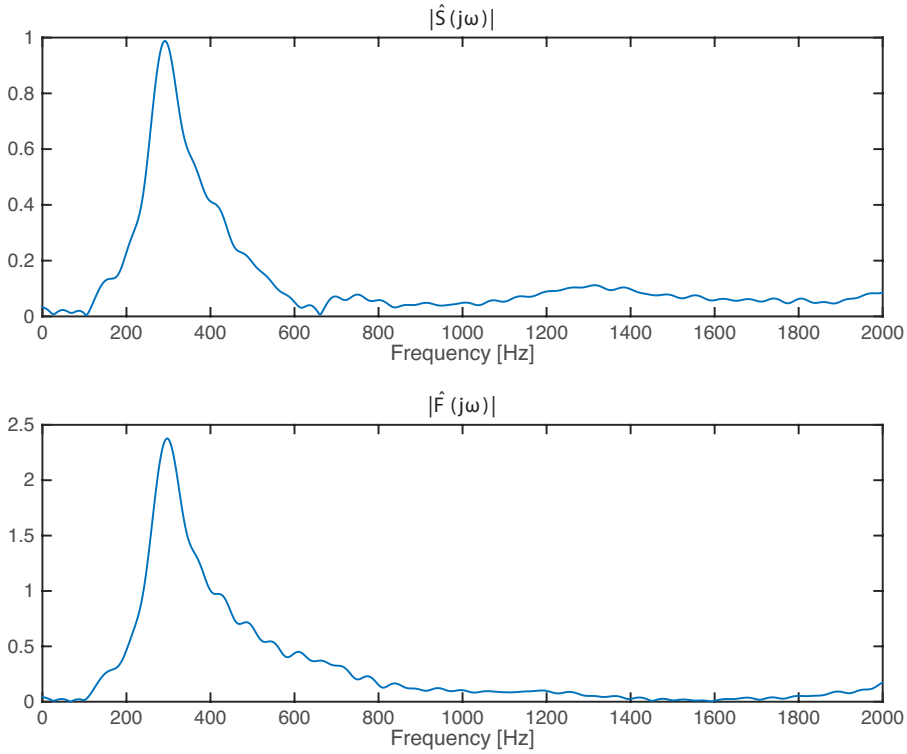

Figure 8.2: Impulse response magnitudes of the FIR filters $\widehat{S}(z)$ (top) and $\widehat{F}(z)$ (bottom) estimated with the duct.

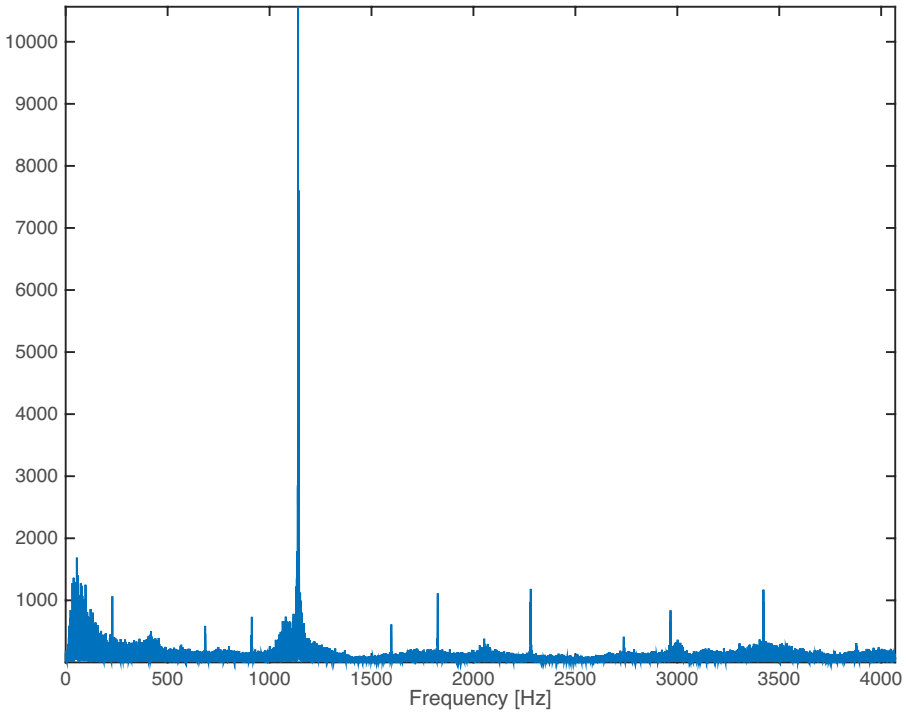

Figure 8.3: FFT of the noise signal produced by the DVB-T fans acquired inside the duct.

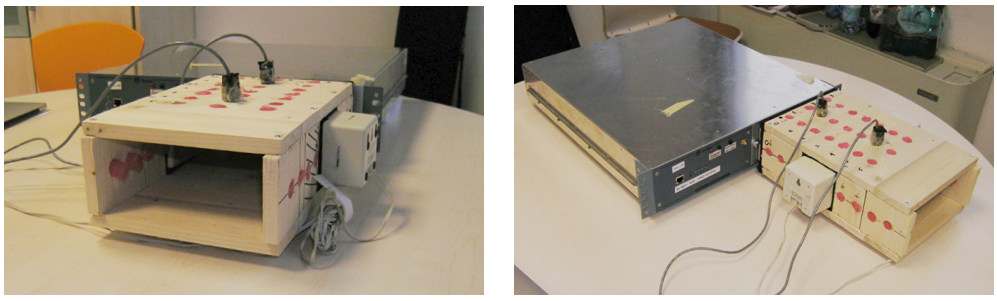

(a) **(b)**

Figure 8.4: Duct applied close to the DVB-T protective grid

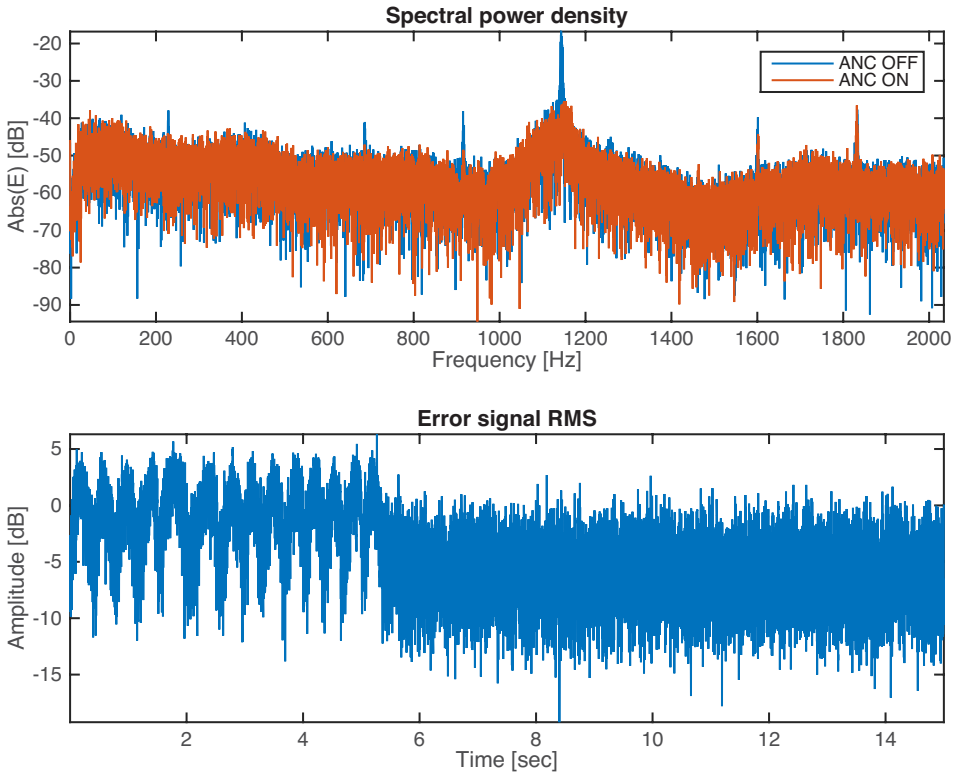

Figure 8.5: Attenuation performance at error microphone using the duct.

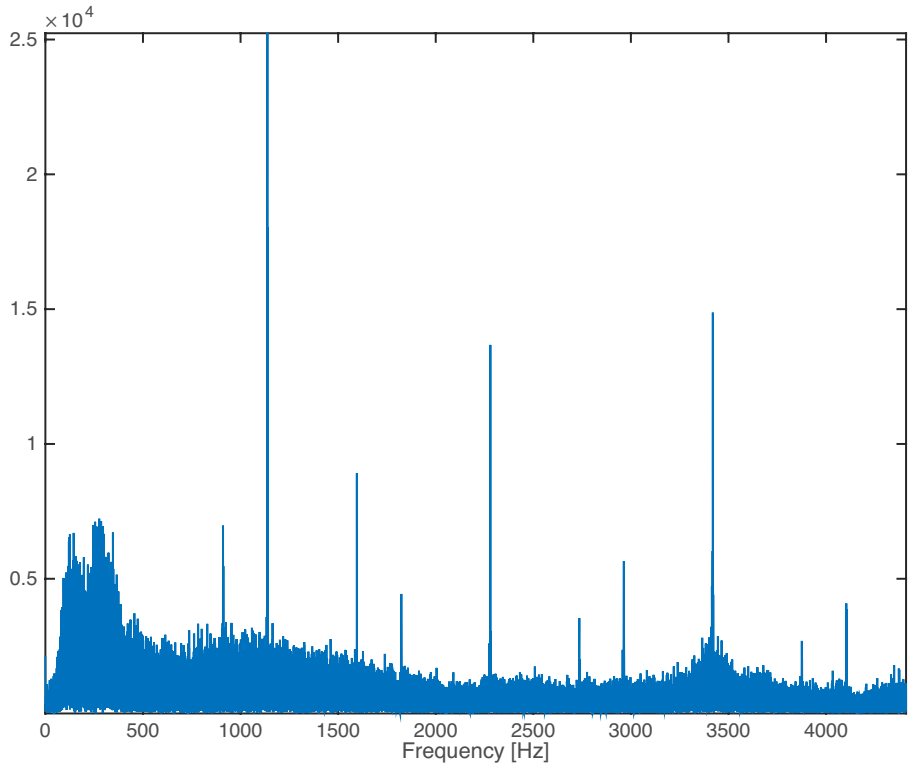

Figure 8.6: FFT of the noise signal produced by the rear side of the DVB-T.

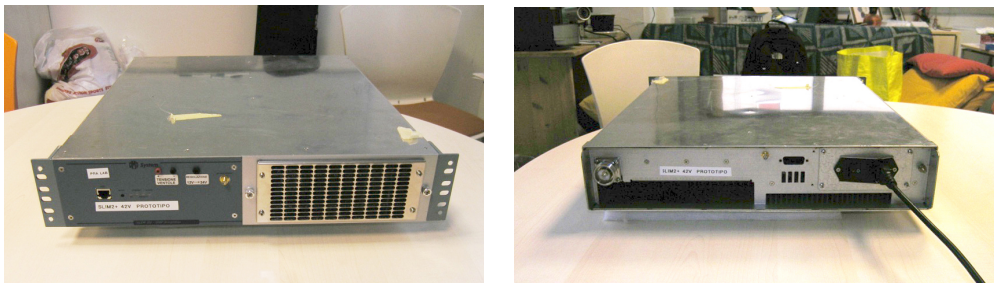

(a) Detail of the front side **(b)** Detail of the rear side

Figure 8.7: DVB-T device under analysis.

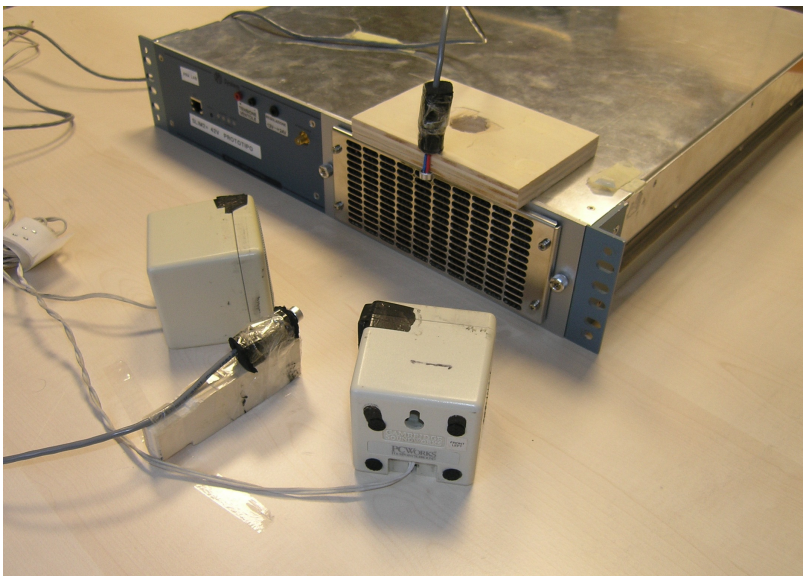

Figure 8.8: Positioning of the ANC sensors and actuators for the control of the DVB-T noise in the free field.

8.2 Test without the duct

This last test concludes the study presented in this thesis. The absence of a duct causes a homogeneous propagation of the noise in the surrounding environment. As discussed in Case 3 of Chapter 7, the use of two loudspeakers leads to better results in the ANC applied to the open field. Accordingly, the same choice was made in this test by placing the two actuators and the error microphone 8 cm away from the fans, as shown in Figure 8.8. The cancellation sources are quite distant from the protective grid, so it is possible to assert that their presence cannot be a hindrance to the cooling performance. The reference microphone is positioned close to the protective grid and in a parallel way with respect to the air flow, so as to limit the flow noise.

The test was performed using an adaptive filter of length $N_W = 98$, and acoustic path estimates of $N_{\widehat{S}} = 80$ and $N_{\widehat{F}} = 74$. The results obtained in this test are similar to the previous one. An attenuation of 5 dB is achieved by applying the proposed method, as shown in Figure 8.9. The fundamental frequency component is completely removed, while the background noise is not attenuated. Despite the attenuation achieved at the error microphone, a noise reduction in the surrounding environment is not appreciable for the same reasons discussed in the previous case.

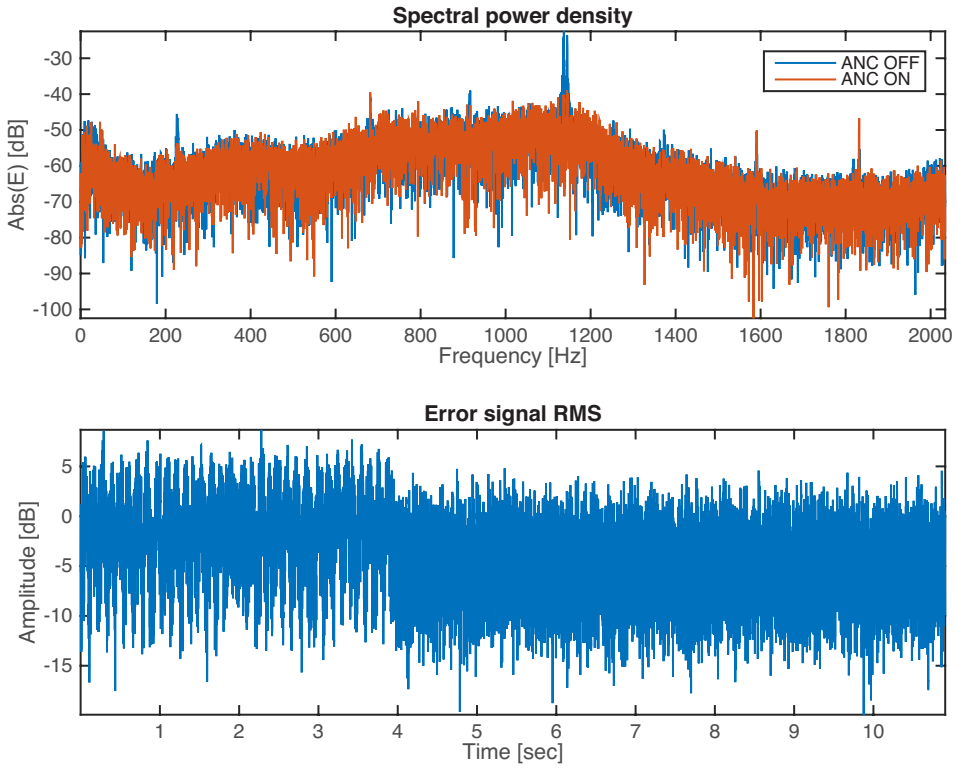

Figure 8.9: Attenuation performance at error microphone in the free field.

Conclusions and future work

In this thesis an ANC method applied to an HVAC system has been studied. The final implementation for the DVB-T case was reached gradually, first by analysing the behaviour of the ANC system implemented on standard physical structures, and subsequently, by adding or removing elements of the system in order to find the best solution to the DVB-T noise problem. The results obtained in the tests meet partially the expectations. In tests, all the theoretical concepts initially discussed have been validated. A high level of noise attenuation is achieved by the implemented ANC systems using synthetic noise sources (single-tone or multiple-tone). Also, if the proper precautions are taken when positioning the sensors and actuators, even a reduction of the noise in the environment is obtained. In particular, it was noted that while the orientation of the speakers does not significantly change the attenuation performance in the vicinity of the error microphone, it can radically change the reduction of noise in the surrounding environment as shown in Case 2 of Chapter 7. Problems arise when there is a strong background noise component. This is the case of the noise produced by the fans of the DVB-T device. The method used in order to optimize the ANC system in the DVB-T case is effective because, contrary to the standard FxLMS-based methodologies, the proposed method does not diverge. The proposed method is similar to those needed for other ANC systems. However, the right combination of all its parts allows the attenuation of the signal produced by the DVB-T device. Despite this, using systems based on the FxLMS algorithm, the performance is limited and only the narrowband components can be reduced, allowing an attenuation of approximately 5 dB in all cases presented previously. This limit in performance is due to many factors. The implemented system attempts to remove the noise from two sources, i.e. the two fans. But a single-channel ANC system is used for this purpose, when it would be more appropriate to use a multi-channel implementation, with a reference microphone and a speaker for each noise source. Also as discussed in Chapter 8, the DVB-T device has additional sources of noise in addition

to the two fans. To ensure that the noise cancellation is perceptually appreciable, it would be appropriate to implement an ANC system also for the other noise sources. A comprehensive study on the DVB-T device radiation pattern can be useful in order to identify the main noise sources, not limited to an evaluation of the noise emitted by the cooling fans, but analysing all sides of the device. A better performing DSP is necessary, as the implementation of a multi-channel system requires a higher computational burden and therefore higher costs related to the instrumentation involved. A possible performance improvement can be achieved by making use of physical structures (ducts) to isolate the noise and limit the flow noise that affects the sensors.

Bibliography

[1] D Morgan. An analysis of multiple correlation cancellation loops with a filter in the auxiliary path. *IEEE Transactions on Acoustics, Speech, and Signal Processing*, 28(4):454–467, 1980.

[2] John C Burgess. Active adaptive sound control in a duct: A computer simulation. *The Journal of the Acoustical Society of America*, 70(3): 715–726, 1981.

[3] Lueg Paul. Process of silencing sound oscillations, June 9 1936. US Patent 2,043,416.

[4] Sen M Kuo and Dennis R Morgan. Active noise control: a tutorial review. *Proceedings of the IEEE*, 87(6):943–973, 1999.

[5] Sen M Kuo, Issa Panahi, Kai M Chung, Tom Horner, Mark Nadeski, and Jason Chyan. Design of active noise control systems with the tms320 family. *Texas Instruments*, 1996.

[6] Yoshinobu Kajikawa, Woon-Seng Gan, and Sen M Kuo. Recent advances on active noise control: open issues and innovative applications. *APSIPA Transactions on Signal and Information Processing*, 1:e3, 2012.

[7] Sen M Kuo and Dennis Morgan. *Active noise control systems: algorithms and DSP implementations*. John Wiley & Sons, Inc., 1995.

[8] Colin Hansen, Scott Snyder, Xiaojun Qiu, Laura Brooks, and Danielle Moreau. *Active control of noise and vibration*. CRC Press, 2012.

[9] Luigi Piroddi. Active control of noise and vibrations - educational material. Master degree in Computer Engineering - Sound and Music Engineering, 2012/13.

[10] JR Glover. Adaptive noise canceling applied to sinusoidal interferences. *IEEE Transactions on Acoustics, Speech, and Signal Processing*, 25 (6):484–491, 1977.

[11] Yegui Xiao. A new efficient narrowband active noise control system and its performance analysis. *IEEE Transactions on Audio, Speech, and Language Processing*, 19(7):1865–1874, 2011.

[12] Yegui Xiao, Liying Ma, Khashayar Khorasani, and Akira Ikuta. A new robust narrowband active noise control system in the presence of frequency mismatch. *IEEE Transactions on Audio, Speech, and Language Processing*, 14(6):2189–2200, 2006.

[13] Sen M Kuo and Ajay B Puvvala. Effects of frequency separation in periodic active noise control systems. *IEEE Transactions on Audio, Speech, and Language Processing*, 14(5):1857–1866, 2006.

[14] Ryan Leonard Rust. Active noise control of a two-fan exhaust-mounted array using near-field control sources and error sensors. 2010.

[15] GIACOMO LAITA. Active noise control: a case study. 2013.

[16] V Vinay, V Roopashree, SV Narasimhan, and M Shivamurti. Active noise control using variable step-size griffiths' lms (vglms) algorithm on real-time platform. 2010.

[17] Pooya Davari and H Hassanpour. A robust feedforward active noise control system with a variable step-size fxlms algorithm: Designing a new online secondary path modelling method. *International Journal of Engineering-Transactions A: Basics*, 21(3):231, 2008.

[18] CC Boucher, SJ Elliott, and PA Nelson. Effect of errors in the plant model on the performance of algorithms for adaptive feedforward control. In *IEE Proceedings F-Radar and Signal Processing*, volume 138, pages 313–319. IET, 1991.

[19] Jared K Thomas, Stephan P Lovstedt, Jonathan D Blotter, and Scott D Sommerfeldt. Eigenvalue equalization filtered-x algorithm for the multichannel active noise control of stationary and nonstationary signals. *The Journal of the Acoustical Society of America*, 123(6): 4238–4249, 2008.

[20] Laszlo Sujbert. A new filtered lms algorithm for active noise control. *Active 99*, pages 1101–1110, 1999.

[21] Victor E DeBrunner and Dayong Zhou. Hybrid filtered error lms algorithm: another alternative to filtered-x lms. *IEEE Transactions on Circuits and Systems I: Regular Papers*, 53(3):653–661, 2006.

[22] Shigeyuki Miyagi and Hideaki Sakai. Mean-square performance of the filtered-reference/filtered-error lms algorithm. *IEEE Transactions on Circuits and Systems I: Regular Papers*, 52(11):2454–2463, 2005.

[23] Orlando José Tobias and Rui Seara. Leaky-fxlms algorithm: stochastic analysis for gaussian data and secondary path modeling error. *IEEE Transactions on speech and audio processing*, 13(6):1217–1230, 2005.

[24] David A Cartes, Laura R Ray, and Robert D Collier. Lyapunov tuning of the leaky lms algorithm for single-source, single-point noise cancellation. In *American Control Conference, 2001. Proceedings of the 2001*, volume 5, pages 3600–3605. IEEE, 2001.

[25] Yegui Xiao and Jing Wang. A new feedforward hybrid active noise control system. *IEEE Signal Processing Letters*, 18(10):591–594, 2011.

[26] Cheng-Yuan Chang and Sen M Kuo. Complete parallel narrowband active noise control systems. *IEEE Transactions on Audio, Speech, and Language Processing*, 21(9):1979–1986, 2013.

[27] STMicroelectronics. Reference manual: Stm32f405/415, stm32f407/417, stm32f427/437 and stm32f429/439 advanced arm®-based 32-bit mcus, . URL http://www.st.com/content/ccc/resource/technical/document/reference_manual/3d/6d/5a/66/b4/99/40/d4/DM00031020.pdf/files/DM00031020.pdf/jcr:content/translations/en.DM00031020.pdf.

[28] STMicroelectronics. Stm32f4discovery discovery kit user manual, . URL http://www.st.com/content/ccc/resource/technical/document/user_manual/70/fe/4a/3f/e7/e1/4f/7d/DM00039084.pdf/files/DM00039084.pdf/jcr:content/translations/en.DM00039084.pdf.

[29] Texas Instruments. Pcm1808-q1 adc data sheet. URL http://www.ti.com/lit/ds/symlink/pcm1808-q1.pdf.

[30] Philips Semiconductors. I2s bus specification. URL https://www.sparkfun.com/datasheets/BreakoutBoards/I2SBUS.pdf.

[31] Cirrus Logic. cs43l22 dac data sheet. URL https://www.cirrus.com/en/pubs/proDatasheet/CS43L22_F2.pdf.

[32] Cambridge SoundWorks. Pcworks fourpointsurround speaker system. URL http://dl.owneriq.net/7/7bb8732f-4b07-4a7e-b1ed-abab98b12f30.pdf.

[33] Pico Technology. Picoscope 2200a series data sheet. URL https://www.picotech.com/download/datasheets/PicoScope2200ASeriesDataSheet.pdf.

[34] Branko Somek, Martin Dadić, and Mladen Maletić. Active noise control in ducts. *AUTOMATIKA: časopis za automatiku, mjerenje, elektroniku, računarstvo i komunikacije*, 42(1-2):5–12, 2001.

[35] Simranjit Sidhu. *Implementation of Active Noise Cancellation in a Duct*. PhD thesis, Simon Fraser University, 2013.

[36] Xun Li, D Leclercq, Xiaojun Qiu, A Zander, and Colin H Hansen. Active control of higher order duct modes propagating in a large exhaust stack. *Proc. The Eighth Western Pacific Acoustics, Melbourne*, 2003.

[37] Finn Jacobsen. Propagation of sound waves in ducts. *Lecture note–Advanced Acoustics, Acoustic Technology, Ørsted DTU*, 2005.

[38] STMicroelectronics. Stm32f2xx standard peripheral library, . URL http://www.st.com/content/ccc/resource/technical/document/user_manual/59/2d/ab/ad/f8/29/49/d6/DM00023896.pdf/files/DM00023896.pdf/jcr:content/translations/en.DM00023896.pdf.

[39] Antti Lankila. *Simulation Model for an Active Noise Control System-Development and Validation*. PhD thesis, HELSINKI UNIVERSITY OF TECHNOLOGY, 2008.

[40] Stephen J Elliott and Philip A Nelson. Active noise control. *IEEE signal processing magazine*, 10(4):12–35, 1993.

[41] Iman Tabatabaei Ardekani and Waleed H Abdulla. Effects of imperfect secondary path modeling on adaptive active noise control systems. *IEEE transactions on control systems technology*, 20(5):1252–1262, 2012.

[42] I Tabatabaei Ardekani and Waleed H Abdulla. Theoretical convergence analysis of fxlms algorithm. *Signal Processing*, 90(12):3046–3055, 2010.

[43] Stephan P Lovstedt. Improving performance of the filtered-x least mean square algorithm for active control of noise contatining multiple quasi-stationary tones. 2008.

[44] Timothy Ma, Gowtham Bellala, and Kifung Chu. Active noise cancellation headsets.

[45] Liang Wang and Woon-Seng Gan. Convergence analysis of narrowband active noise equalizer system under imperfect secondary path estimation. *IEEE transactions on audio, speech, and language processing*, 17 (4):566–571, 2009.

[46] Sen M Kuo, Ajay B Puvvala, and Woon S Gan. Convergence analysis of narrowband active noise control. In *2006 IEEE International Conference on Acoustics Speech and Signal Processing Proceedings*, volume 5, pages V–V. IEEE, 2006.

[47] I Tabatabaei Ardekani and Waleed H Abdulla. On the convergence of real-time active noise control systems. *Signal Processing*, 91(5): 1262–1274, 2011.